PUBLICATIONS OF
THE UNIVERSITY OF EASTERN FINLAND

Dissertations in Forestry and Natural Sciences

HEIKKI YLI-OLLILA

METHODS TO ANALYZE LONGITUDINAL MOTION OF THE CAROTID WALL

HEIKKI YLI-OLLILA

Methods to Analyze Longitudinal Motion of the Carotid Wall

Publications of the University of Eastern Finland
Dissertations in Forestry and Natural Sciences
No 270

Academic Dissertation
To be presented by permission of the Faculty of Science and Forestry for public examination in the Auditorium 2 in Kuopio University Hospital, Kuopio, on August, 18, 2017, at 12 o'clock noon.

Department of Applied Physics

Grano Oy
Jyväskylä, 2017
Editors: Research Dir. Pertti Pasanen,
Profs. Pekka Kilpeläinen, Kai Peiponen, and Matti Vornanen

Distribution:
University of Eastern Finland Library / Sales of publications
P.O.Box 107, FI-80101 Joensuu, Finland
tel. +358-50-3058396
www.uef.fi/kirjasto

ISBN: 978-952-61-2521-3 (printed)
ISSNL: 1798-5668
ISSN: 1798-5668
ISBN: 978-952-61-2522-0 (PDF)
ISSN: 1798-5676 (PDF)

Author's address:

Kanta-Häme Central Hospital
Department of Radiology
Ahvenistontie 20
13530 Hämeenlinna
FINLAND
email: heikki.yli-ollila@khshp.fi

Supervisors:

Docent Tiina Laitinen, Ph.D.
Kuopio University Hospital
Department of Clinical Physiology and Nuclear Medicine
P.O.Box 100
70029 KYS
FINLAND
email: tiina.m.laitinen@kuh.fi

Professor Tomi Laitinen, M.D Ph.D.
Kuopio University Hospital
Department of Clinical Physiology and Nuclear Medicine
P.O.Box 100
70029 KYS
FINLAND
email: tomi.laitinen@kuh.fi

Docent Mika Tarvainen, Ph.D.
University of Eastern Finland
Department of Applied Physics
P.O.Box 1627
70211 KUOPIO
FINLAND
email: mika.tarvainen@uef.fi

Reviewers:

Professor Tapio Seppänen, Ph.D
University of Oulu
Machine Vision Group
P.O.Box 4500
90014 OULU
FINLAND
email: tapio.seppanen@oulu.fi

Docent Tom Kuusela, Ph.D
University of Turku
Laboratory of Quantum Optics
Vesilinnantie 5
20014 TURKU
FINLAND
email: tom.kuusela@utu.fi

Opponent:

Professor Jari Hyttinen
Tampere University of Technology
Faculty of Biomedical Sciences and Engineering
P.O.Box 527
33101 TAMPERE
FINLAND
email: jari.hyttinen@tut.fi

ABSTRACT

Longitudinal movement of the common carotid artery wall is a novel parameter and postulated to represent an independent index of arterial wellbeing. This thesis describes methods to accurately measure and characterize the longitudinal motion from B-mode ultrasound videos. In addition, multiple local arterial stiffness indices computed from the waveform of the longitudinal motion have been devised. This thesis focuses on exploring the complexity of the longitudinal waveform instead of plain motion amplitude measurements that have been published previously.

Two separate study populations were collected, which both included 19 healthy subjects. A 2D cross-correlation and contrast optimization based motion tracking method was developed and used to track the longitudinal and radial motion of the carotid wall from imaged ultrasound videos. The characterization of the longitudinal motion was conducted with principal component analysis and transfer function analysis. Applanation tonometry as well as known arterial stiffness indices computed from the radial motion of the artery wall were used as reference stiffness indices.

The results revealed that the motion tracking was reproducible and three different longitudinal waveforms could be observed: antegrade oriented, bidirectional and retrograde oriented. There was a clear linear relationship between the blood pressure and the longitudinal motion of the carotid wall. It was also observed that the longitudinal motion of the inner artery wall priors on average at about 19 ms the longitudinal motion of the outer wall. In addition, there was a 17 % reduction of the longitudinal motion amplitude (on 1 Hz frequency) in the outer arterial wall compared to that in the inner wall. The strongest correlations to the reference stiffness indices were found with those indices describing the complexity of the longitudinal waveform, RAlength (i.e. the length of the hysteresis curve formed by plotting the diameter change graph and the longitudinal motion against each other) and the 2nd

principal component, and the correlation between the peak velocity and acceleration of the longitudinal motion. The peak Spearman correlations were between the RAlength and compliance coefficient ($r = 0.80$, $p < 0.001$) and the 2nd principal component of the outer carotid wall layer and the distensibility coefficient ($r = 0.63$, $p < 0.01$). The peak-to-peak amplitude of the longitudinal motion did not correlate significantly with the reference stiffness indices in a healthy population.

The results indicate that the complexity indices of the longitudinal waveform are a good addition to the toolbox for measuring the state of the vascular system. The indices are repeatable and they display a higher correlation than the previously published amplitude indices of longitudinal motion with arterial stiffness. It seems that arterial stiffening primarily starts to modify the finer details of the longitudinal waveform before there is any amplitude reduction in the longitudinal motion.

National Library of Medicine Classification: QT 34.5, QT 36, WG 595.C2, WN 208

Medical Subject Headings: Carotid Artery, Common; Biomechanical Phenomena; Vascular Stiffness; Elasticity; Motion; Blood Pressure; Ultrasonics; Ultrasonography; Video Recording; Principal Component Analysis

Yleinen suomalainen asiasanasto: kaulavaltimot; biomekaniikka; jäykkyys; joustavuus; venyminen; liikeanalyysi; verenpaine; ultraääni; ultraäänitutkimus; kuvantaminen; videokuvaus

To Maika

Acknowledgements

This thesis was carried out in the Department of Clinical Physiology, Nuclear Medicine and Clinical Neurophysiology, Kuopio University Hospital, and the Department of Applied Physics, University of Eastern Finland, during 2012 – 2016. I would like to thank all of the people who have contributed to the studies. Most of all I would like to highlight the following people who have contributed to my work significantly:

Firstly, I would like to express my deepest gratitude to my supervisors Chief Physicist Tiina Laitinen, Ph.D., Professor Tomi Laitinen, M.D. Ph.D. and Adjunct Professor Mika Tarvainen, Ph.D. Tiina Laitinen was my principal supervisor, an eminent medical physicist and her inspiring guidance and remarkable enthusiasm for the subject made the completion of this thesis a true pleasure. She always had a solution if I ever was stuck with a problem and she was a constant source of new ideas, even in her sleep. My second supervisor, Tomi Laitinen, is an expert in the field of clinical physiology. His comprehensive knowledge of vascular biomechanics has been a great help to me and his encouraging way of providing feedback always kept me motivated. Mika Tarvainen is an inexhaustible databank when it comes to signal analysis and processing. Even though his office was a small trip away, he was always available and literally ready to travel the extra mile to help me at any time.

I thank the former Head of the Physics Department in the University of Oulu, Matti Weckström, M.D. Ph.D. His critical thinking and ambition towards learning inspired me to take my first steps in the world of science. Matti was one of the co-writers in Studies I and II. He passed away during the writing of this thesis. I will be forever grateful that I had the privilege to know Matti and that he took time out of his busy schedule to be a part of my research project and to counsel me in my previous studies.

I want to acknowledge the reviewers of this thesis Professor Tapio Seppänen, Ph.D. and Adjunct Professor Tom Kuusela, Ph.D. Their valuable comments improved my thesis significantly. I also want to thank Ewen MacDonald, Ph.D. for the linguistic corrections of this thesis.

I thank the joyful staff of the Department of Clinical Physiology, Nuclear Medicine and Clinical Neurophysiology, Kuopio University Hospital, for taking me as one of your own, when I was making my measurements and working as a specializing physicist. In particular, I thank the former creepers of the zero-zero-floor Tuomas*, Elisa*, Salla, Laura, Helena, Alisa, Hanna, Lepi, Matti, Minna and Mikko for making my working days a pleasure. *Equal contribution.

I would like to thank all of my friends from the A.I. Virtanen Institute who have brought me joy and happiness on the floor ball arena, on the disc golf field and in the overall hang-a-rounds. May the Force be with you.

I would like to thank my parents Mervi and Raimo and my brother Jarmo for always being there for me. You are my backbone and without you, I would have never made it this far.

I was fortunate to enjoy significant financial support from Doctoral Programme in Medical Physics and Engineering, Kuopio University Hospital (EVO 5031320, 5031316 and VTR 5031356), Science Foundation of Kuopio University Hospital, Aarne and Aili Turunen Foundation, Foundation for the Promotion of Technological Advances, Aleksanteri Mikkonen Foundation, Finnish Foundation for Cardiovascular Research, Antti and Tyyne Soininen Foundation and International Doctoral Programme in Biomedical Engineering and Medical Physics. I am truly grateful for each of the above-mentioned organizations for believing in my studies.

I dedicate my thesis to my beloved wife Maika. You are my inspiration, motivation and the love of my life. Thank you for putting up with me throughout this writing process and thank you for not being jealous of my love of science.

Tampere, March 2017 *Heikki Yli-Ollila*

LIST OF ABBREVIATIONS

2D	Two dimensional
3D	Three dimensional
A	Acceleration
AA	Aortic augmentation
Aix	Augmentation index
Aix@75	Augmentation index at heartrate of 75 beats per minute
ampl	Amplitude
ante	Antegrade direction
avg	Average
AO	Longitudinal motion of adventitia layer
AO_{ampl}	Peak-to-peak amplitude of the longitudinal motion of adventitia layer
AO_{ante}	Antegrade amplitude of the longitudinal motion of adventitia layer
AO_{dev}	Average deviation of the longitudinal motion of adventitia layer from its initial location
AO_{retro}	Retrograde amplitude of the longitudinal motion of adventitia layer
CC	Cross-sectional compliance coefficient
CCA	Common carotid artery
CV	Coefficient of variation
D	Diameter
D_{avg}	Average diameter of the artery
DBP	Diastolic blood pressure
DC	Cross-sectional distensibility coefficient
D_d	Diastolic diameter of the artery
dev	Deviation
DICOM	Digital imaging and communications in medicine
D_s	Systolic diameter of the artery
ECG	Electrocardiograph
E_Y	Young's elastic modulus
HDL	High-density lipoprotein

IA	Longitudinal motion between intima-media and adventitia layers
IA_{ampl}	Peak-to-peak amplitude of the longitudinal motion between intima-media and adventitia layers
IA_{ante}	Antegrade amplitude of the longitudinal motion between intima-media and adventitia layers
IA_{dev}	Average deviation of the longitudinal motion between intima-media and adventitia layers from its initial location
IA_{retro}	Retrograde amplitude of the longitudinal motion between intima-media and adventitia layers
IMT	Intima-media thickness
IO	Longitudinal motion of intima-media layer
IO_{ampl}	Peak-to-peak amplitude of the longitudinal motion of intima-media complex
IO_{ante}	Antegrade amplitude of the longitudinal motion of intima-media complex
IO_{dev}	Average deviation of the longitudinal motion of intima-media complex from its initial location
IO_{retro}	Retrograde amplitude of the longitudinal motion of intima-media complex
LDL	Low-density lipoprotein
P1	First peak on the aortic pressure curve
PC	Principal component
PCA	Principal component analysis
PP	Pulse pressure
PP_c	Carotid pulse pressure
PWV	Pulse wave velocity
RAlength	Length of the hysteresis curve formed by plotting the diameter change graph and the longitudinal motion against each other's
retro	Retrograde direction
ROI	Region of interest

SBP	Systolic blood pressure
SD	Standard deviation
V	Velocity
Z	Characteristic impedance

NOTATIONS

$\| \|$	Absolute value
$( )^T$	Transpose
$( )^*$	Complex conjugate
α	Cronbach's alpha
λ	Eigenvalue
λ_v	Vector containing all eigenvalues
ρ	Blood density
θ	Angle
σ^2	Variance
$\Phi(\omega)$	Phase response (function of angular frequency ω)
ω	Angular frequency
$\boldsymbol{a}(i,j)$	Weighting factor matrix
$A(\omega)$	Amplitude response (function of angular requency ω)
arg	Argument; the phase angle in complex domain obtained as ratio between real and imaginary parts
$\boldsymbol{C}(x,y)$	Correlation matrix
$C_{XY}(f)$	Coherence function
$det( )$	Determinant
f	Frequency
f_0	Original frequency
$f(x)$	Function
$f[k]$	Discrete function
$F[n]$	Discrete Fourier transform
F_s	Sampling frequency
$\boldsymbol{\mathcal{F}}$	Continuous Fourier transform
$\boldsymbol{H}$	Eigenspace

$\boldsymbol{I}$	Identity matrix
$\boldsymbol{I}(x,y)$	Surrounding pixels intensities of an image
$\boldsymbol{I}_x(x,y)$	Slope of an image in x-direction
$\boldsymbol{I}_y(x,y)$	Slope of an image in y-direction
$\boldsymbol{I}_{xy}(x,y)$	Cross-product of the x and y slopes of an image
L	Length of signal / number of measurements
p	Characteristic polynomial
$\boldsymbol{PC}$	Matrix containing principal components in rows and subjects in columns
$P_{XX}(f)$	Power spectrum of an input signal
$P_{YY}(f)$	Power spectrum of an output signal
$P_{XY}(f)$	Cross-power spectrum
r	Correlation coefficient
$\boldsymbol{R}$	Correlation matrix
t	Time
$TF(f)$	Transfer function
$TF(dB)$	Transfer function in decibels
U	Power of a window function
$w(n)$	Window function
x	Observation
$x(i)$	i:th observation
X	Input signal in frequency space
$\boldsymbol{X}$	Matrix
y	Observation
$y(i)$	i:th observation
Y	Output signal in frequency space
$\boldsymbol{Y}$	Matrix

LIST OF ORIGINAL PUBLICATIONS

This thesis is based on data presented in the following articles, referred to by the Roman numerals I–IV, and on previously unpublished data collected and analyzed by our research group.

I Yli-Ollila H, Laitinen T, Weckström M and Laitinen T. Axial and Radial Waveforms in Common Carotid Artery: An Advanced Method for Studying Arterial Elastic Properties in Ultrasound Imaging. *Ultrasound in Med Biol 39: 1168-1177, 2013.*

II Yli-Ollila H, Laitinen T, Weckström M and Laitinen T. New indices of arterial stiffness measured from longitudinal motion of common carotid artery in relation to reference methods, a pilot study. *Clin Physiol Funct Imaging 36: 376-388, 2016.*

III Yli-Ollila H, Tarvainen MP, Laitinen TP and Laitinen TM. Principal component analysis of the longitudinal carotid wall motion in association with vascular stiffness, a pilot study. *Ultrasound in Med Biol 42: 2873-2886, 2016.*

IV Yli-Ollila H, Tarvainen MP, Laitinen TP and Laitinen TM. Transfer function analysis of the longitudinal motion of the common carotid artery wall. *Front Physiol 7: 651, 2016.*

The above publications are included at the end of this thesis with their copyright holders' permission.

AUTHOR'S CONTRIBUTION

The publications of this thesis are original research papers and the author has been the first author of papers I-IV and the corresponding author of papers I-III. The named co-authors have made significant contributions to all of the articles. The author participated in all data acquisitions described in the publications and has conducted all of the data analysis and formulated the results presented in the publications. In addition, the author developed the fully functioning ultrasound video analysis software, which was used in studies I-IV to analyze the motion and stiffness of the common carotid artery wall. All of the studies were carried out in Kuopio University Hospital and in the University of Eastern Finland.

Contents

1 Introduction

The primary function of the circulatory system is to convey oxygen and nutrients to all of the cells in the body by circulating blood first through the lungs and then around the rest of the body [1]. The circulatory system has four main components: the heart, arteries, veins and micro vessels. Any malfunction in the circulatory system can lead to local ischemia and therefore damage to those tissues that are located behind the point of failure in the cardiovascular system. At present, cardiovascular diseases are the leading global cause of death in the world [2-4].

There are two main pathogenetic processes affecting arterial wellbeing: arteriosclerosis, systemic, age-related arterial stiffening of blood vessels [5, 6], and atherosclerosis, a progressive nodular disease in which there is an accumulation of lipids and eventually calcium and other crystallized materials within artery walls [5, 7]. There are reliable methods to diagnose advanced vascular diseases such as the presence of atherosclerotic plaques. However, the field of cardiovascular diseases is currently moving from late state detection and treatment to early detection and prevention [8, 9]. New methods for population screening, allowing an early detection of arterial disease are needed because the development of cardiovascular disease begins already in childhood long before there are any clinical manifestations [10-14]. In addition, atherosclerosis develops in a non-uniform fashion [15, 16] and there are other diseases causing arterial stiffening [5, 6]. Therefore, multiple different measures are crucial if one wishes to gather a complete picture of the cardiovascular status and to detect the early signs of the arterial stiffness [17, 18]. Thus, early detection, with lifestyle changes, and possibly pharmacological treatment, could delay or even prevent the progression of the arterial stiffness [19].

The longitudinal motion of the common carotid artery wall is a newly found characteristic depicting vascular function. Details

of the driving force and the role of different anatomical and physiological phenomena affecting the motion are still unclear. However, the amplitude of the motion has been shown to correlate with the markers of early-stage arteriosclerosis [20, 21] and the atherosclerotic plaque burden [22]. Thus, the longitudinal motion of the carotid wall is a potential new index for assessing arterial wellbeing.

In this thesis, methods to measure and characterize the longitudinal motion of the common carotid artery wall were developed and validated in human trials. Whereas other studies have focused on the amplitude of the longitudinal motion, this thesis emphasizes the benefits of making more comprehensive use of the longitudinal motion signal as well as examining the rate of change of the motion and the waveform of the motion. The purpose of the thesis is to gather detailed information about the longitudinal motion waveform and to develop a comprehensive toolbox for measuring arteriosclerotic changes in the common carotid artery.

2 Common carotid artery

2.1 ARTERIAL ANATOMY

The common carotid artery is a large elastic artery with an internal diameter of approximately 6.7 mm [23]. The left common carotid artery starts as one of the branches in the arch of aorta; it then runs upwards under the cover of the sternocleidomastoid muscle to the upper border of the thyroid cartilage where the common carotid artery divides into the internal and external carotid arteries [24]. The diameters of the internal and external carotid arteries are 6.0 mm and 5.2 mm, respectively [23]. In addition, the composition of the artery changes from being elastic artery to a more muscular artery after the bifurcation [25].

The artery wall can be divided into three larger layers that can be distinguished from each other, as shown in Figure 2.1. The innermost layer is called the intima. The intima layer consists of the endothelium; this is one cell layer thick and overlying a thin subendothelial surface of connective tissue [25]. The middle layer is called media and it consists of smooth muscle cells, which regulate the tonus of the vessel, and helps the vessel to withstand the pulsatile blood flow and pressure [25]. The media layer is connected to the intima layer by internal elastic lamina, which is a thin layer containing elastic fibers [26]. Finally, the outermost layer is called the adventitia. The adventitia layer consists of flexible fibrous connective tissue, which helps to prevent rupturing of the artery during body movements [26]. The adventitia layer is connected to the media layer by a thin layer called the external elastic lamina, which is made of condensed sheets of elastic fibers [26]. The elastic fibers allow the adventitia layer to move separately from the media layer in the longitudinal direction; this seems to be the case as the maximum longitudinal shear strain has been reported to occur between the media layer and the adventitia layer [27]. The

common carotid artery is at the borderline, where the large elastic artery type changes into a more muscular artery type [28] and thus the media and the adventitia layers are the thickest layers [29]. On the other hand, diseases like atherosclerosis can affect the thickness of the intima and media layers, especially thickening of the intima layer [30].

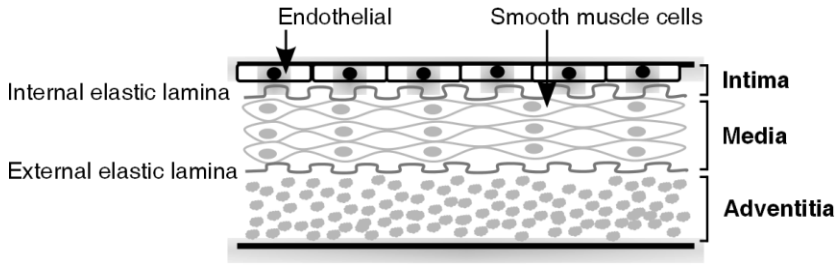

Figure 2.1: *Cross-sectional visualization of an artery wall. The three main layers intima, media and adventitia are displayed on the right side and the separating elastic laminas are displayed on the left side.*

2.2 ARTERIAL PHYSIOLOGY AND BIOMECHANICS

In Section 2.1, the diameter of the common carotid artery was estimated to be 6.7 mm. In reality, the diameter of the artery changes cyclically, following the pressure changes inside the artery [31, 32]. During diastole, the diameter of the common carotid artery can be 5.7 mm [33] and during systole, when the brachial blood pressure rises in the healthy population from 80 mmHg to 130 mmHg [34], the diameter of the artery increases by approximately 1 mm. To be more exact, the pulse pressure is about 11-14 mmHg higher in the common carotid artery than in the brachial artery [35].

The diameter change in the common carotid artery is not parabolic but displays two separate peaks as visualized in Figure 2.2. The first peak follows the forward propagating pulse pressure, which has originated from the contracting heart. The second peak is due wave reflection from the periphery [36].

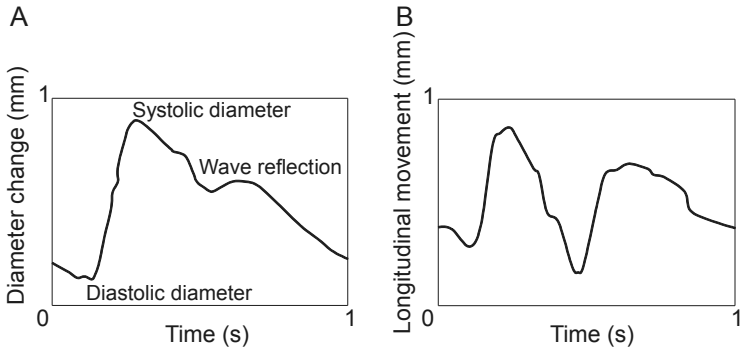

Figure 2.2: *Illustration of heartbeat-long carotid wall motion waveforms. A, diameter change waveform; B, longitudinal waveform of the intima-media layer.*

Every time a blood vessel branches into smaller vessels or tapers or stiffens, there are alternation in the resistance to blood flow. The resistance change within the arterial tree always creates a reflection for the propagating pressure wave. A sum of these wave reflections, mainly from the lower body, is visible on the diameter curve as a second, smaller peak after the maximum systolic diameter [36].

As elastic artery stretches and its diameter enlarges, the artery buffers the energy of the pulse pressure into the artery wall and as the diameter returns to its original position, the stored energy is released back to the circulation. This ability of storing and releasing the energy from the blood flow is called the Windkessel effect [37]. According to Poiseuille's law, resistance is inversely proportional to blood vessel radius to the fourth power [38]. Therefore, the smallest arteries and arterioles are responsible for the main resistance (i.e. the peripheral resistance) against which the heart muscle has to combat. The buffering of the pulse pressure energy in large arteries stabilizes the pulsatile blood flow and reduces the energy needed by the heart muscle to push the blood through the circulatory system [37]. If the Windkessel effect is compromised, this elevates the pulse pressure, and thus a greater force is needed to drive the required blood volume ahead.

The endothelium is a key regulator of vascular homeostasis [39]. It is an active barrier between the blood and tissue as well as a signal transducer in the circulation i.e. it influences the vessel wall phenotype [40]. Under normal conditions, endothelial regulation maintains the normal vascular tone, blood volume flow, limiting vascular inflammation as well as the proliferation of smooth muscle cells by sensing hemodynamic forces, regulating substances and adjusting permeability [40-42]. The vascular homeostasis may become disturbed if endothelial function is compromised, for instance by attenuated shear stress of the artery wall or by prolonged exposure to cardiovascular risk factors [39].

2.3 ARTERIAL STIFFNESS

There are multiple causes for arterial stiffening and often the diseased stiffening process starts in childhood or in young adulthood [12-14]. Arterial stiffness can be either systemic or local [43] but in general the stiffness affects to different degrees, depending on the different locations in the arterial tree [44-46].

Arteriosclerosis is a diffuse, age-related disease and a major cause of systemic arterial stiffening and thickening [5, 6]. Arteriosclerosis has been demonstrated to increase the risk of cardiovascular disease [47-49]. The mechanical properties of an artery are primarily set by the media layer [50-52] and arteriosclerosis is primarily a disease of the media layer; in this layer, there are elevation in the collagen level accompanied by a decline in the elastin content as well as changes in the collagen type present in the tissue [53].

Atherosclerosis is one nodular form of arteriosclerosis [5] and a major cause of local arterial thickening. The thickening of the artery involves pathological changes of the intima layer and is commonly a disease of the larger and coronary arteries [5]. The genesis of atherosclerosis is a sum of multiple factors. The imbalance of high-density (HDL) and low-density lipoproteins (LDL) in the blood circulation and structural damage within the

endothelium of the artery wall, likely caused by the elevated blood pressure level [54, 55], are the main contributors to the accumulation of the LDL into the arterial walls [56]. The LDL are involved in the transfer of cholesterol from the liver to the vessels but when these LDL particles become embedded under the endothelium of the artery wall, free oxygen radicals oxidize the LDL [57]. This evokes an inflammatory process that leads, over the years, though multiple phases, into local plaque formation on the inner surface of the artery wall [7]. The development of a plaque takes years and due to local artery wall enlargement, it can exert minimal or even no effects on the blood flow for decades [58]. However, the accumulation of fat within the arterial wall locally changes the arterial elasticity prior to the visible formation of the plaque.

There are other forms of arteriosclerosis; for instance arterioloclerosis, which is a sclerosis affecting the smaller arteries and arterioles [6], Mönckeberg's arteriosclerosis, which involves degeneration of smooth muscle cells and mostly affects the arteries of the extremities in elderly populations [5], and hyaline arteriosclerosis, which is caused by the deposition of hyaline in the small arteries and arterioles [59].

Some degree of the arterial stiffening and thickening is part of inevitable, normal ageing process. It has been evaluated that between the years 10 to 50, the intima layer accumulates approximately 10 mg of cholesterol per a gram of tissue [5]. In addition, by the age of 25 years, approximately 30-50 % of the aortic inner surface area is displaying evidence of fatty streaks [5]. This diffuse thickening of the intima layer, affecting all arteries, must be discriminated from local fibromuscular plaques that are a characteristic of atherosclerosis.

2.4 ADVERSE EFFECTS OF ARTERIAL STIFFNESS

Arterial stiffness affects the wellbeing of the cardiovascular system in multiple ways. The stiffness decreases the compliance of the artery wall and hence increases the total impedance of the

artery, causing a weakening of the performance of the vascular system [60] and compromising the Windkessel effect of the artery [37].

Stiffening of the large elastic arteries reduces the natural mismatch between the impedances of large elastic arteries and muscular arteries. A loss of the impedance mismatch results in a loss of wave reflection at the border of the two artery types and hence a greater proportion of the pulse pressure energy is transferred to the periphery [61, 62]. As the pulse pressure becomes increased, due to the compromised Windkessel effect, and because a larger proportion of the pressure energy is transferred to the periphery due to the loss of impedance mismatch, the elevated pulse pressure in periphery is capable of damaging the blood vessels of the target organs [63, 64]. In addition, the dynamic tone (i.e. endothelial function) in small arteries is affected by the pulse pressure [65, 66]. The increased pulse pressure might disturb the autoregulation of organs such as the brain and the kidneys, which tune the input resistance of the blood flow by the pulse pressure and mean arterial pressure [64].

Due to the reduced compliance, stiff arteries conduct pressure waves faster than their more elastic counterparts [67], as revealed by the widely used Moens-Korteweg equation, which states that arterial stiffness is proportional to pulse wave velocity (PWV) to the second power [68]:

$$\mathrm{PWV} = \sqrt{\frac{\mathrm{E_Y}\ \mathrm{IMT}}{2r\rho}} \tag{2.1}$$

where r is the radius of the artery, ρ is blood density, E_Y is Young's elastic modulus and IMT is the thickening of the intima-media. The faster pressure wave propagation leads to a situation where the pulse pressure, which originates from the heart, reflects back to the heart from the periphery during systole i.e. the time when the heart muscle is still contracting, and thus further elevates the systolic blood pressure [69]. This introduces an extra burden on the left ventricle of the heart,

which is the part responsible for pumping the blood around the body. This extra burden weakens the cardiac function [70, 71] and can cause dilated cardiomyopathy i.e. pathological dilatation of the left ventricle [72]. In addition, the shift of the arrival time of the pressure wave reflection from diastole to systole worsens the perfusion pressure of the coronary arteries and weakens the nutrient intake of the heart muscle [62].

In complicated atherosclerosis, the plaque may burst or rupture, causing occlusion of the artery and trigger ischemia in the target organ fed originally by that artery.

2.5 MEASURING ARTERIAL BIOMECHANICS

Arterial stiffening is a complex phenomenon and thus multiple stiffness measuring modalities are needed to cover all aspects of the arterial stiffness. For instance, local arterial stiffness can be measured from the diameter change of the artery with ultrasound imaging [33]. Systemic arterial stiffness can be estimated with PWV measurement [73] or with pulse waveform analysis with applanation tonometry [74]. Measurements of the endothelial function of arteries [75, 76] and the IMT [77] are indices of general arterial wellbeing and have been considered as surrogate markers of atherosclerotic disease.

2.5.1 Diameter change of the artery

The proportion of blood pressure and diameter change reflects local arterial stiffness [78]. When the artery is stiff, a larger amount of inner pressure is needed to stretch the artery. Therefore, in stiff arteries, a smaller diameter change between the diastolic and systolic phases [79, 80]. However, the elevated pulse pressure in stiff arteries decreases the effect of diameter change reduction and therefore blood pressure information is needed as a scaling factor if one wishes to make a more accurate estimation of the local arterial stiffness.

The diameter change of carotid artery can be measured by carotid ultrasound imaging and multiple stiffness indices exist

for evaluating the local stiffness. The cross-sectional distensibility coefficient (DC) represents the strain on the arterial wall at a given pulse pressure and is a reflection of the mechanical stress of the artery [79]. DC is a significant predictor of future cardiovascular diseases and mortality [81] and can be calculated as follows [43]:

$$\mathrm{DC} = \frac{D_s^2 - D_d^2}{D_s^2\, PP_c} \tag{2.2}$$

where D_s is systolic diameter of the artery, D_d is diastolic diameter of the artery and PP_c is pulse pressure in carotid artery.

The cross-sectional compliance coefficient (CC), measures the relation between the volume change of the artery and the pulse pressure. Commonly in the noninvasive measurements of the CC, the compliance is assumed independent of the blood pressure and the volume change of the artery is believed to be attributable only to the distension of the artery, not to its elongation [79]. The CC can be calculated as follows [43]:

$$\mathrm{CC} = \frac{\pi({D_s}^2 - {D_d}^2)}{4\, PP_c} \tag{2.3}$$

E_Y is an estimate of the pressure change per square area theoretically needed for a 100% increase in artery diameter [82]. The formula for E_Y is presented below. However, calculating of E_Y from IMT assumes that the wall is homogeneous and therefore E_Y values may be underestimated [43]:

$$\mathrm{E_Y} = \frac{3}{\mathrm{DC}}\left[1 + \frac{{D_s}^2}{(D_d + 2\ \mathrm{IMT})^2 - {D_d}^2}\right] \tag{2.4}$$

The characteristic impedance of the common carotid artery (Z) relates arterial pressure to blood flow velocity in the absence of wave reflection [43]. Since in *in vivo* measurements the wave reflection is always present, a mathematical estimation of the Z can be calculated:

$$Z = \sqrt{\frac{E_Y \, IMT \, \rho}{D_{avg}}} \tag{2.5}$$

where D_{avg} is the average diameter of the artery, IMT is intima-media thickness and ρ is density of the blood, which is commonly approximated as 1060 kg/m^3 [83].

In addition to the local stiffness indices, the ultrasound measurement of the artery diameter change can also be used for a rough estimation of the systemic stiffness. The timing of the first and second peaks in the diameter curve reflects systemic stiffness. The pressure signal propagates faster in stiff arteries [69] and this causes the first peak in the diameter curve to occur sooner in the common carotid artery if the ascending aorta and distal end of the common carotid artery are stiff. Commonly, a greater change is observable in the timing of the second peak: as the pressure wave travels faster through the smaller arteries in the periphery, the second peak in the carotid diameter curve occurs sooner and starts to merge with the first peak [52, 62, 80]. This merging of the first and second pressure peak also affects the diameter change of the artery: while the stiffness of the artery makes it more difficult to move the artery wall, the drastically elevated peak blood pressure due to the wave reflection can stretch the artery wall significantly.

2.5.2 Applanation tonometry and pulse wave velocity

In applanation tonometry, the blood pressure signal is measured commonly from the radial artery with a pen-like tonometer. Then the measured pressure signal is mathematically transferred into aortic pressure waveform from which multiple arterial wellbeing indices are computed. Although it is not a direct pressure measurement from aorta, the estimated aortic pressure waveform is accurate in most cases [84].

Arterial wellbeing can be estimated from the aortic pressure curve [85]. Commonly used indices are aortic augmentation (AA), i.e. the pulse pressure in aorta, and augmentation index (Aix), which is defined as follows:

$$\mathrm{Aix} = \frac{\mathrm{SBP} - P1}{\mathrm{SBP} - \mathrm{DBP}} \tag{2.6}$$

where SBP is systolic blood pressure in aorta, DBP is diastolic blood pressure in aorta, *P1* is the primary aortic peak pressure before the reflected pressure waveform. Both indices have been displayed to increase in patients with hypercholesterolemia [86] and to be associated with cardiovascular risk [74, 87]. Aix is dependent of heart rate [88, 89] and therefore Aix is often adjusted for the heart rate. Commonly the Aix value is corrected to show the corresponding Aix value at a heart rate of 75 beats per minute (Aix@75) [89]. Aix is also affected by sex, age and height [88] and therefore is more of an arterial wellbeing index than a stiffness index.

Applanation tonometry can also be used for defining the PWV in arteries. The PWV measures the average arterial stiffness in a large segment of the arterial tree [73, 90]. Commonly the PWV is measured between the common carotid and femoral arteries [43, 91] but also a measurement between carotid and radial arteries is used to estimate the stiffness of brachial artery or, in general, the muscular artery stiffness [92]. The carotid-femoral PWV has been shown to predict cardiovascular diseases and mortality in multiple studies [68, 73, 93]. The carotid-radial PWV has been shown to reflect coronary artery disease [94]. In a comparative study, the carotid-radial PWV could not predict the cardiovascular outcome of end-stage renal disease patients unlike the carotid-femoral PWV [95].

2.5.3 Endothelial function of artery

The gold standard for measuring endothelial function is angiography with acetylcholine injection but due to its invasiveness and radiation exposure, it cannot be used in population screening [96]. The most widely used noninvasive method for estimating endothelial function of arteries is flow-mediated dilatation (FMD) as measured commonly from brachial artery with ultrasound imaging. Other arteries could be used for the measurement, but brachial artery is easy to

measure. In addition, smaller arteries are technically challenging, whereas in larger arteries the vasodilatation might be difficult to perceive, even in arteries with normal endothelial function [97].

In the FMD measurement, blood flow into brachial artery is blocked in general for 5 minutes using a cuff [98]. Ultrasound imaging is used to image the diameter of the brachial artery approximately 5–10 cm above the antecubital fossa for duration of 3 minutes [99]. Although the blood pressure and flow declines, the diameter of the brachial artery remains almost the same or even increases lightly while the cuff is applied. After release of the cuff, the local blood flow increases dramatically, causing shear stress to the endothelium of the artery wall. The self-regulation of the endothelium triggers a cascade of responses to the increased shear stress by dilating the artery [41]. As a result of these changes in endothelial function, the diameter of the brachial artery increases by approximately 0.2-0.3 mm within a minute and then slowly returns to its initial position. The peak FMD can be calculated as:

$$\text{FMD} = \frac{D_{max} - D_{BL}}{D_{BL}} \tag{2.7}$$

where D_{max} is maximum diameter and D_{BL} is mean baseline diameter.

As an arterial wellbeing index, the reduced FMD has been shown to be associated with type 2 diabetes [76], body mass index and smoking [75]. The disadvantages of the FMD measurement is that it is slow compared to many other arterial wellbeing indices, inter-observer variation has been an issue and the accuracy of the measurement depends on the quality of the imaging equipment/software being used [41].

2.5.4 Intima-media thickness

The measurement of the combined thickness of the two innermost arterial wall layers is commonly made with ultrasound imaging from common carotid artery. Normal values for IMT in adults are 0.592 ± 0.10 for men and 0.572 ± 0.08

mm for women [100]. In addition, the IMT increases by about 5.7 ± 0.4 μm/year with aging [100].

IMT is used to evaluate the stage of a nodular atherosclerotic disease and therefore is not a direct index of arterial stiffness but rather an index of arterial wellbeing [77]. However, the elevated IMT does exhibit a high correlation with arterial stiffness and it has also been noted to correlate directly to smoking [13], body mass index [13], hypercholesterolemia [13, 101], type 2 diabetes [102], myocardial ischemia [103] and inversely to the HDL level [104].

Although IMT is strongly associated with atherosclerosis, there are other reasons that can cause thickening of the carotid artery wall. For example, local hemodynamics, shear stress and elevated blood pressure are known influencers on artery wall thickening [105]. However, an IMT value over 0.9 mm in common carotid artery is thought to be abnormal and IMT over 1.3-1.5 mm or IMT 50% greater than the IMT of the surrounding artery is considered as evidence of the presence of an atherosclerotic plaque [106-108].

2.6 LONGITUDINAL MOTION OF THE ARTERY WALL

2.6.1 Measurement methods

The longitudinal motion occurring in the carotid artery wall was first detected in 1950s when invasively studying dogs' carotid arteries with piezo-electric crystals [109]. In that experiment, the amplitude of the longitudinal motion was evaluated to be insignificant compared to the diameter change. Five decades later, the longitudinal carotid wall motion was evaluated noninvasively in human trials and found to have an equal magnitude range as the diameter change of the carotid artery [110].

The tracking of the longitudinal motion of the carotid wall with ultrasound imaging is more challenging than the change of the artery diameter, due to limited resolution of ultrasound imaging in the longitudinal direction. The detailed

characteristics of ultrasound imaging will be presented in Chapter 3. Despite the measurement challenges, ultrasound imaging has quickly become the gold standard for measuring the longitudinal carotid wall motion. Multiple methods to measure the longitudinal motion with ultrasound imaging have been presented in the literature [111-123] and a summary of the methods is displayed in Table 2.1.

The majority of the proposed longitudinal motion tracking methods are based on clinical video data of common carotid artery. There are a few exceptions e.g. the use of the raw radio frequency signals of the ultrasound devices, which provide better control of the imaging data and thus superior possibilities for motion tracking [117-119, 123]. The ultrasound devices were equipped with 4-13 MHz transducers and they were capable of imaging frequencies varying from 25 Hz to 192 Hz. In general, the imaging has been performed in a breath hold for a duration of less than 5 seconds and the tracking of the longitudinal motion was performed for the intima-media complex of the carotid far wall. The reason for handling the intima and the media layers as combined unit is that the intima layer is not clearly distinguishable from the media layer in ultrasound imaging [124]. In addition, most of the visible longitudinal motion is believed to occur between the media and adventitia layers [27, 119]. Five of the studies listed in Table 2.1 performed the longitudinal motion tracking also for the adventitia layer, in order to quantify the longitudinal strain between the arterial layers. Only two of the listed studies used surrounding tissues as their origin for evaluating the longitudinal motion, others used the location of the ultrasound transducer as the origin.

The published motion tracking algorithms are mainly based on 2D cross-correlation, details of which will be described in Section 5.1.1. The major differences of the used algorithms are the size and the amount of the motion-tracked structures (i.e. regions of interest, ROIs) as well as the method used for updating the motion-tracked structures, i.e. the reference ultrasound images for the 2D cross-correlation analysis; as they are subject to variations in the function of time [125, 126].

Table 2.1. *Methods to track longitudinal motion of the carotid wall. Abbreviations: i, intima; m, media; a, adventitia; st, surrounding tissue; hb, heartbeat; RF, radio frequency; -, unknown parameter.*

Reference	Algorithm	Regions	ROI size	Format	Frame rate	Length	Frequency
Albinsson et al. 2014	Lagrangian speckle tracking	i-m	0.57-1.61 × 0.36-1.09 mm²	Video	55 Hz	Several hb	12 MHz
Cinthio et al. 2005	Echo tracking	i-m	0.1 × 0.1 mm²	Video	55 Hz	5.5 s	12 MHz
Gastounioti et al. 2011	Kalman filtering	i-m, a, st	1.6 × 1 mm²	Video	25 Hz	3 s	7.5 MHz
Gastounioti et al. 2013	Finite impulse response filtering	i, a	1.5 × 1.0 mm²	Video	25 Hz	3 s	7.5 MHz
Golemati et al. 2003	Speckle tracking	i-m, a, st	3.2 × 2.5 mm²	Video	25 Hz	3 s	7.5 MHz
Golemati et al. 2012	Weighted least-squares optical flow	i-m, a	1.5 × 1.0 mm²	Video	25 Hz	3 s	7.5 MHz
Idzenga T. et al. 2012	Coarse-to-fine echo tracking	i-m-a	-	RF	43 Hz	3 s	13 MHz
Larsson et al. 2015	Speckle tracking and median filtering	i	5.4 × 0.3 mm²	RF	43,2 Hz	-	12 MHz
Numata T. et al. 2007	Speckle tracking	i-m-a	2.8 × 0.2 mm²	RF	192 Hz	-	10 MHz
Svedlund and Gan. 2011	Velocity vector imaging	i	-	Video	-	-	8 MHz
Zahnd et al. 2011	Contour guided speckle tracking	i-m	1.5 × 0.24 mm²	Video	26 Hz	> 2 hb	8 MHz
Zahnd et al. 2013	Kalman filtering	i-m	1.5 × 0.3 mm²	Video	26 Hz	2 hb	10 MHz
Zahnd et al. 2014	2D+t volume trajectory estimation	i-m	1.5 × 0.3 mm²	Video	26 Hz	2 hb	8 MHz
Zahnd et al. 2015	Optical flow (real time)	i-m	2.45 × 0.30 mm²	RF	91 Hz	3.28 s	4 MHz

Commonly, one ROI from each motion tracked arterial layer is selected, but the amount of structures from a single layer is known to vary up to five [127]. The size of the motion-tracked ROI can be as small as a single "point" used in optical flow [123] and in vector velocity imaging [127], which are methods capable of describing the vector field generated by the spatio-temporal image brightness variations between subsequent frames. More commonly, the motion-tracked ROI size being used varies from 0.1 × 0.1 mm^2 with the so-called echo tracking method to 3.2 x2.5 mm^2 area with the speckle tracking method. More discussion on speckles is provided in Section 3.6. The update procedure of the reference ROI is based on previous motion-tracked video frames. Some algorithms do not update the reference ROI at all [115]. Others use a previous unfiltered video frame or multiple subsequent video frames with different filtering techniques to form the new reference ROI [113, 114, 121, 122].

All the presented algorithms, except one recent real-time application [123], are based on offline analysis of the gathered ultrasound data.

2.6.2 Waveform and driving force

The longitudinal motion of the common carotid wall has been reported to be bidirectional: First, the intima-media complex moves along the direction of the blood flow (antegrade direction) and this is then followed by backward motion, i.e. retrograde motion [128, 129]. A visualization of a typical longitudinal motion waveform reported in the literature is presented in Figure 2.2. In addition, other types of longitudinal motion patterns have been reported, where the main motion is in the retrograde direction [129-131].

The driving force for the longitudinal motion in the common carotid artery is unclear. The blood pressure has been shown to correlate with the longitudinal motion of the carotid wall [130, 132] and it has been speculated that the friction of the blood flow as well as the diameter change causing longitudinal shear or the physical motion of the contracting heart, or a combination of these phenomena, could drive the longitudinal motion [129,

133]. In addition, breathing [112] and arterial stiffness [20, 21] have been observed to influence the longitudinal motion waveform, as has the presence of atherosclerotic plaques, as these can alter the direction of the longitudinal motion in the artery wall [22, 134, 135].

The fact that retrograde oriented longitudinal motion waveforms exist, emphasizes the plausible effect of the physical motion of the heart or the larger diameter change prior the carotid bifurcation as a driving force. Nevertheless, in a smaller study, no significant correlation was found between the amplitude of the longitudinal motion and the physical motion of the ascending aorta [128]. However, in the same study, a preliminary connection was found between the cyclic rotation of the left ventricle and the longitudinal motion of carotid artery.

In a study conducted in pigs, catecholamines were observed to exert an effect on the amplitude and waveform of the longitudinal motion [136]. With very simplified generalization, both the α- and β-receptor activations have an effect on the vasculature and the heart: α-receptor activation evokes vasoconstriction, β_1 increases heart rate as well as cardiac muscle contractility and therefore cardiac output and β_2 causes vasodilatation [136]. In the study, epinephrine (agonist at α-, β_1- and β_2-adrenergic receptors) was intravenously administered at rate 200 μg/h, which was raised to 400 μg/h after a plateau in blood pressure and heart rate had been reached. During continuous epinephrine infusion, a higher bolus (0.1 mg) of norepinephrine (α-agonist) was given and longitudinal motion of the carotid wall was imaged. Ten minutes after the bolus, a constant infusion (25 mg/h) of metoprolol (β-blocker) was initiated. After total β-blockade, another 0.1 mg bolus of norepinephrine was delivered. The low constant infusion of epinephrine was reported to cause a decrease in pulse pressure, due to the greater affinity of epinephrine for β_2-receptors (causing vasodilatation) than for α-receptors (causing vasoconstriction). The reduction of pulse pressure was associated with a decrease in the longitudinal motion amplitude. More interestingly, norepinephrine was observed to

double the longitudinal amplitude, even during β-blockade, and hence Ahlgren et al. concluded that longitudinal motion was strongly related to α-adrenoceptor activation [136]. The study also claimed that in addition to the motion amplitude change, the high levels of norepinephrine and epinephrine in the circulatory system changed the longitudinal waveform such that it became multiphasic.

The same group has also stated in another recent small study on pigs that there seemed to be no significant correlation between the viscous drag of the blood flow and the longitudinal motion of the artery wall [137]. However, there are opposite findings from an experiment conducted in humans; it was claimed that the timing of the blood flow velocity graph matched with the antegrade longitudinal motion of the intima-media complex [128].

Overall, it seems that there are multiple components, physical, humeral and structural, affecting the longitudinal artery wall kinetics. The roles of these factors are still largely unknown.

2.6.3 Relation to arterial stiffness

Despite the lack of deeper understanding of the origin of the longitudinal artery wall motion, multiple studies have linked the longitudinal motion, and especially the amplitude of the motion, with different indices describing cardiovascular health: Diabetic patients have been reported to display reduced longitudinal motion amplitudes [21]. The reduced longitudinal motion has also been associated with the carotid plaque burden [22] as well as with coronary heart disease and with cardiovascular disease [138]. In addition, a link between major adverse cardiac events in mid- and high-risk patients and reduced amplitude of the longitudinal motion of the carotid wall was reported in a one-year follow-up study [139]. Cardiovascular risk factors such as ageing and high blood pressure have been associated with a reduction in the extent of the longitudinal motion [132]. The longitudinal motion of the common carotid artery wall is independent on the carotid IMT

[20, 131]. In addition, the retrograde amplitude of the longitudinal motion has been found to have a better discrimination power than the IMT to separate healthy individuals from cardiovascular risk patients [131].

In addition to the amplitude measurements, the acceleration of the longitudinal motion has been investigated; this parameter displays a strong and graded association between the peak acceleration of the longitudinal wall motion and the severity of the carotid stenosis [140].

2.6.4 Mathematical modelling

Under certain mathematical circumstances and assumptions, e.g. that blood behaves as a Newtonian fluid, the pulsatile blood flow through arteries can be modelled by the Navier–Stokes equations and Womersley equations. Fluid-structure interactions are always present *in vivo* and hence the resulting shear stress and motion of the artery wall are nowadays commonly modelled as well. Previously the arterial motion was only modelled as a diameter change but the latest arterial modelling studies have also considered the longitudinal motion such as in the Koiter shell model [134, 141, 142].

Mathematical modelling is a tool with which to evaluate theories and therefore a way to understand underlying causalities between signals and moreover a tool to predict future outcomes. Currently the modelling of the longitudinal motion is in its early developmental stage, but already it has achieved a good agreement with results from *in vivo* studies [134, 141, 142]. The reduction of the longitudinal motion amplitude in atherosclerotic arteries is visible through modelling [134] and thus in agreement with measured data [22]. With computational modelling, new information has been gained from stenotic coronary arteries: unlike the diameter change of the artery, the longitudinal motion of the inner artery wall has been demonstrated to be highly dependent on the geometry of the stenotic lesion [134].

3 Ultrasound imaging

The human ear can hear sound waves that have a frequency of 20-20,000 Hz. Waves that have higher frequencies are called ultrasound. Typically, frequencies from 3 to 20 MHz are used in clinical imaging devices [143].

The B-mode is the most used image modality in ultrasound imaging. In B-mode imaging, an anatomical, cross-sectional 2D image is formed based on the echoes reflecting from the tissue borders. Often the sound velocity is assumed to be constant (1540 m/s) in all soft tissues. When the sound propagation velocity and the time difference between the sounds being emitted and reflected are known, the point of reflection can be easily calculated.

Ultrasound imaging is fast, cheap and a widely available method with which to investigate superficial vessels. Other beneficial properties of ultrasound imaging are its good spatial and temporal resolution in superficial targets like the common carotid artery as well as its safety [144]. Thermal and cavitation effect produced by the clinical ultrasound imaging devices are insignificant [145] and the patient is not exposed to ionizing radiation in contrast to the situation with X-ray imaging.

3.1 TRANSDUCERS

Ultrasound transducers transform the electrical signal of the ultrasound device into a pressure wave using piezoelectric crystals (i.e. elements), and vice versa. The transducers are formed by coupling multiple independently acting elements together with varying configurations [146]. Modern transducers have a large bandwidth, in order to transfer and receive pulses of different frequencies. The large bandwidth is necessary for good axial resolution [146].

There are three different basic shapes that are used in 2D transducers: linear, sector and curved. In linear transducers, the elements are placed on the same plane in a row. This setup allows to the creation of a rectangular ultrasound field. The width of the image and the number of scan lines are constant at all tissue levels. This is an advantage when imaging targets in the near field [146]. In a sector transducer, the elements are placed tightly together and by the use of an acoustical lens located after the piezo elements, they form a fan-like ultrasound field that is narrow in the near field and widens as a function of distance. [146] Sector transducers are good for imaging through tight spaces but they have a poor near field resolution. Curved transducers are a mix of the two above-mentioned transducer types. The shape of the ultrasound field is fan-like, offering a wide field of view of the sector transducer. However, the piezo elements are widely positioned, as in linear transducers but on a curved surface, thus offering better near field resolution than can be acquired with a sector transducer. In general, linear transducers are used on superficial targets, sector transducers can be used, for example, to image between the ribs and curved transducers are used in greater imaging depths and for a larger field of view of the abdominal region [146].

3.2 FOCUSING

Each piezo element in an ultrasound transducer forms an individual ultrasound wave. These ultrasound waves are focused by two techniques. 1) The physical shape of the transducer either focuses (linear transducer) or defocuses (curved transducer) the pulses. 2) The ultrasound beams can also be focused by control pulses from the ultrasound device [146]. By controlling the timing of each piezo element with a precise protocol, the ultrasound beams can be made to form a field, which theoretically focuses on a single point [147]. The primary focus zone is where the scanline density of the ultrasound field is highest. For example, if the focus point is on

the central axis of the transducer, the generated ultrasound waves from the middle of the transducer reach the desired focus depth first. The ultrasound waves from the edge of the transducer have to travel a longer distance to the focal point, and hence by adjusting the delay of transferring and receiving ultrasound waves from the center of the transducer towards the edges, this results in focused ultrasound scanlines at the desired focusing point. The delay is chosen in a manner that the sum of the waves' travel time and the delay imposed on the electrical echo signal are the same for each piezo element [146]. If one wishes to estimate the echo time, the ultrasound velocity is assumed to be constant in soft tissues, which in reality is not exactly true [147]. In practice, all the focusing is conducted semi-automatically by the clinical ultrasound device and the user only needs to choose the focusing depth or depths, in addition examining multiple focusing depths is also possible if one has access to different transfer and receive patterns.

The focusing area can be extended in the axial direction (the direction along the ultrasound beam) by non-uniform excitation of the piezo elements, i.e. using lower amplitudes in the edge of the transducer than those in the middle. With this approach, the focusing area extends in the axial direction, but also a broadening of the ultrasound field will occur, which is unsatisfactory for lateral resolution and thus choosing the size of the focus zone always involves a compromise [146].

3.3 SLICE THICKNESS

In the above sections, the ultrasound beams were addressed in the axial and lateral directions. However, since the ultrasound imaging is based on echoes from the tissue borders (i.e. sites where acoustical impedance varies) and the echoes as well as the transferred ultrasound waves are all three dimensional (3D), the elevation direction (i.e. the direction perpendicular to the axial and lateral directions) must be considered.

The transferred 3D ultrasound beam causes echoes from targets situated close, but actually out of the intended scan plane. These redundant echoes result in the introduction of acoustical noise in the image and therefore limit the penetration of the beam and reduce contrast in the final images [146]. The slice thickness is not infinitely thin but defined by these echoes from the elevation plane; at any given plane, the slice thickness is equal to the width of the beam in the elevation direction. The width of the beam in the elevation direction is always narrowest at the focus depth [146]. The slice thickness can be improved by the use of multi-row arrays. In multi-row arrays, the piezo elements are aligned in a matrix form; the simple single row alignment is expanded for instance into a five row configuration. Similar focusing techniques as in the lateral direction can be used in the elevation direction, in order to reduce the beam width and thus the slice thickness [146].

In general, it is recommended to keep the slice thickness as narrow as possible. However, as this increases the resolution in the elevation direction, it also makes the ultrasound measurement more difficult. In small imaging targets, the small slice thickness easily causes the region of interest to move out of the imaging plane, if the imaging projection is even slightly non-optimal.

3.4 SPATIAL RESOLUTION

The wavelength of the ultrasound imaging (sound propagation velocity per frequency of the ultrasound) determines the theoretical axial resolution: the higher the sound frequency the better the axial resolution. The depth of imaging does not affect the axial resolution, as the frequency of the ultrasound is constant at all depths [146]. The pitfall of increasing the ultrasound frequency is the higher ultrasound absorption of the tissue and thus deeper tissues cannot be imaged if one utilizes higher frequencies [147].

The lateral resolution is defined by the number of scan lines and the geometry of the ultrasound transducer, or in other words, by the proportion of the width of the ultrasound field and the number of consecutive piezo elements detecting the echo [147]. In practice, the lateral resolution can be improved by focusing the ultrasound beam and increasing the bandwidth as well as the central frequency of the transmitted pulse [147]. Unlike the axial resolution, beyond the focus point the lateral resolution decreases as a function of depth as every ultrasound beam diverges at greater depth [147]. Therefore, the transducer type and the focus point being used is crucial when lateral resolution is important.

3.5 TEMPORAL RESOLUTION

In traditional ultrasound imaging, the number of transmit events equals to the number of scan lines to be formed and this results in frame rates up to 30-60 Hz [146]. However, with modern ultrasound imaging devices, multiple focused coded beams along different directions can be sent simultaneously. This process is more efficient than the traditional method and increases the frame rate (i.e. the temporal resolution) of imaging [148]. The maximum frame rate is ultimately defined by physics, as the sound propagation velocity limits how fast the data can be gathered from the medium, but in practice, the limit is set by the performance of the ultrasound device [147]. There are multiple image plane and quality adjustments that affect the frame rate and usually manufacturers have allowed the user to manipulate the settings and hence decide between image quality and frame rate.

Both the depth and the width of the image plane affect the frame rate as a larger image plane contains a larger amount of data. If the lateral and axial resolutions are kept constant, the data amount to be processed by the ultrasound device increases linearly with the image plane size and therefore the frame rate drops accordingly [146]. In 2D cardiac imaging, frame rates over

260 Hz can be achieved by narrowing the field of view and reducing line density i.e. lateral resolution [149].

Another key modulator of the frame rate is the complex use of the transducer elements. The use of multiple focuses simultaneously is an example of this kind of imaging protocol. In addition, increasing the focus depth reduces the frame rate. Harmonic imaging is another imaging protocol reducing the frame rate; in this approach, the transducer processes the harmonics of the received wave reflections. In addition, the simultaneous use of different ultrasound imaging modalities, i.e. B-mode and Doppler imaging, also reduces the frame rate, as the transducer is actually measuring the two modalities in turn.

In general, the more post-processing and the more complex use of the transducer elements that is applied, the larger the negative effect on the temporal resolution. Ultrasound imaging is always an optimization problem, balancing between the spatial and temporal resolutions.

3.6 SPECKLE

There are some problems encountered in medical imaging with ultrasound; the echo amplitudes and distributions are random from surfaces that are too rough or detailed for the ultrasound wavelength in use [146]. Due the random scatter distribution of the detailed surfaces, the final B-mode images suffer from random brightness fluctuations called 'speckles', and these can be more dominant than the acquisition noises from other sources [146, 147]. The speckles are attributable to interferences between the transduced and reflected wave: the frequency of the waves are the same but the phase difference causes alternating amplification and abatement of the signal between the transducer and the point of reflection [150]. Overall, speckles reduce the image quality and create a "pixelated" effect.

Since the speckles are artifacts and not real anatomical structures, multiple methods for speckle reduction have been developed, in general by mathematical filtering [151-154].

However, the speckles are useful for motion tracking purposes since they are not completely random artifacts but their location is based on real anatomy. Therefore, in ultrasound imaging, the motion tracking is often referred to as speckle tracking. In addition, if successful motion tracking is desired, the speckle reduction algorithms of the ultrasound device are set to a minimum.

3.7 ULTRASOUND OF COMMON CAROTID ARTERY

The common carotid artery is a superficial vessel and thus higher sound frequencies can be used for better axial resolution. Importantly, the lateral resolution of the ultrasound is crucial when studying the longitudinal motion of the carotid wall. Therefore, an appropriate depth of the focus point is important if one wishes to increase the lateral resolution, as it is the finer details within the artery wall that allow the accurate motion (speckle) tracking along the vessel wall.

The intima layer has higher acoustical impedance compared to the blood and thus great numbers of the sound waves travelling from the blood to the intima reflect back on the intima surface. This provides good contrast between the lumen of the vessel and the intima layer in the ultrasound image; the lumen does not cause wave reflection and thus appears black in the ultrasound image and the intima layer shines bright white, as illustrated in Figure 3.1. The fine details of the media layer are harder to distinguish as it tends to be shadowed by the more reflective intima layer. The media layer appears to be a thin black layer between the bright intima and adventitia layers. The adventitia consists of fibrous tissue, which causes a large amount of sound reflection. With respect to the longitudinal motion analysis of the carotid wall, the ultrasound imaging is a good modality; the three arterial layers are clearly visible, there are a significant amount of speckles on the artery layers to visualize the longitudinal motion, both the spatial and the temporal resolution of the ultrasound imaging are good, the

imaging is noninvasive and non-harmful. In addition, ultrasound imaging is fast, cheap and a widely available technique.

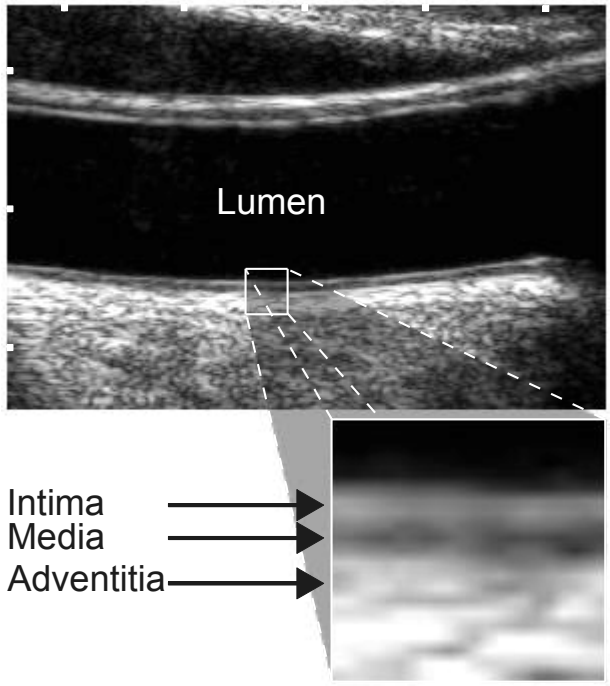

Figure 3.1: *Ultrasound image of a common carotid artery. The white ticks on top and on left border of the image are placed 5 mm apart from another.*

4 Aims

This thesis focuses on the development of methods to study the longitudinal motion of the common carotid artery wall and its relation to arterial stiffening. More specifically, the investigation of the longitudinal motion was divided into four sub-studies:

I. To propose a contrast optimized motion-tracking technique to measure the longitudinal arterial wall motion and to compute several novel, potential stiffness indices. The repeatability of the proposed method was also tested.

II. To validate the developed method by comparing the longitudinal measurements against more widely used arterial stiffness indices.

III. To devise more detailed characterization methods for the complex waveform of the longitudinal motion.

IV. To examine the kinetic energy transfer from the blood pressure to the inner wall layers and from there to the outermost wall layer.

5 Materials and Methods

5.1 METHODS TO ANALYZE LONGITUDINAL MOTION

5.1.1 Tracking method (Study I)

The speckle tracking algorithm used in the longitudinal motion analysis has been developed in Matlab (Versions 2007b and 2014b, The MathWorks Inc., Natick, MA, USA) working environment and it can be applied on B-mode DICOM ultrasound videos to track the 2D motion of the arterial wall. The algorithm is based on the use of robust 2D cross-correlation and an adaptive contrast optimization technique. To improve the tracking accuracy, the matrix size of the original video frame was interpolated to be fourfold in Studies I and II and due to increased computing power, to be ninefold in Studies III and IV. This artificially improves the resolution of the ultrasound video and creates a larger amount of pixels to be available for the 2D cross-correlation analysis.

The interpolation was made by using a bicubic algorithm, which uses 16 pieces of information to create new intermediate pixels, virtually increasing the resolution. Four of these data points are the original intensity values of the surrounding pixels ($\boldsymbol{I}(x,y)$, where x = [0,1] and y = [0,1]), four are the partial derivatives of the surrounding pixels' intensities along the x-axis ($\boldsymbol{I}_x(x,y)$, where x = [0,1] and y = [0,1]), four are the partial derivatives of the surrounding pixels' intensities along the y-axis ($\boldsymbol{I}_y(x,y)$, where x = [0,1] and y = [0,1]) and four are the cross-derivatives of the surrounding pixels' intensities ($\boldsymbol{I}_{xy}(x,y)$, where x = [0,1] and y = [0,1]). The used data points are of the form:

$$\boldsymbol{I}(x,y) = \sum_{i=0}^{3}\sum_{j=0}^{3} \boldsymbol{a}(i,j)x^i y^j \qquad (5.1)$$

$$\boldsymbol{I_x}(x,y) = \sum_{i=0}^{3}\sum_{j=0}^{3} \boldsymbol{a}(i,j) i x^{i-1} y^{j} \tag{5.2}$$

$$\boldsymbol{I_y}(x,y) = \sum_{i=0}^{3}\sum_{j=0}^{3} \boldsymbol{a}(i,j) x^{i} j y^{j-1} \tag{5.3}$$

$$\boldsymbol{I_{xy}}(x,y) = \sum_{i=0}^{3}\sum_{j=0}^{3} \boldsymbol{a}(i,j) i x^{i-i} j y^{j-1} \tag{5.4}$$

where x and y are the coordinates of the surrounding pixels (i.e. [0,1]) and $\boldsymbol{a(i,j)}$ is a matrix of size 4 × 4, containing unknown weighting factors. The known sixteen data points are used to determine the unknown weighting factors used in creating the interpolated image. In other words, we have 16 unknowns and 16 linear equations and thus the weighting factors can be calculated.

Once the weighting factors have been defined, the intensity values of the interpolated image's pixels can be calculated using the same Formulas 5.1 – 5.4. However, in this scenario, the matrix $\boldsymbol{a}$ is known and the matrixes $\boldsymbol{I}$, $\boldsymbol{I_x}$, $\boldsymbol{I_y}$ and $\boldsymbol{I_{xy}}$ are unknown.

From the interpolated images, the motion tracking was made with 2D cross-correlation. In 2D cross-correlation, a group of selected pixel values from the image (a region of interest, ROI) is compared to the pixel values of the next video frame. The tracking target is assumed to move as a whole to where the best matching pixel values are found in the subsequent video frame. After the inter-frame motion estimation, the ROI data is updated to the current content of the ROI area and the updated ROI data is used for the motion estimation of the next frame. The procedure is automatically continued throughout a cardiac cycle, then checked and approved by the user. Consecutive heartbeat-long motion traces are parsed together with linear detrending.

In order to save computing time, the 2D cross-correlation and the interpolation are only computed for a subset of the next video frame (template). The preselected subset requires assumptions of the velocity of the motion of the selected target. In the case of the arterial wall motion, the small amplitude and

relatively slow radial and longitudinal motions of the wall makes it possible to use a rather small image subset for the motion-tracking.

In the 2D cross-correlation, the un-normalized correlation matrix is defined as follows:

$$\boldsymbol{C}(x,y) = \sum_{m=0}^{M-1} \sum_{n=0}^{N-1} \boldsymbol{I}(m,n)\boldsymbol{R}^{*}(m-x, n-y) \tag{5.5}$$

where $\boldsymbol{R}$ is P × Q ROI matrix, $\boldsymbol{I}$ is M × N image matrix, $\boldsymbol{C}$ is M+P-1 × N+Q-1 correlation matrix and the asterisk denotes complex conjugate. The coordinates of the maxima within the correlation matrix reveals where the ROI should be positioned on the image in order to achieve the highest correlation between the two.

In order to improve the motion-tracking accuracy and to reduce noise from the image, an adaptive contrast optimization technique was applied. In the contrast optimization algorithm, the intensity values of the whole ultrasound video frame i+1 are changed based on the intensity values in ROI i, where i indicates

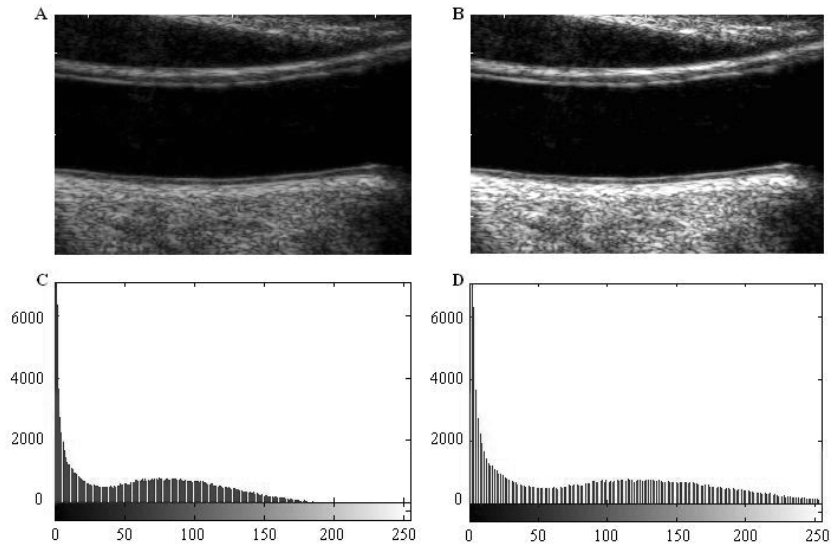

Figure 5.1: *Example of the contrast optimization technique. A, an ultrasound image of common carotid artery; B, a contrast optimized ultrasound image; C, 8-bit histogram of the original image; D, 8-bit histogram of the optimized image.*

the current frame. This is achieved by obtaining the minimum and maximum intensity values inside the ROI i and by stretching the histograms of the ROI i and image i+1 accordingly. In addition, the optimization algorithm cuts out 1% of the lowest and highest intensity values so that single bright (or dark) pixels should not affect the contrast optimization. This procedure intentionally over- and under-exposes the surrounding areas of the ROI since most of the time, the intensity values in the full video frame are in the wider spectrum rather than inside the ROI. See Figure 5.1 for an illustration of the technique.

5.1.2 Indices of longitudinal motion (Studies I and II)

The developed motion-tracking software automatically computes multiple indices describing the longitudinal motion of the artery wall. There are indices describing the peak-to-peak (ampl), antegrade (ante) and retrograde (retro) amplitude of the longitudinal motion, see Figure 5.2. In addition, there is an index reflecting the main direction of the longitudinal motion i.e. the average deviation (dev) of the longitudinal motion during a heartbeat, see Figure 5.2. Additionally, there are rate of change indices describing the maximum velocity (V) and acceleration (A) occurring in the longitudinal motion graphs, see Figure 5.3. The rate of change indices contain the magnitude and the direction information of the changes: a negative sign indicates a change in motion, which has been directed against the blood flow (retrograde direction), and positive sign indicates a change in motion in the opposite direction (antegrade direction). In addition, there are the absolute values of the same indices. All these indices are computed separately for the longitudinal motion of the intima-media complex (IO), the longitudinal motion of the adventitia layer (AO) and the longitudinal motion between the intima-media complex and adventitia layer (IA), respectively.

Two indices were created to utilize every time point of the heartbeat-long longitudinal motion graphs to describe the complexity of the longitudinal motion. The first one is called

RAlength, which is the length of the curve that plotting the diameter change graph against the longitudinal motion graph forms, see Figure 5.2. The figure represents the dyssynchrony and hysteresis between the diameter change curve and the longitudinal motion of the carotid wall [110] and thus the amplitude of the motion in both directions has an effect on the value of the RAlength. The second index Polydeg describes the complexity of the longitudinal motion waveform; the higher the value of Polydeg, the more complex is the motion waveform. Polydeg is the degree of the polynomial function needed to fit the function to the measured data points of the longitudinal motion of the intima-media complex. The criterion for acceptable fit was set to $r > 0.95$, where r is Pearson's correlation coefficient.

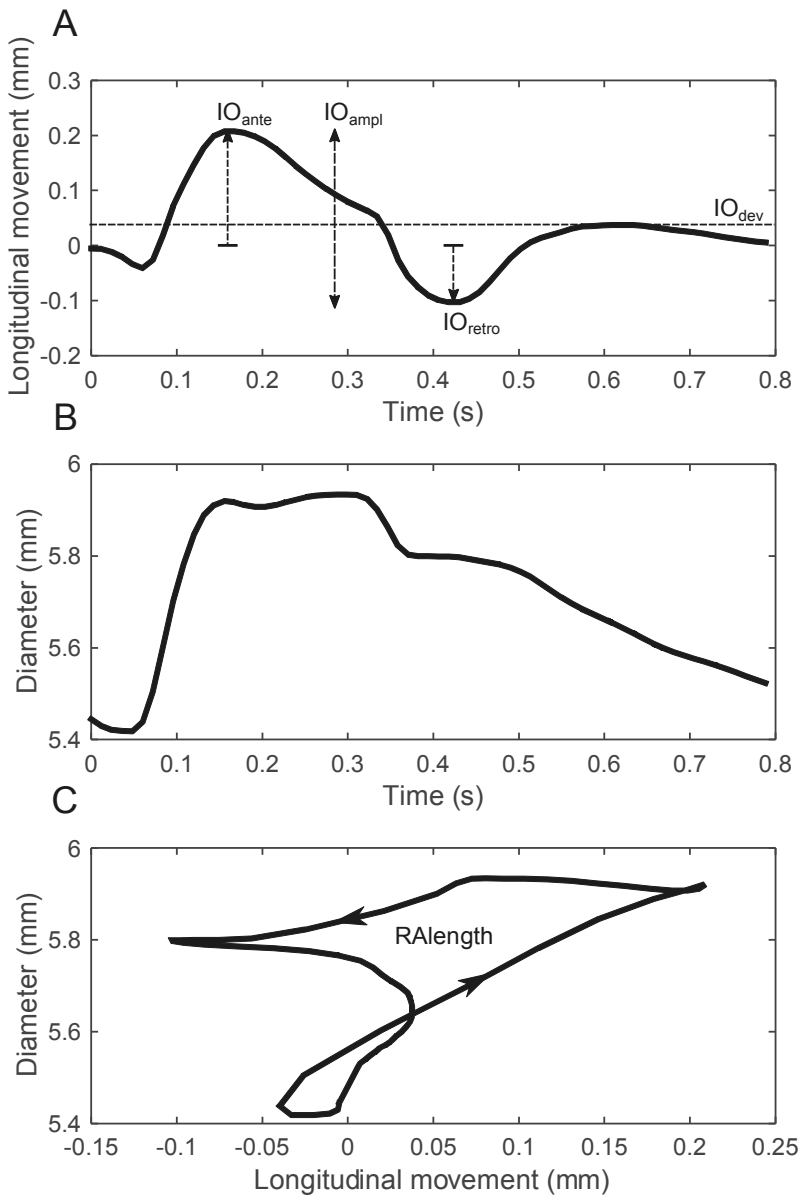

Figure 5.2: *Illustration of the indices derived from the carotid longitudinal movement of the intima-media complex. A, longitudinal movement during a heartbeat; B, diameter during a heartbeat; C, diameter curve plotted against longitudinal movement curve.* IO_{ante}*, amplitude towards antegrade direction;* IO_{retro}*, amplitude towards retrograde direction;* IO_{ampl}*, peak-to-peak amplitude;* IO_{dev}*, average; deviation from the initial position; RAlength, the length of the hysteresis curve.*

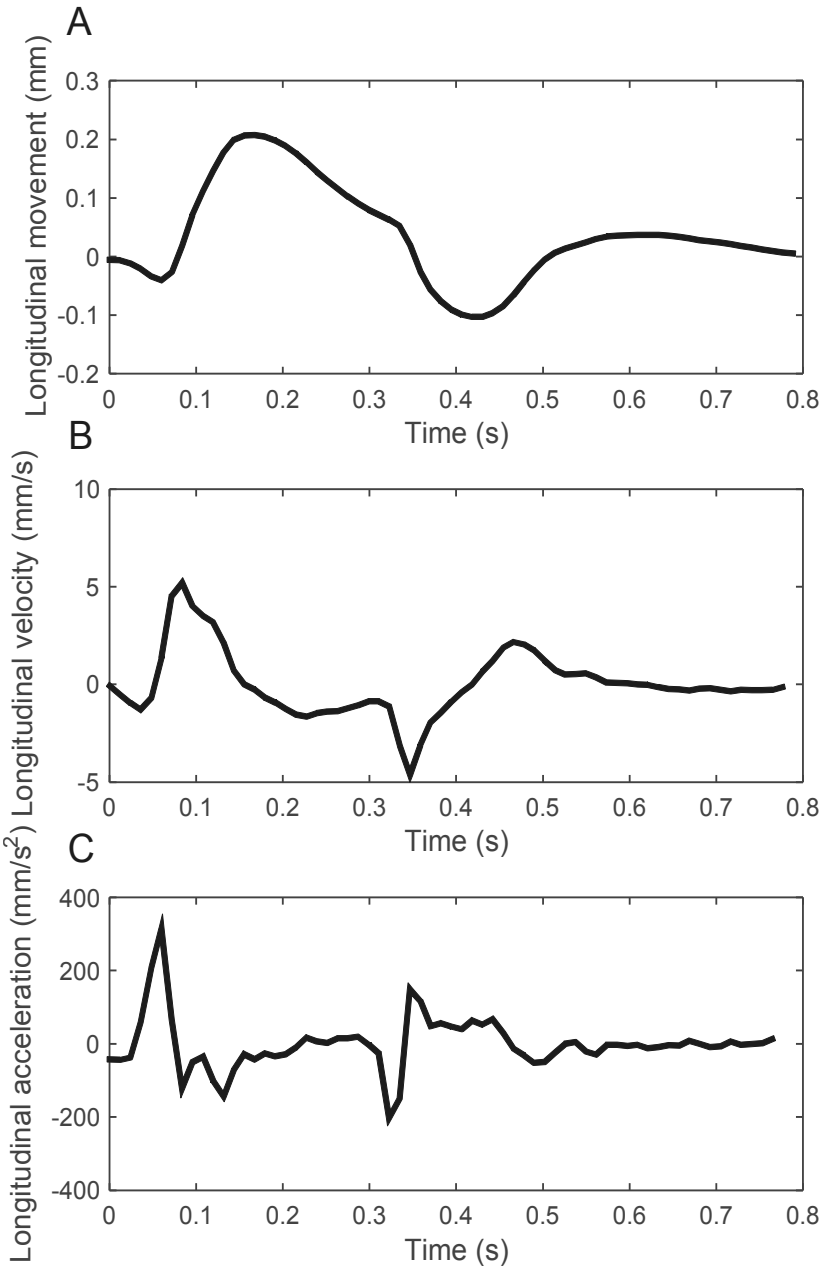

Figure 5.3: *Rate of change of the carotid longitudinal movement of the intima-media complex. A, longitudinal movement of the artery; B, velocity of the longitudinal movement; C, acceleration of the longitudinal*

5.1.3 Waveform analysis (Study III)

The principal component analysis (PCA) is a widely used method for compressing information and for making predictive models in large correlated data sets. The analysis works by creating a new set of linearly uncorrelated indices called principal components (PCs). The PCs are obtained by orthogonal transformation of the data, i.e. by projecting the data in a new coordinate system defined by eigenvectors and eigenvalues of a data correlation matrix. The first PC is defined to contain most of the variance present in the original data.

If one assumes that matrix $\boldsymbol{X}$ is size M × N and contains M observations i.e. time points of the motion traces from N subjects, then the PCA can be made in the following steps. First, the size M × M correlation matrix $\boldsymbol{R}$ is formed as:

$$\boldsymbol{R} = \frac{1}{M}\boldsymbol{X}\boldsymbol{X}^T \tag{5.6}$$

where T designates the matrix transposition. Eigen decomposition is used to solve the eigenvalues and their corresponding eigenvectors of the correlation matrix. Eigenvalues are the roots of the characteristic polynomial p:

$$p(\lambda) = \det(\boldsymbol{R} - \lambda\boldsymbol{I}) \tag{5.7}$$

where λ is the eigenvalue, $\boldsymbol{I}$ is M × M identity matrix and det designates determinant. Eigenvectors can be calculated by solving the linear equation:

$$(\boldsymbol{R} - \lambda_v\boldsymbol{I})\boldsymbol{H} = 0 \tag{5.8}$$

where $\boldsymbol{H}$ is eigenspace, a matrix containing the eigenvectors: $\boldsymbol{H} = [v_1, v_2, \ldots, v_M] \in \mathbb{R}^{M \times M}$ and λ_v is a vector containing all the eigenvalues. Finally, the PC values can be calculated by sorting the eigenvalues and the corresponding eigenvectors in the eigenspace in descending order, thus the eigenvector explaining most of the variance of the original data is on top, and by multiplying the eigenspace with the data matrix $\boldsymbol{X}$:

$$\boldsymbol{PC} = \boldsymbol{H}^T\boldsymbol{X} \tag{5.9}$$

where $\boldsymbol{PC}$ is a matrix containing M pieces of principal components (rows) for N subjects (columns).

The eigenvectors are orthogonal and thus independent from each other's. The eigenvector corresponding to the largest eigenvalue and its equivalent PC values represent the most of the variance within the large data set, i.e. highlight the main features of the data. The sum of the eigenvalues is one and the proportion of the data variance represented by a certain eigenvector and its corresponding PC values can be calculated by dividing the corresponding eigenvalue by the sum of all the eigenvalues.

5.1.4 Transfer function analysis (Study IV)

The Fourier transform is a continuous function used widely in signal processing for different frequency analysis applications. The Fourier theorem states that any given periodic signal can be expressed as a linear combination of sine waves and that the Fourier transform can identify the amplitude and the phase of the sine waves. The continuous Fourier transform is defined as:

$$\mathcal{F}\{f(x)\} = \int_{-\infty}^{\infty} f(x)e^{-i\omega x}dx \tag{5.10}$$

where ω is an angular frequency ($\omega = 2\pi f$, where f is frequency in Hz). When observing a specific angular frequency ω, the corresponding amplitude of the function $f(x)$ is

$$A(\omega) = |\mathcal{F}\{f(x)\}| \tag{5.11}$$

and the corresponding phase is

$$\phi(\omega) = \arg(\mathcal{F}\{f(x)\}) \tag{5.12}$$

where arg is a function operating on complex numbers, giving the angle between the positive real axis and the line from origin to the complex value.

In signal analysis where signals are commonly discrete, a discrete version of the Fourier transform is used:

$$F[n] = \sum_{k=0}^{N-1} f[k] e^{-i\frac{2\pi}{N}nk} \tag{5.13}$$

The corresponding inverse transforms for the continuous and discrete signals are, respectively:

$$f(x) = \frac{1}{2\pi} \int_{-\infty}^{\infty} \mathcal{F}\{f(x)\} e^{i\omega x} d\omega \tag{5.14}$$

and

$$f[k] = \frac{1}{N} \sum_{n=0}^{N-1} F[n] e^{i\frac{2\pi}{N}nk} \tag{5.15}$$

To form an accurate power spectrum from a discrete signal, the original signal must be prepared properly. First, the linear trend of the signal is removed and the signal is zero averaged because without zero averaging an additional, artificial power disturbs the lower frequencies of the signal spectrum. After the trend removal and the zero averaging the signal must be windowed to force the signal to be periodic (i.e. constraining the start and the end of the signal to zero). Windowing is always applied because using no window function is the same as using a rectangular window. Despite its good frequency resolution, the rectangular window is often avoided since it causes spectral leakage.

In this thesis, the Hanning window was used due to its widespread popularity in signal processing. For example, the Hanning window is one of the recommended windows in the

popular Welch's method of estimating the transfer function between two signals [155]. The Hanning window is defined as:

$$w(n) = 0.5 - 0.5\cos\left(\frac{2\pi n}{L-1}\right) \tag{5.16}$$

where L is the number of data points within the discrete signal.

When the discrete signal has been windowed, a Fourier transform is applied, transforming the time domain signal into a frequency domain. For the use of a transfer function analysis, power spectrums are computed separately to the input and output signals. In addition, a cross-power spectrum is needed:

$$P_{XX}(f) = \frac{X(f)X^*(f)}{LF_sU}, \tag{5.17}$$

$$P_{YY}(f) = \frac{Y(f)Y^*(f)}{LF_sU}, \tag{5.18}$$

$$P_{XY}(f) = \frac{X(f)Y^*(f)}{LF_sU} \tag{5.19}$$

where P_{XX} is the power spectrum of the input signal, P_{YY} is the power spectrum of the output signal and P_{XY} is the cross-power spectrum. X is the Fourier transform of the windowed input signal as Y is the Fourier transform of the windowed output signal. The asterisk designates a complex conjugate (i.e. a sign change of the imaginary part of the complex number). L is the length of the time series signal, F_s is the sampling frequency and U is the power of the used window function. The power of the window function can be computed as:

$$U = \frac{1}{L}\sum_{n=1}^{L} w(n)^2 \tag{5.20}$$

Compensation for the power of the used window function is needed to scale the spectrum values thus the total power equals

the variance of the original signal in the time domain. The power of the Hanning window is 0.375.

The time invariant transfer function is defined as a quotient of the cross spectrum of the input and output signals (P_{XY}) and the power spectrum of the input signal (P_{XX}):

$$TF(f) = \frac{P_{XY}(f)}{P_{XX}(f)} \tag{5.21}$$

This gives the transfer function in a complex frequency space. By using Formulas 5.11 and 5.12, the complex values can be transformed into the amplitude and phase values. Commonly a Bode plot is used to describe the transfer functions. In the Bode plot, the amplitude part and the phase part are displayed in separate graphs and the amplitude is presented in decibels (dB) and the phase in degrees. The transformation from the absolute values to the decibel values can be made with the following formula:

$$TF(dB) = 10 \log_{10} TF(f) \tag{5.22}$$

A coherence function is used to find the linear relationship between the input and the output signals of the transfer function analysis. The magnitude-squared coherence between input and output signals can be computed as:

$$C_{XY}(f) = \frac{|P_{XY}(f)|^2}{P_{XX}(f)P_{YY}(f)} \tag{5.23}$$

The values of coherence function C_{XY} are always between 0 and 1 with one referring to a direct, linear relationship between the input and the output signals and 0 representing zero linearity between the input and the output. Even though the coherence of the input and the output signals is zero, there still might be a nonlinear relationship between the two signals. Nevertheless, if the coherence between the signals is zero, the corresponding transfer function is useless, since it only represents the linear relationship between the input and the output.

5.1.5 Estimation of carotid blood pressure (Studies II – IV)

The carotid blood pressure level differs from the brachial blood pressure level and the waveform resembles more the aortic waveform than brachial waveform [156]. Therefore, it is better to use carotid blood pressures rather than brachial pressures when observing the effect of blood pressure on carotid artery wall. Applanation tonometry can be used to estimate noninvasively the systolic and diastolic carotid blood pressure levels: the estimation requires an applanation tonometry measurement on the carotid artery to acquire the carotid pressure waveform and a reference blood pressure measurement from brachial artery [79]. The brachial blood pressures can be changed into carotid blood pressures by a build-in transfer function of the applanation tonometer [79].

Furthermore, the computed carotid systolic and diastolic blood pressure levels can be used for continuous estimation of the carotid blood pressure waveform. For this purpose, the diameter change of the common carotid artery is traced with ultrasound and linearly transformed into a blood pressure signal by changing the average systolic diameter into the carotid systolic pressure and the average diastolic diameter into the carotid diastolic pressure. The linear relationship between the blood pressure and the diameter change in the common carotid artery has been validated previously [32, 157-159].

5.2 EXPERIMENTS TO VALIDATE THE ANALYSIS

5.2.1 Study populations

This thesis consist data from two different experimental setups using different study populations. See Table 5.1 for a description of the study populations. All subjects were healthy, non-smoking volunteers and recruited from the Kuopio area in Finland. One subject was omitted from the studies because of the finding of a left bundle branch block. None of the remaining participants had any history of heart or cardiovascular diseases.

The first setup (Studies I and II) was intended for developing the motion-tracking algorithm to observe the longitudinal motion of the carotid wall and for validating the method against known arterial stiffness measurements. The second setup (Studies III and IV) was for characterizing the waveform of the longitudinal motion and for studying the linear relationship between the longitudinal motion of the intima-media complex and the adventitia layer using transfer function analysis.

The age variation in the first study population was intentionally large to test the operation of the algorithm in multiple age groups and to ensure that there was stiffness variation for the side-by-side comparison with previously known stiffness indices.

Table 5.1: *Description of the study population included in Studies I-IV.*

	Study I & II	**Study III & IV**
Number of subjects (after exclusions)	19	20 (19)
Gender (females/males)	11/8	10/9
Age range (years)	24-73	19-49

5.2.2 Data acquisition

In both studies, the data acquisition was conducted in a similar manner. The volunteers were instructed not to drink coffee 2h before the measurements and the measurement itself was standardized. First, the height and weight of the volunteer were asked. Then, the volunteer was placed in the supine position and three ECG-electrodes were attached to the volunteer's chest representing V5 lead and the cuff of an automatic blood pressure monitor (Omron, M4-I, Matsusaka, Kyoto, Japan) was placed on the left upper arm. The ECG was measured continuously throughout the measurement protocol. After a minimum of 10 minutes rest, the diastolic and systolic blood pressures were measured from the left brachial artery. The ultrasound imaging of the left common carotid artery was performed immediately after the blood pressure measurement.

After the ultrasound acquisition the blood pressure values were measured again and an average of the two blood pressure measurements was calculated. The scheme of the measurements is presented in Figure 5.4.

The 5-seconds ultrasound imaging for Studies I and II was obtained with a clinical ultrasound device (Acuson Sequoia 512, Siemens, Mountain View, CA, USA) equipped with 14 MHz linear transducer (Acuson 15L8-S, Siemens, Mountain View, CA, USA). The 5-minute imaging for Studies III and IV was acquired with a Philips EPIQ 7 clinical ultrasound device, equipped with an 18 MHz linear transducer (Philips, L18-5, Best, The Netherlands). A longitudinal view of the left common carotid artery was acquired, approximately 1 cm to caudal direction from the carotid bifurcation. The imaging parameters are presented in Table 5.2. Due to the restrictions of the Philips EPIQ 7 ultrasound imaging device, the 5–minute imaging for Studies III and IV was done in 30 separate 10-second-long parts, which were collected consecutively. The typical delay between the clips was under half a second. The long acquisition was intended to allow the completion of the transfer function analysis.

Applanation tonometery measurement (SphygmoCor version 9; AtCor Medical Inc., Itasca, IL, USA) was utilized at the end of the protocol, using a pen-like pressure probe (SPT-301B; Millar Instruments, Houston, TX, USA). The pulse wave analysis was performed on both radial and carotid arteries.

With the first study population, all the above-mentioned measurements were repeated on the subsequent day. The repetition was made in order to test the repeatability and the reproducibility of the measurements, by analyzing the same video twice and by analyzing videos collected on subsequent days, respectively.

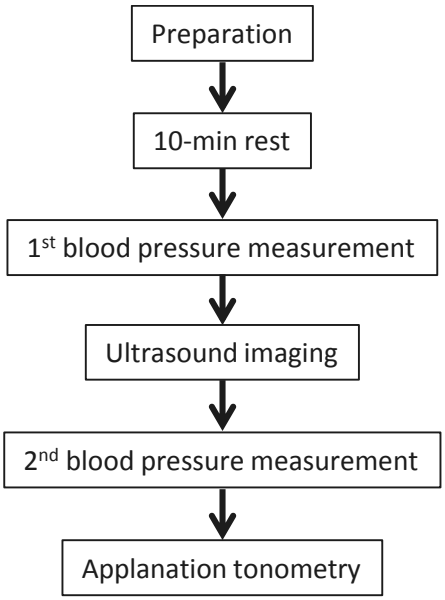

Figure 5.4: *Representation of the study protocol being used. The preparation phase includes the attachment of the ECG electrodes on the chest of the volunteer and the installment of the cuff of the blood pressure meter on the left upper arm of the volunteer.*

Table 5.2: *Used ultrasound devices and imaging parameters in Studies I-IV.*

	Study I & II	**Study III & IV**
Ultrasound device	Acuson Sequoia 512	Philips EPIQ 7
Ultrasound transducer	Acuson 15L8-S	Philips L18-5
Length of ultrasound video	5 s	30 × 10 s
Image acquisition rate	25 Hz	85 Hz
Repeated measurement on the following day	Yes	No

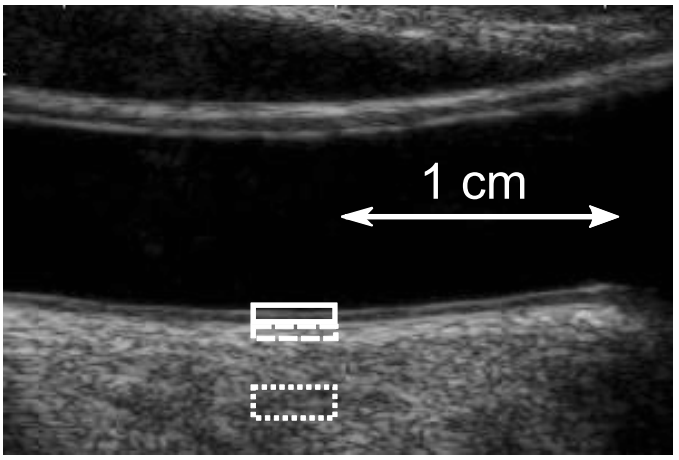

Figure 5.5: *Ultrasound image of the common carotid artery. The typical locations of the regions of interest (ROI) used in the longitudinal motion-tracking are 1 cm before carotid bifurcation. Solid line, intima-media ROI; dashed line, adventitia ROI; dotted line, surrounding tissue ROI.*

5.2.3 Data processing and analysis

The collected ultrasound videos were analyzed offline by the developed motion tracking method. The motion tracking of the longitudinal motion was performed separately on the intima-media complex, on the adventitia layer and on the surrounding tissues, which was used as a reference point for the longitudinal motion. The typical ROI locations are displayed in Figure 5.5. The average ROI sizes were (width × height) 2.76 × 0.50 mm^2 (intima-media complex), 3.02 × 0.46 mm^2 (adventitia layer) and 4.85 × 1.56 mm^2 (surrounding tissues) in Studies I and II as well as 2.58 × 0.33 mm^2, 2.58 × 0.30 mm^2 and 2.58 × 1.15 mm^2, respectively, in Studies III and IV. In order to reduce artefacts caused by the movement of the ultrasound transducer, the motion of the surrounding tissues was subtracted from the longitudinal traces of the intima-media complex and the adventitia layer. In addition, the longitudinal motion between the intima-media and the adventitia was computed.

The ECG-signal was measured simultaneously with the ultrasound imaging and the R-peaks of the ECG were automatically recognized using Matlab code. The information

from the R-peaks was used to chop the ultrasound video into heartbeat-long sequences on which the motion tracking was performed. In Studies I-III, the heartbeat-long motion traces were used to form an average heartbeat-long motion traces for every individual. In Study IV, the heartbeat-long motion traces were edited together to form continuous motion traces for the transfer function analysis. The longitudinal stiffness indices, presented in Section 5.1.2, were computed from the heartbeat-long average graphs.

For the validation of the created stiffness indices, reference stiffness indices were used. DC, CC, E_Y and Z were computed from the diameter curve, which was estimated using the same motion tracking method alongside the longitudinal motion. In addition, from the results of applanation tonometry, AA, Aix, Aix@75 and PWV could be defined. The carotid blood pressure values needed in the stiffness index calculations were estimated from the applanation tonometry.

The waveform characterization was made with the PCA. The PC values were computed for every time point of every recorded motion curve: the diameter change curve, the longitudinal motion of the intima-media complex, the longitudinal motion of the adventitia layer and the longitudinal motion between the intima-media complex and the adventitia layer. Only the two first minutes of the gathered 5-minute-long data were used for the PCA. More specifically, the 2-minute-long data was cut in half and both minute-long ultrasound videos were used to form robust heartbeat-long averaged longitudinal wall motion traces. The average longitudinal motion graph of the intima-media complex and the adventitia layer, defined from the first minute of the video, was used as a primary data in the study and the second minute was only used in the repeatability analysis.

The whole 5-minute-long ultrasound videos were used in the transfer function analysis. The transfer function analysis was used to characterize how the energy from the blood pressure becomes transformed into the longitudinal wall motion of the common carotid artery, by estimating the carotid blood pressure

as presented in Section 5.1.5 and by the use of the presented transfer function analysis. In addition, the linear relationship between the longitudinal motion of the intima-media complex and adventitia layer was described using the transfer function analysis. To estimate the impact of the main direction of the longitudinal motion on the transfer function, additional quartile transfer functions between the carotid blood pressure and the longitudinal motion of the common carotid artery wall were computed. In this analysis, the study population was divided into quartiles according to the main direction of the longitudinal motion. The motion direction was evaluated from the measured IO_{dev} value. The upper and lower quartiles of the study population were used to form two separate quartile transfer functions: one representing the population with antegrade oriented longitudinal waveform and the other representing the population with the retrograde oriented longitudinal waveform.

In addition, for the transfer function analysis, a specific heartbeat band was defined in order to have a single subject specific amplitude and a phase value from the transfer functions. These values were used in a correlation analysis to study the connections between the amplitude and phase parts of the transfer functions with the arterial stiffness indices. The heartbeat band was 0.5 Hz wide and centered on the peak of the power spectrum of the measured subject specific blood pressure data. The width of the band was selected based on the average heart rates within the study population; the bandwidth 0.5 Hz, centered on each subject's peak on the power spectrum and it covered the frequencies where other subjects' peaks were in their power spectrums. When computing the average amplitude and phase values within the 0.5 Hz wide heartbeat band, the amplitude and phase values were neglected from those frequencies where the coherence of the transfer function was below 0.5.

5.2.4 Statistical analysis

Due to skewed distributions of some of the measured indices, a Spearman's rank correlation coefficient was used. Using a rank

correlation coefficient also confers the benefit that a linear relationship between two indices does not need to be expected. The relationship between the two correlates can be for example sigmoidal but the Spearman's rank correlation coefficient can still detect the conformity between the two correlates.

For studying the repeatability of the measured indices, a Pearson's correlation coefficient, a Cronbach's alpha and a coefficient of variation of repeated measurements (CV) were utilized. Here, Pearson's correlation coefficient was used instead of Spearman's rank correlation coefficient since a linear relationship must be assumed between two repeated measurements of the same index. The coefficient of variation of repeated measurements is defined as:

$$\mathrm{CV}(\%) = 100\frac{\mathrm{SD}}{\mathrm{Mean}} \tag{5.24}$$

where SD is the standard deviation between the repeated measurements and Mean is the average of the repeated measurements. The Cronbach's alpha is defined as:

$$\alpha = \frac{L}{L-1}\left(1 - \frac{\sum_{i=1}^{L}\sigma_{Yi}^2}{\sigma_X^2}\right) \tag{5.25}$$

where L is the number of measurements that are repeated, σ_{Yi}^2 is the variance of the i:th measurement for the current sample and σ_X^2 is the variance of all measurements. In general, Cronbach's alpha values over 0.8 are considered suitable for individual diagnostics [160].

The risk level was chosen thus a p-value lower than 0.05 was considered as statistically significant. The p-value 0.05 means that there is only a 5 % probability to obtain the same result by change.

5.3 ETHICAL CONSIDERATIONS

All the studies in this thesis were non-invasive and pain free. The studies were conducted according to the Declaration of Helsinki (1969, latest revision in 2013) and approved by the Ethics Committee of the Kuopio University Hospital. A written informed consent was obtained from all the subjects.

6 Results

6.1 REPEATABILITY OF THE MEASUREMENTS

The in-house-build algorithm for tracking the longitudinal motion of the common carotid artery was tested with 19 healthy volunteers. Fourteen indices describing the longitudinal motion amplitude and twelve additional indices describing the rate of change of the longitudinal motion were devised in this thesis. The median and interquartile range (IQR) values of the study population is displayed in Tables 6.1 and 6.2.

Table 6.1: *Median, interquartile range (IQR), repeatability and reproducibility values of the longitudinal motion indices of the common carotid artery. Repeatability is defined by measuring the indices twice from the same ultrasound video and reproducibility is defined by measuring the indices from two different ultrasound videos, imaged on subsequent days. Pearson's correlation coefficients (r) which did not achieve $p < 0.05$ are left out. CV is coefficient of variation and a is Cronbach's alpha.*

Longitudinal			**Reproducibility**			**Repeatability**		
index	**Median**	**IQR**	**CV**	**α**	**r**	**CV**	**α**	**r**
IA_{ante} (mm)	0.06	0.14	72.3	0.57		46	0.86	0.76
IO_{ante} (mm)	0.06	0.28	36.1	0.93	0.86	28.5	0.96	0.92
AO_{ante} (mm)	0.07	0.14	71.1	0.67	0.58	20.2	0.97	0.95
IA_{retro} (mm)	0.23	0.30	46.1	0.78	0.65	32.3	0.92	0.85
IO_{retro} (mm)	0.30	0.37	28.6	0.90	0.82	21	0.95	0.90
AO_{retro} (mm)	0.08	0.14	65.2	0.49		36	0.85	0.76
IA_{ampl} (mm)	0.29	0.21	29.8	0.73	0.58	19	0.89	0.81
IO_{ampl} (mm)	0.43	0.23	16.3	0.80	0.67	13.8	0.88	0.78
AO_{ampl} (mm)	0.22	0.06	48.5	-0.48		22.4	0.71	0.57
IA_{dev} (mm)	-0.05	0.13	97.1	0.81	0.69	97.2	0.91	0.84
IO_{dev} (mm)	-0.04	0.13	92.3	0.81	0.69	117.5	0.79	0.65
AO_{dev} (mm)	-0.04	0.13	115.4	0.75	0.60	100.8	0.90	0.82
Polydeg	7.00	2.00	25.1	0.62		13.8	0.94	0.90
RAlength (mm)	1.48	0.59	9.80	0.94	0.89	7.4	0.97	0.94

The repeatability results of these indices are displayed also in Tables 6.1 and 6.2. The repeatability of the amplitude indices was good overall; 12 out of 14 indices exceeded the Cronbach's alpha value 0.8 and none was under 0.7, evidence that the developed motion-tracking algorithm was working properly, even when using a low imaging frequency of 25 frames per second. The repeatability of the rate of change parameters was also good, as 9 out of 12 indices exceeded the Cronbach's alpha value of 0.8 and only V_{IA} and A_{IA} had poorer repeatability. The reproducibility from the two separately imaged videos was adequate, as Cronbach's alpha varied between 0.57 – 0.95, revealing that the longitudinal motion preserves its waveform from day to day. The reproducibility of indices IO_{ante}, IO_{retro}, IO_{ampl}, IA_{dev}, IO_{dev} and RAlength exceeded the Cronbach's alpha value of 0.8, indicating that they would be suitable for individual diagnostics. In contrast, IA_{ante}, AO_{retro}, AO_{ampl} and Polydeg displayed poor reproducibility.

Table 6.2: *Median, interquartile range (IQR) and repeatability values of the rate of change indices of the longitudinal carotid wall motion. CV is coefficient of variation, a is Cronbach's alpha and r is Pearson's correlation coefficient.*

Longitudinal			**Repeatability**		
index	**Median**	**IQR**	**CV**	**α**	**r**
V_{IA} (mm/s)	-1.44	3.83	-234	0.57	0.41
V_{IO} (mm/s)	-2.09	7.94	128	0.99	0.98
V_{AO} (mm/s)	-1.01	3.92	217	0.94	0.88
A_{IA} (mm/s^2)	-41.66	108.19	-213	0.57	0.41
A_{IO} (mm/s^2)	-28.94	182.49	114	0.98	0.96
A_{AO} (mm/s^2)	-19.48	118.62	180	0.93	0.88
$\lvert V_{IA} \rvert$ (mm/s)	1.75	1.14	22.0	0.80	0.67
$\lvert V_{IO} \rvert$ (mm/s)	3.15	2.39	15.4	0.92	0.86
$\lvert V_{AO} \rvert$ (mm/s)	1.93	1.52	19.1	0.91	0.84
$\lvert A_{IA} \rvert$ (mm/s^2)	54.93	39.20	29.5	0.77	0.63
$\lvert A_{IO} \rvert$ (mm/s^2)	84.37	77.14	23.2	0.89	0.85
$\lvert A_{AO} \rvert$ (mm/s^2)	61.74	32.47	25.8	0.84	0.73

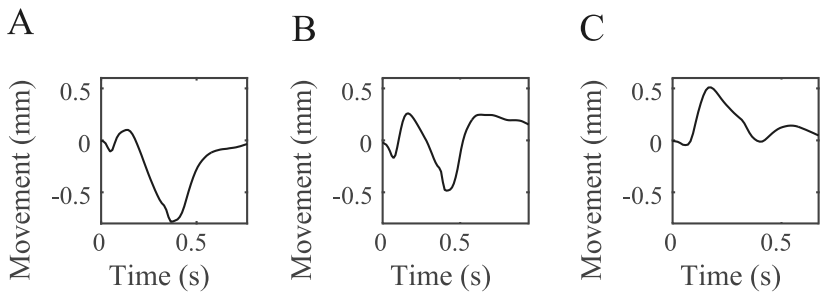

Figure 6.1: *Three different, representative longitudinal motion waveforms of intima-media complex. A, retrograde oriented waveform; B, bidirectional waveform; C, antegrade oriented waveform.*

Three different longitudinal motion patterns occurring in the common carotid artery were found: 1) an antegrade oriented longitudinal motion, 2) a retrograde oriented longitudinal motion and 3) a bidirectional longitudinal motion where the longitudinal motion occurred first in the antegrade direction and was immediately followed by a retrograde motion. Examples of the motion patterns are presented in Figure 6.1.

6.2 VALIDATION OF STIFFNESS INDICES

The proposed new arterial stiffness indices, derived from the longitudinal motion curves, were validated against widely known arterial stiffness indices. The known stiffness index values and their variation within the study population as well as the results of the correlation analysis are presented in Tables 6.3 and 6.4. The peak-to-peak amplitude indices of the longitudinal carotid wall motion displayed a weak, not statistically significant correlation to known arterial stiffness indices, but the antegrade component of the longitudinal motion between the intima-media complex and the adventitia layer was directly related to the weight ($r = 0.56$, $p < 0.05$) and the height ($r = 0.60$, $p < 0.01$) of the subject as well as to the measured systolic ($r = 0.48$, $p < 0.05$) and pulse pressure ($r = 0.49$, $p < 0.05$). From the rate of change indices, the $|A_{IA}|$ was inversely related to AA ($r = -0.49$, $p < 0.05$), Aix ($r = -0.54$, $p < 0.05$) and Aix@75 ($r = -0.52$, $p <$

0.05). A_{AO} was inversely related to age (r = -0.54, p < 0.05) and directly to CC (r = 0.47, p < 0.05). RAlength and Polydeg displayed clear inverse correlations to AA (r = -0.65, p < 0.01 and r = -0.46, p < 0.05, respectively) and to Aix@75 (r = -0.60, p < 0.01 and r = -0.53, p < 0.05, respectively).

Table 6.3: *Median and interquartile range (IQR) values of the clinical characteristics and the Spearman's correlations between the longitudinal motion indices and the clinical characteristics.*

	SBP (mmHg)	**DBP (mmHg)**	**PP (mmHg)**	**Age (years)**	**Weight (kg)**	**Height (cm)**
Median	119	76	46	38	65	173
IQR	21	11	14	22	16	17
IA_{ante}	**0.48***	0.29	**0.49***	-0.35	**0.56***	**0.60†**
IO_{ante}	0.35	0.23	0.44	-0.35	0.40	0.43
AO_{ante}	0.11	-0.03	0.34	-0.33	0.40	0.30
IA_{retro}	-0.40	-0.29	**-0.48***	0.04	-0.32	-0.23
IO_{retro}	-0.27	-0.21	-0.37	0.12	-0.26	-0.15
AO_{retro}	-0.01	0.06	-0.16	0.21	-0.29	-0.23
IA_{ampl}	-0.14	-0.12	-0.21	-0.11	0.00	0.13
IO_{ampl}	-0.05	-0.03	-0.08	-0.10	0.07	0.26
AO_{ampl}	0.40	0.29	**0.47***	-0.16	0.23	0.26
V_{IA}	-0.01	0.19	-0.00	-0.16	-0.06	0.05
V_{IO}	0.23	0.07	**0.46***	**-0.51***	0.37	0.38
V_{AO}	0.10	0.17	0.24	-0.45	0.15	0.32
A_{IA}	-0.21	0.04	-0.15	-0.23	-0.21	0.03
A_{IO}	0.06	0.01	0.23	**-0.57***	0.28	0.41
A_{AO}	0.03	0.06	0.19	**-0.54***	0.04	0.23
$\lvert V_{IA} \rvert$	-0.19	**-0.52***	0.14	-0.09	**0.58†**	0.42
$\lvert V_{IO} \rvert$	0.03	-0.05	0.15	-0.26	0.33	0.40
$\lvert V_{AO} \rvert$	0.17	0.01	0.40	-0.24	0.32	0.10
$\lvert A_{IA} \rvert$	-0.05	-0.40	0.25	-0.13	**0.66†**	0.37
$\lvert A_{IO} \rvert$	0.35	0.15	0.43	-0.05	**0.54***	0.43
$\lvert A_{AO} \rvert$	0.18	0.09	0.32	-0.06	0.13	-0.20
RAlength	-0.08	-0.44	0.17	**-0.66†**	0.29	0.41
Polydeg	-0.10	-0.43	0.26	-0.43	0.32	0.18

*p < 0.05, †p < 0.01

Table 6.4: *Median and interquartile range (IQR) values of the reference stiffness indices and the Spearman's correlations between the longitudinal motion indices and the reference stiffness indices.*

	DC (1/Pa)	**CC (m^2/Mpa)**	**Z (Ω)**	**AA (mmHg)**	**Aix (%)**	**Aix@75 (%)**	**PWV (m/s)**
Median	24.22	0.68	7.43	5.00	18.00	10.00	7.60
IQR	10.44	0.39	1.94	5.00	16.00	17.50	1.95
IA_{ante}	0.02	0.21	-0.01	-0.24	-0.29	-0.32	0.25
IO_{ante}	-0.09	0.12	0.07	-0.24	-0.30	-0.34	0.27
AO_{ante}	0.07	0.22	-0.08	-0.22	-0.28	-0.36	0.10
IA_{retro}	0.23	0.06	-0.19	-0.06	0.04	0.11	-0.34
IO_{retro}	0.22	0.10	-0.21	0.01	0.08	0.10	-0.25
AO_{retro}	0.15	0.06	-0.14	0.18	0.20	0.24	-0.17
IA_{ampl}	0.19	0.16	-0.16	-0.24	-0.16	-0.13	-0.20
IO_{ampl}	0.18	0.25	-0.18	-0.21	-0.18	-0.17	-0.06
AO_{ampl}	0.16	0.34	-0.18	0.07	-0.02	-0.04	0.10
V_{IA}	0.20	0.36	-0.21	0.27	0.19	0.18	-0.08
V_{IO}	0.15	0.32	-0.24	-0.34	-0.41	**-0.46***	0.00
V_{AO}	0.16	0.40	-0.21	-0.24	-0.28	-0.30	0.23
A_{IA}	0.30	**0.49***	-0.30	0.17	0.13	0.13	-0.09
A_{IO}	0.27	0.41	-0.37	-0.43	-0.45	**-0.50***	0.02
A_{AO}	0.29	**0.47***	-0.35	-0.31	-0.35	-0.41	0.10
$\lvert V_{IA} \rvert$	0.21	0.29	-0.15	-0.40	-0.44	**-0.48***	0.09
$\lvert V_{IO} \rvert$	0.17	0.31	-0.16	-0.21	-0.23	-0.24	0.22
$\lvert V_{AO} \rvert$	-0.12	-0.09	0.09	-0.36	-0.39	-0.33	0.05
$\lvert A_{IA} \rvert$	0.01	-0.04	0.01	**-0.49***	**-0.54***	**-0.52***	0.12
$\lvert A_{IO} \rvert$	-0.07	-0.00	0.12	0.00	-0.09	-0.16	0.41
$\lvert A_{AO} \rvert$	-0.03	-0.08	0.03	-0.02	-0.07	-0.12	-0.07
RAlength	**0.68‡**	**0.80‡**	**-0.67†**	**-0.65†**	**-0.61†**	**-0.60†**	**-0.55***
Polydeg	0.26	0.34	-0.23	**-0.46***	**-0.47***	**-0.53***	-0.37

*p < 0.05, †p < 0.01, ‡p < 0.001

6.3 WAVEFORM CHARACTERIZATION

A PCA was used to characterize the longitudinal waveform of the common carotid artery in a healthy population of 19 subjects. The two most significant eigenvectors were derived to describe the longitudinal waveform and PC values were utilized as weighting coefficients to fit the eigenvectors to the measured longitudinal motion signal. The repeatability of the PC values was good as Cronbach's alpha values were greater than 0.85 in all measured 1st and 2nd PC values.

The two most significant eigenvectors are displayed in Figure 6.2. Based on the corresponding eigenvalues, the two most significant eigenvectors summarize 99.5 % of the variance in the diameter change curve and over 92 % of the variance of the longitudinal motion of the different wall layers of the common carotid artery. The first eigenvector alone explained 97.9 % of the variance within the diameter change curve and 87.2 % of the variance within the longitudinal motion between the intima-media complex and the adventitia layer. In addition, the first eigenvectors defined from the longitudinal motion of the individual wall layers intima-media and adventitia explained 83.1 % and 80.8 % of the variation within the study population, respectively.

The relationships between the more conventional peak-to-peak amplitude indices and the PC values are displayed in Table 6.5. In addition, the relationships between the deviation of the longitudinal motion (describing the direction of the motion) and the PC values are shown in the same table. The peak-to-peak amplitudes and average deviation values exhibited high correlations with the 1st PC values, measured from the corresponding artery layers. On average, over 70 % of the data variation in the deviation indices and over 50 % of the data variation in the amplitude indices was represented by the corresponding 1st PC values. The 2nd PC values did not correlate with the longitudinal peak-to-peak values and explained on average, roughly 35 % of the data variation in the corresponding deviation values.

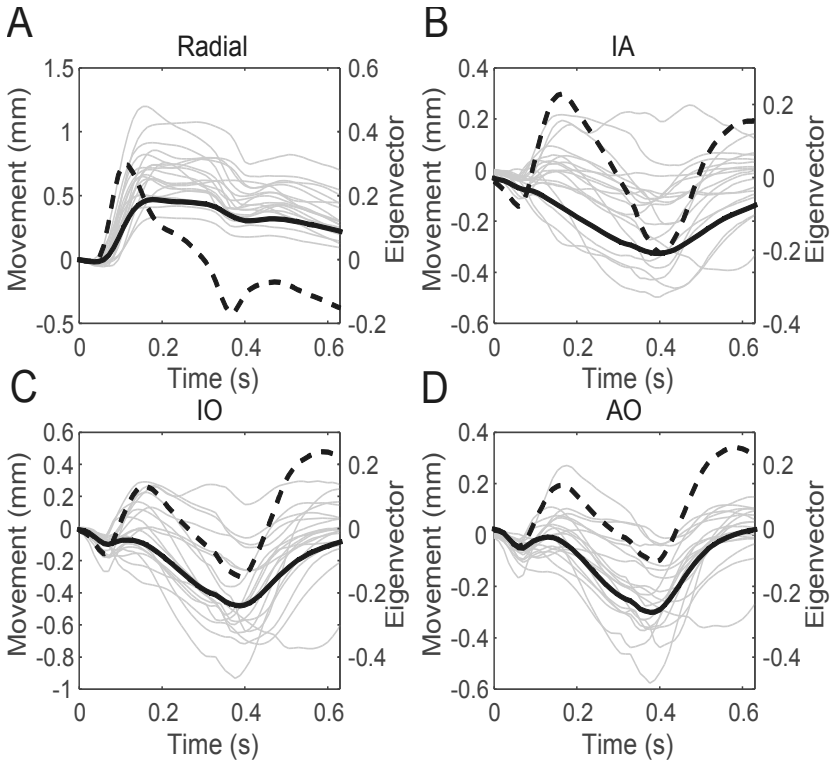

Figure 6.2: *The two most significant eigenvectors derived from the diameter change (radial) and longitudinal movement curves. The thick solid line is the 1st eigenvector and the dashed line is the 2nd eigenvector. The thinner lines are the original motion traces.*

The correlations between the PC values, clinical characteristics of the study population and the measured arterial stiffness indices are displayed in Table 6.6. In addition, the medians and IQR values of the clinical characteristics and the arterial stiffness indices are presented in the same table. The 1st PC defined from the diameter change curve revealed a clear correlation to with multiple stiffness indices, i.e. a direct correlation with DC ($r = 0.58$, $p < 0.01$) and CC ($r = 0.81$, $p < 0.001$) and an inverse correlation with PWV ($r = -0.53$, $p < 0.05$). The 2nd PC showed no signs of any correlation with arterial stiffness. In addition, the values of the 1st PC of the longitudinal motion between the different arterial wall layers displayed no correlation to arterial stiffness. However, the 1st PC exhibited a direct relationship with the pulse pressure ($r = 0.52$, $p < 0.05$).

The 2nd PCs correlated with reference arterial stiffness indices. Especially the 2nd principal component derived from the longitudinal motion of the adventitia layer showed a clear correlation to local arterial stiffness: a direct correlation with DC ($r = 0.63$, $p < 0.01$) and CC ($r = 0.53$, $p < 0.05$) as well as an inverse correlation with E_Y ($r = -0.58$, $p < 0.01$) and Z ($r = -0.59$, $p < 0.01$). In the same dataset, the peak-to-peak amplitudes of the longitudinal wall motions displayed no correlation to the arterial stiffness indices.

Table 6.5: *The Spearman's correlations of the principal components (PCs), derived from the diameter change curve (radial) and longitudinal motion curve, to the peak-to-peak amplitudes (ampl) and average deviations (dev) of the longitudinal motion.*

PC	IA_{dev}	IO_{dev}	AO_{dev}	IA_{ampl}	IO_{ampl}	AO_{ampl}
Radial 1st PC	0.02	0.01	0.08	0.19	0.18	0.09
Radial 2nd PC	-0.10	-0.12	-0.25	-0.19	0.10	0.41
IA 1st PC	**-0.90‡**	**-0.85‡**	**-0.61†**	**0.58†**	**0.53***	0.27
IA 2nd PC	0.48*	0.43	0.16	-0.10	-0.18	-0.10
IO 1st PC	**-0.86‡**	**-0.93‡**	**-0.79‡**	**0.62†**	**0.73‡**	**0.55***
IO 2nd PC	**0.65†**	**0.61†**	0.42	-0.14	-0.13	0.06
AO 1st PC	0.45	**0.62†**	**0.78‡**	-0.25	**-0.62†**	**-0.76‡**
AO 2nd PC	**0.53***	**0.65†**	**0.70‡**	-0.06	-0.18	-0.16

*$p < 0.05$, †$p < 0.01$, ‡$p < 0.001$

Table 6.6. *Median and interquartile range (IQR) values of the clinical characteristics and the arterial stiffness indices. In addition, the Spearman's correlations between the principal components (PCs), derived from the diameter change curve (radial) and longitudinal motion curve, and the clinical characteristics as well as the arterial stiffness indices.*

	Gender	**Age (years)**	**SBP (mmHg)**	**DBP (mmHg)**	**PP (mmHg)**	**DC (1/Pa)**	**CC (m^2/Mpa)**	**E_Y (Mpa)**	**Z (Ω)**	**AA (mmHg)**	**Aix (%)**	**Aix@75 (%)**	**PWV (m/s)**
Median		28.00	114.5	69.00	46.00	29.14	0.93	0.41	6.06	4.00	10.00	3.00	7.00
IQR		6.50	18.25	8.25	11.5	6.00	0.36	0.14	0.74	5.00	16.00	18.00	1.20
Radial 1st PC	0.10	-0.37	0.04	**-0.56***	0.25	**0.58†**	**0.81‡**	**-0.49***	**-0.52†**	-0.04	-0.02	-0.26	**-0.53***
Radial 2nd PC	-0.29	0.18	0.28	0.25	0.23	0.07	0.00	0.04	-0.01	0.03	0.02	0.28	0.00
IA 1st PC	0.08	0.00	0.29	-0.32	**0.47***	-0.28	-0.16	0.09	0.33	-0.06	-0.11	-0.09	-0.29
IA 2nd PC	0.17	0.16	**-0.46***	0.13	**-0.54***	0.21	0.08	**-0.50***	-0.18	0.15	0.22	0.16	0.31
IO 1st PC	-0.02	0.02	0.35	-0.30	**0.52***	-0.29	-0.11	0.09	0.34	0.05	-0.02	-0.05	-0.32
IO 2nd PC	-0.08	-0.02	-0.27	-0.04	-0.29	0.43	0.35	**-0.55***	-0.38	0.04	0.11	0.01	-0.04
AO 1st PC	0.00	-0.05	0.27	-0.09	0.41	-0.12	0.04	0.08	0.15	0.05	-0.02	-0.03	-0.19
AO 2nd PC	-0.02	-0.20	-0.32	-0.28	-0.25	**0.63†**	**0.53***	**-0.58†**	**-0.59†**	-0.19	-0.12	-0.18	-0.31

*p < 0.05, †p < 0.01, ‡p < 0.001

6.4 TRANSFER FUNCTION ANALYSIS

A transfer function analysis was used to determine the plausible linear relationship between the longitudinal motion of the intima-media complex and the adventitia layer in a population of healthy subjects. In addition, the transfer function between the blood pressure signal and the longitudinal motion of the intima-media complex was investigated.

The ideal signal for transfer function analysis would have been a continuous signal but due to the restrictions of the imaging device, the 5-minute signal had to be collected in 10-seconds-long sections. In addition, motion artifacts and changing image quality caused additional cuts to the 10-seconds motion traces and thus the length of the final signals used in the study varied between 1 and 10 seconds.

The power spectrums of the measured signals are displayed in Figure 6.3. The main power in all of the power spectrums was in the 0-3 Hz band, with a peak on the 1.1 Hz frequency. In the power spectrums of the longitudinal wall motion, there was an additional peak in the 0.2 Hz frequency compared to the power spectrum of the blood pressure signal.

The transfer function between the longitudinal motion of the intima-media complex and the adventitia layer is displayed in Figure 6.4. The average coherence function value in the observed frequency band 0-5 Hz was 0.80, with no large deviations in the coherence values. The values of the amplitude part of the transfer function were negative throughout the observed spectrum, with the maximal decrease being -1.6 dB on the 1.0 Hz frequency. The -1.6 dB decrease is equivalent to a 17 % amplitude reduction in the longitudinal motion of the adventitia layer compared to the intima-media complex. The phase part of the transfer function reveals intima-media complex leading the adventitia layer in the band 0-3 Hz. At higher frequencies, the adventitia layer was in front of the intima-media complex, but there is no notable power on the

high frequencies. In the 1.0 Hz frequency, where the amplitude part of the transfer function had its minimum, the delay between the longitudinal motion of the intima-media complex and the adventitia layer was 6.8 degrees.

The transfer function between the blood pressure signal and the longitudinal motion of the intima-media complex is shown in Figure 6.5. The average coherence value on the band from 0 Hz to 5 Hz was 0.68. The coherence declined to merely under 0.5 on individual frequency bands from 1.8 Hz to 2.0 Hz and from 3.6 Hz to 3.9 Hz. In addition, the coherence peaked over 0.7 on 1.1 Hz and 2.7 Hz frequencies. The amplitude part of the transfer function behaved as a low-pass filter with a notch on the 1 Hz frequency. The phase part displayed extensive variation in the frequencies 0.5-1.5 Hz where the heart muscle operates and the phase values on the 0.5 Hz wide heartbeat band correlated with known arterial stiffness indices Aix@75 ($r = 0.66$, $p < 0.01$) and E_Y ($r = -0.50$, $p < 0.05$). The amplitude part of the heartbeat band did not correlate with the stiffness indices.

The quartile transfer functions between the blood pressure signal and the longitudinal motion of the intima-media complex, computed from the upper and lower quartiles of the study population arranged according to IO_{dev} value, are presented in Figure 6.6. The amplitude parts of the quartile transfer functions are similar to each other and to the corresponding whole population transfer function. The most notable difference is on the phase parts around 1 Hz frequency. The upper quartile (i.e. the population whose longitudinal motion waveform was antegrade oriented) transfer function exhibited a positive phase (peak at 37 degrees) and the lower quartile (i.e. the retrograde oriented population) transfer function displayed a clearly negative phase (peak at -117 degrees). The coherence function could be considered as another differentiator between the quartile transfer functions. The maximum coherence was achieved between 2-3 Hz in the upper quartile transfer function and at 1 Hz in the lower quartile transfer function. There was only a small peak in the 2-3 Hz band in the lower quartile transfer function.

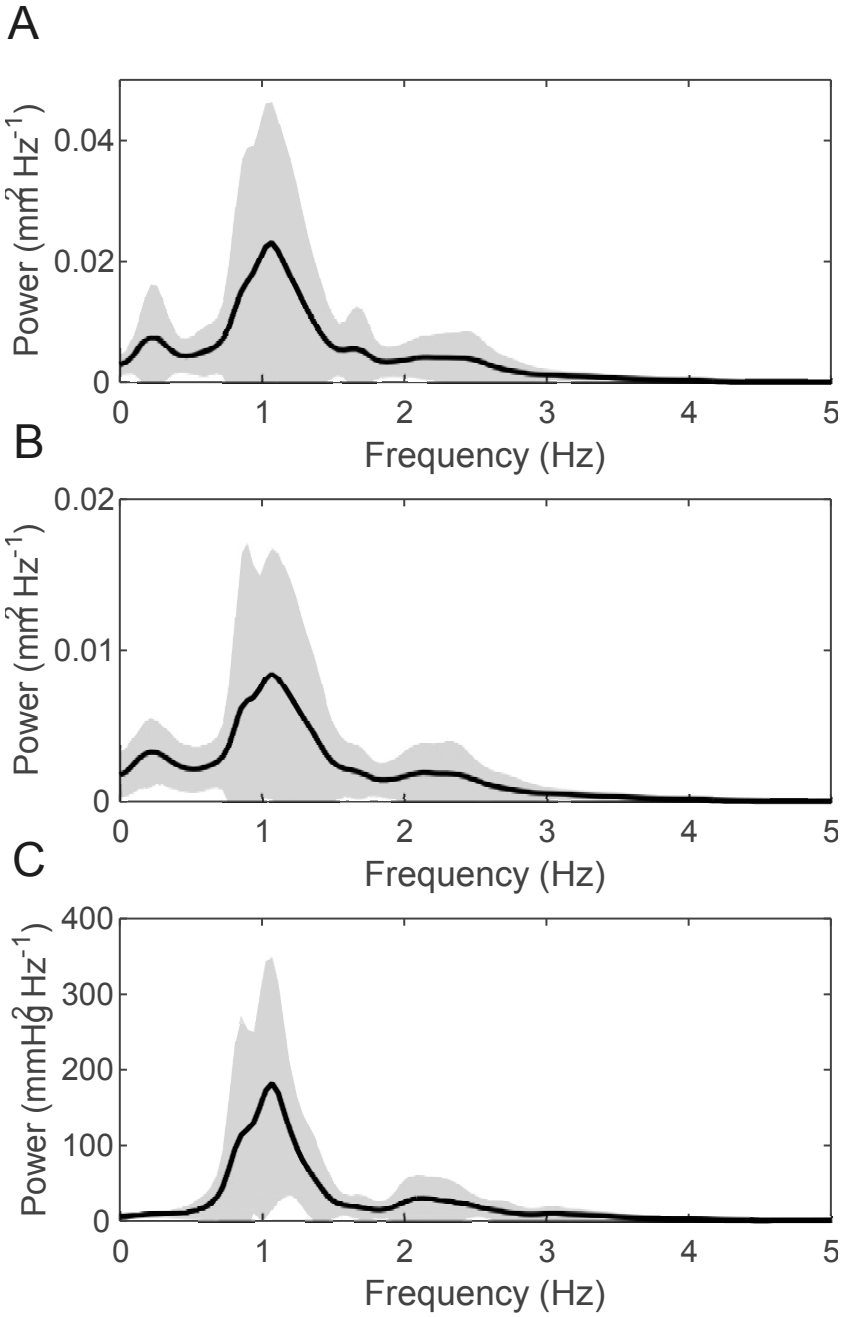

Figure 6.3: *Power spectrums of: A, the longitudinal movement of the intima-media complex; B, the longitudinal movement of the adventitia layer; C, the blood pressure signal. Solid line represents the average of the population and standard deviation is shown by the gray background.*

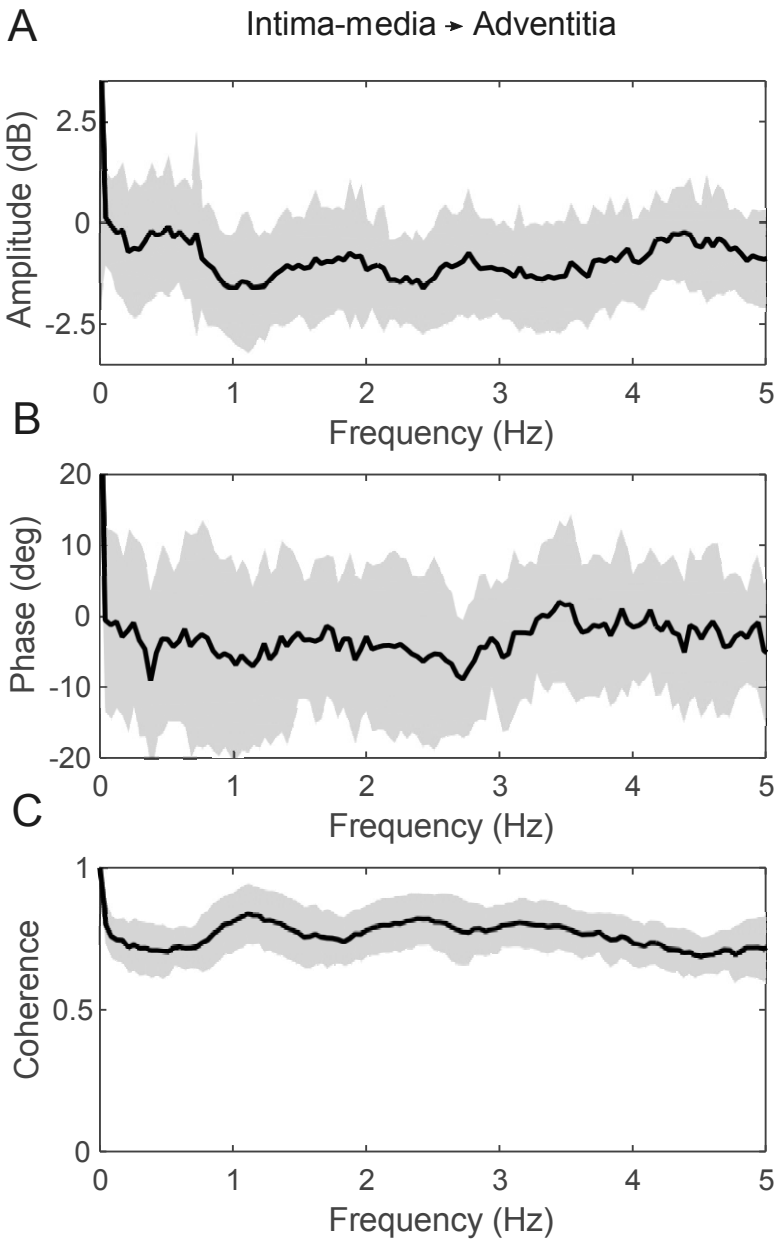

Figure 6.4: *Transfer function between the longitudinal movement of the intima-media complex and the adventitia layer. A, amplitude part; B, phase part; C, coherence function. The solid line represents the mean value and the gray background is the standard deviation.*

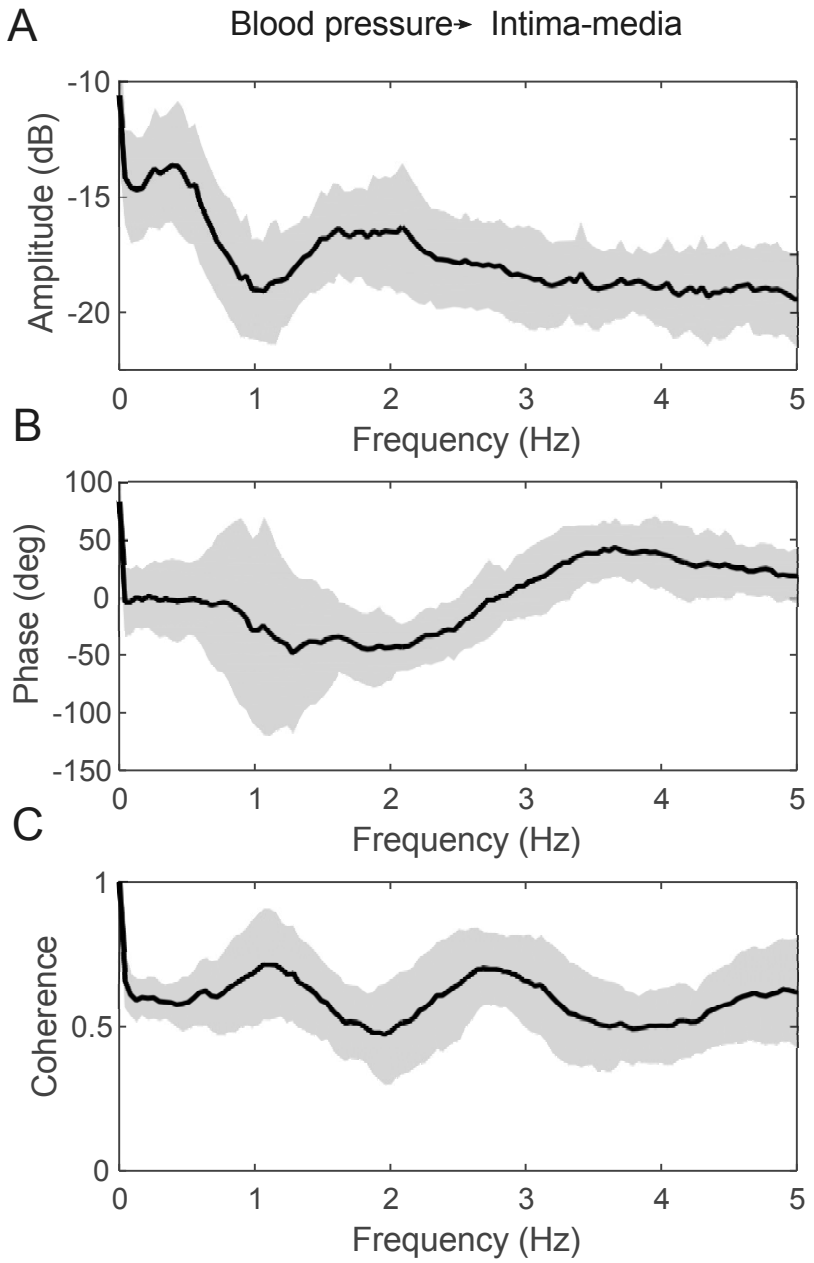

Figure 6.5: *Transfer function between the blood pressure signal and the longitudinal movement of the intima-media complex. A, amplitude part; B, phase part; C, coherence function. The solid line represents the mean value with the gray background as the standard deviation.*

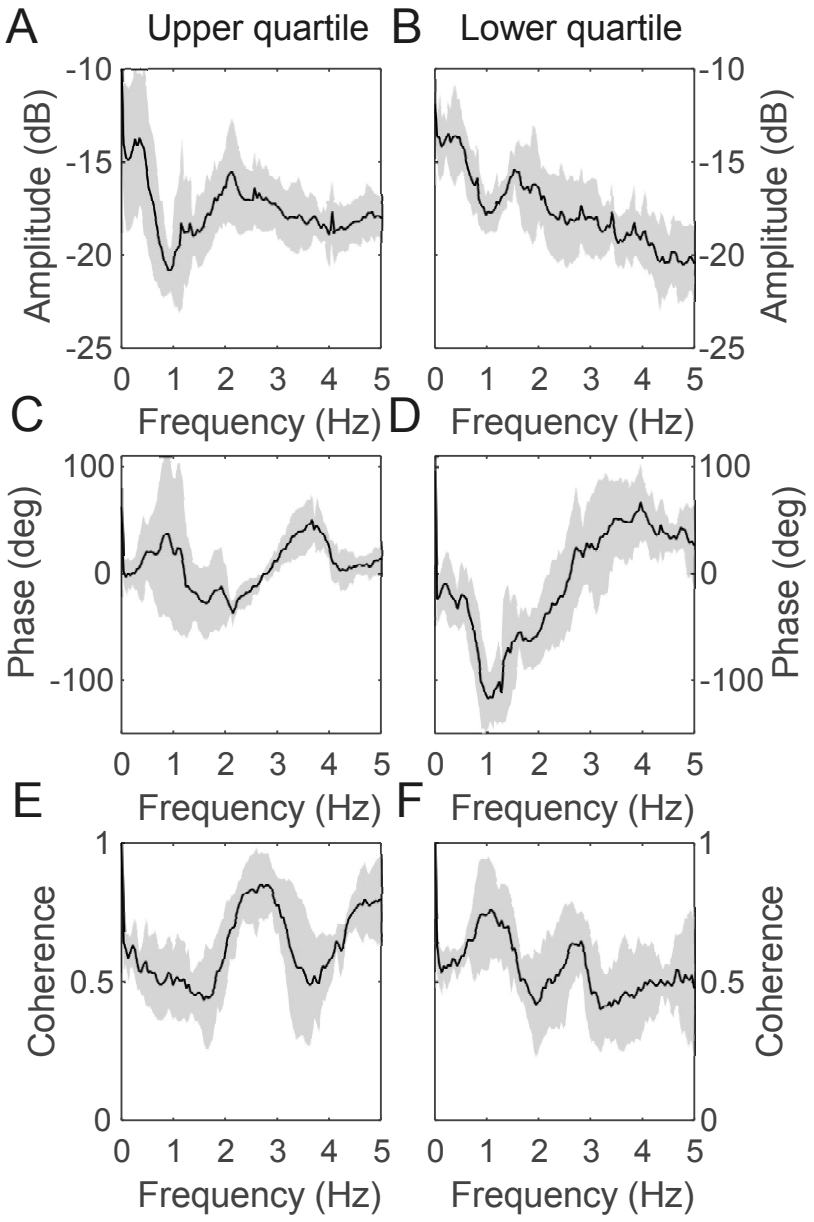

Figure 6.6: *Quarter transfer functions between the blood pressure signal and the longitudinal movement of the intima-media complex. A, C and E display the amplitude part, the phase part and the coherence function, respectively, of the upper quartile. B, D and F display the amplitude part, the phase part and the coherence function, respectively, of the lower quartile. The solid line represents the mean value with the gray background being the standard deviation.*

7 Discussion

In this thesis, accurate methods were developed to measure the longitudinal motion of the common carotid artery wall and to characterize the waveform of the motion. In addition, multiple arterial stiffness and wellbeing indices, computed from the longitudinal motion waveform, were devised. The indices' repeatability was tested and found to be suitable for population studies and some for individual diagnostics. The stiffness indices were also successfully validated against commonly known arterial stiffness and arterial wellbeing indices. In addition, the waveform of the longitudinal motion was found to vary extensively but nonetheless to exhibit a relationship with arterial stiffness.

7.1 MEASURING LONGITUDINAL MOTION

The noninvasive detection of the arterial stiffening in its early stage is increasingly becoming a topic of interest to researchers. The longitudinal wall motion has been proposed to provide novel information about vascular wellbeing but understanding of the longitudinal kinetics is somewhat limited. In addition, the tools to study the motion have been at the development stage, as the longitudinal motion of the artery wall is a challenging parameter due to limited lateral resolution of the ultrasound transducers. However, ultrasound has quickly become the gold standard for studying the longitudinal motion of the common carotid wall. Increasing amounts of the published motion-tracking algorithms operating on ultrasound are based on the radio frequency data of ultrasound devices, but these are not commonly available in clinical ultrasound imaging devices [117-119, 123]. The raw radio frequency signal is more robust than the compressed B-mode image data of the clinical devices but still the motion-tracking method presented here relies on the B-

mode video data. There were two reasons behind this decision: firstly, the ultrasound scanners which we could utilize during this thesis, did not allow the user to access the radio frequency data and secondly, methods based on the radio frequency data cannot be widely used; in contrast, the B-mode video based algorithms can be easily adopted to all current clinical ultrasound scanners.

The longitudinal motion-tracking method presented here differs from the majority of the other published methods in three ways: firstly, the method is the only one that uses contrast optimization to reduce noise from the ultrasound images. Secondly, a bicubic interpolation is used to increase in a virtual way, the resolution of the video frame matrix and thus it achieves a more precise estimation of the longitudinal motion than can be obtained from the limited lateral resolution of the ultrasound transducers. Thirdly, this method uses an additional region of interest to track the longitudinal motion in the surrounding tissues; this is not a feature commonly described in the literature. The motion of the surrounding tissues is reduced from the longitudinal traces of the intima-media complex and the adventitia layer. In this way, all artefacts caused by the motion between the ultrasound transducer and skin are minimized.

The bicubic interpolation, which virtually increases the spatial resolution of the ultrasound video frame matrix, has been used successfully as a way to acquire a more precise measurement of the longitudinal motion [111]. There are also more simplified interpolation methods such as bilinear and nearest neighbor, which can be approximately 7 to 10 times faster than the bicubic method. The bilinear interpolation has been used in one previous publication but the authors considered that the bicubic interpolation may have been a better method but the bilinear interpolation was used to reduce computing time [112]. The problem, in the case of motion-tracking, is that almost no enhancement is reached with nearest neighbor interpolation and that the bilinear method is more vulnerable to artefacts (pixels standing out conspicuously),

compared to the bicubic method. A general problem is that interpolating new pixels to the original data is only an estimation of the increased image resolution without certainty and the estimation can be therefore lead to discrepancies. Nevertheless, generally in image resizing, the bicubic method is preferred over nearest neighbor and bilinear methods, unless the time needed to perform the interpolation is crucial [161, 162].

Although the measurement of the longitudinal motion of the common carotid wall is challenging, the method presented in this thesis proved to be suitable for studying this phenomenon. The overall day-to-day reproducibility of the longitudinal measurements was good. The method of Cinthio and Ahlgren [112] is the one with the most direct comparison to the presented method since it uses image interpolation and referential ROI in the surrounding tissues and since CV value was computed between measurements of subsequent days. Cinthio and Ahlgren were able to achieve a CV value 12.5 % in their day-to-day reproducibility of the peak-to-peak motion amplitude between the intima-media complex and the surrounding tissues. The corresponding CV value was 10.5 % for a motion tracking method based on velocity vector imaging, averaging the longitudinal motion for a 1 cm space [127]. Our corresponding CV value was 16.3 %. The slightly better value with the method by Cinthio and Ahlgren might be because they used a higher frame rate in their ultrasound imaging (55 Hz). The use of the high frame rate was likely to remove motion artifacts, which are visible in the intima-media complex using lower frame rates. Svedlund and Gan [127] did not report imaging frame rate that they used and furthermore they motion tracked a long segment of the artery wall, which is known to contain different longitudinal motion amplitudes [133]. In addition, the vector velocity imaging was not able to detect the multiphasic form of the longitudinal motion, as has been reported in other studies [127]. Another difference possibly affecting the reproducibility is the fact that Cinthio and Ahlgren used breath hold during imaging while we allowed free breathing. It is debatable whether it is best to image the

longitudinal motion in a breath hold or during free breathing. With free breathing, one needs a longer signal to average out the effect of breathing whereas with breath hold one can acquire a repeatable longitudinal motion signal rather quickly. However, it is obvious that holding the breath is not a natural state and its specific effects on the longitudinal wall motion are unknown.

In the literature, ultrasound transducers with the mean or peak frequency on 4-13 MHz band have been used successfully for longitudinal motion tracking [111-123, 127]. Therefore, the transducers used here (14 MHz and 18 MHz peak frequencies) are one of the highest frequencies used in the longitudinal motion tracking. However, a recent study claimed that modern clinical ultrasound imaging devices (frequency of the transducer < 20 MHz) are sufficient to measure the longitudinal motion of the carotid wall [118]. The application of high frequency ultrasound devices (frequency > 20 MHz) does not seem to achieve any significant additional accuracy in the measurement of the longitudinal motion of the far carotid artery wall [118]. However, ultrasound probes capable of emitting higher frequencies are most likely beneficial for imaging smaller, superficial arteries such as the radial artery.

In the tracking of the longitudinal motion of the carotid wall, it is important to keep the ROI size and location constant as the longitudinal motion has been shown to vary along the common carotid artery [133]. In addition, large ROIs make it impossible to detect the local shear stress changes whereas small ROIs are more subject to tracking errors [115]. In the literature, ROI sizes 0.5-3.2 × 0.1-2.5 mm^2 (lateral and axial measures, respectively) have been generally used for the motion tracking of the intima-media complex [111-123, 127]. The average intima-media ROI sizes used in this thesis were 2.76 × 0.50 mm^2 in Studies I and II and 2.58 × 0.33 mm^2 in Studies III and IV, which are in line with values in the literature. The optimal ROI size is always a compromise between motion-tracking accuracy and detecting the smallest motions.

The limitation of the presented motion tracking method is the update procedure of the ROI data after every frame, based

simply only on the previous frame i.e. the method is an adaptive single frame cross-correlation. The ROI data update is necessary in order to incorporate to the changes occurring inside the ROI: shear strain within the ROI and other deformations or disappearances of the tracked speckles as a function of time. Nevertheless, the ROI updating procedure based on only a single previous frame slowly accumulates errors into the tracked ROI, as the inevitable small errors in the motion-tracking move the ROI slightly away from the correct position and from that point onwards, the motion tracking is being performed on a false measuring site. One automatic solution to this problem is to keep some information of the original ROI data unchanged and only update some features of the ROI data in the current location. A method averaging the original and current ROI data has been applied with good success [120]. Other longitudinal motion tracking methods in the literature have relied on more advanced adaptive cross-correlation techniques i.e. based on finite impulse response filtering [114] or Kalman filtering [113, 114, 121], which mainly differ from the method used here by taking information from n ($n > 1$) ultrasound video frames prior to the current frame, in order to update the content of the ROI. In a comparison study, the Kalman filtering based method was noted to display more reliable motion tracings, when compared to conventional 2D cross-correlation and adaptive single frame cross-correlation [114]. The disadvantage of the Kalman filtering is the increase in the computation time, which can be as much as fivefold compared to the conventional cross-correlation [113]. The key difference in the method presented in this thesis is that it is semiautomatic and relies on the user to check the motion traces after every heartbeat-long motion tracking and to reset the ROI to a proper speckle to be traced for the next cardiac cycle. The potential mismatch between the original and reset ROI locations is corrected by removing the linear trend between the subsequent, heartbeat-long motion traces. The user dependency is a disadvantage but the presented method allows successful motion tracking that can last for several minutes, which is

required in the transfer function analysis. Our method has been used for 5-minute-long motion tracings, while typically in the literature the longitudinal motion has been measured for less than 5 seconds [111-123, 127].

In the future, the three-dimensional ultrasound imaging will most likely allow measurement of the artery wall motion even more accurately and more comprehensively than the current techniques. There is a recent study comparing 2D and 3D cross-correlation motion-tracking algorithms being applied on a modelled carotid artery wall to track radial and circumferential motion [163]. That study stated that 3D displacement estimation clearly outperformed the 2D type and that large inter-frame longitudinal motion made it impossible to estimate the radial and circumferential motion accurately only with 2D cross-correlation. Similarly, we can state that circumferential motion of the artery wall negatively influences the longitudinal motion estimation when using the current 2D techniques and this problem could be fixed by adopting 3D techniques.

7.2 NEW STIFFNESS INDICES

This thesis introduced multiple arterial stiffness and wellbeing indices based on the longitudinal motion of the common carotid artery wall. The indices can be divided into four sub-categories: amplitude indices, rate of change indices, complexity indices and indices characterizing the waveform of the longitudinal motion.

7.2.1 Amplitude indices

Longitudinal amplitude indices are the types on which most of the researchers in this field have concentrated. Instead of focusing only on the peak-to-peak amplitude of the longitudinal motion of the intima-media complex, the adventitia layer and the motion between these layers, this thesis also highlighted partial amplitudes, i.e. the antegrade component and the retrograde component of the longitudinal motion. These partial

amplitudes have also been studied by some researchers [111, 128, 129, 131].

In this thesis, the greatest peak-to-peak amplitudes seemed to be encountered in subjects with the retrograde oriented longitudinal waveform and on average, the retrograde component of the longitudinal motion was greater than the antegrade component. The median peak-to-peak amplitude of the longitudinal motion of the intima-media layer was 0.43 mm, which is in agreement with the average values of the healthy population found in the literature: 0.61 mm [122], 0.64 mm [121], 0.48 mm [115], 0.81 mm [112], 0.54 mm [127], 0.40 mm [127].

The median amplitude of the antegrade component of the longitudinal motion found here was 0.06 mm (IQR 0.22 mm), which is slightly lower than the values reported in the literature: 0.31 mm [111], 0.39 mm [129], 0.35 mm [131] and 0.13 mm [128]. In addition, the retrograde amplitudes were slightly lower in this thesis (median 0.30 mm and IQR 0.37) than values in the literature: 0.71 mm [111], 0.52 mm [129], 0.82 mm [131] and 0.42 mm [128]. The antegrade and retrograde amplitudes are in line with the results of the peak-to-peak amplitude, which was low but comparable with other studies.

Based on our results, it seems that the partial amplitudes play major role when studying arterial stiffness: the antegrade and retrograde amplitudes had higher correlations to known arterial stiffness indices than the longitudinal peak-to-peak amplitudes. In addition, previously the reduced retrograde amplitude of the intima-media has been speculated to reflect an increased cardiovascular disease risk [131].

The exact driving force for the longitudinal motion is still unclear and this complicates the evaluation of the amplitude indices; measuring only the longitudinal amplitude, whether it is the peak-to-peak or partial amplitude, is an incomplete measure of the longitudinal kinetics. The longitudinal motion is the output of some initiating force, and if one wishes to derive a proper stiffness measure, the output needs to be normed with the input. When the driving force is taken into account, the significances of the different longitudinal amplitude indices can

change. However, in this thesis and in many other publications, the longitudinal amplitude alone has been shown to be related to vascular wellbeing [20-22, 131, 132, 138, 139].

7.2.2 Rate of change indices

The results indicate that the rate of change indices display higher correlations with known arterial stiffness indices than the previously more widely studied longitudinal amplitudes. This emphasizes the need to study the longitudinal motion in greater detail, rather than simply focusing on the numerical amplitude of the motion. The highest correlations between the rate of change indices and previously known arterial stiffness indices were achieved with those rate of change indices which included information about the direction of the longitudinal motion. Based on these results, arterial stiffness may have an effect on the main direction of the longitudinal motion, but there is no clear-cut clinical evidence to support this concept; in fact they are at odds with the results of a smaller study on this subject [164].

The challenge with the rate of change indices is the frame rate of the ultrasound acquisition. The frame rate of 25 Hz was found to be sufficient to track the longitudinal motion but for the rate of change indices, especially for the acceleration measurements, a higher frame rate would be beneficial in order to capture the real peak value of the velocity and acceleration of the motion. Nevertheless, the peak rate of change indices, performed with a frame rate 25 Hz, achieved more than adequate repeatability results.

7.2.3 Complexity indices

This thesis introduced two easily measurable indices that describe the complexity of the arterial wall motion. The idea of the indices is to have single value to depict the entire heartbeat-long motion graph. We named the indices as Polydeg and RAlength. Polydeg measures the complexity of the longitudinal motion waveform and RAlength assesses the total two-dimensional motion of the arterial wall during a heartbeat.

The repeatability and the reproducibility of RAlength are good, meaning that the measurement is reliable. According to the results of this thesis, RAlength exhibits a clear correlation with known arterial stiffness indices. A larger study with hundreds of subjects was also conducted to evaluate the connection between the longitudinal wall motion and known indices of arterial stiffness [20]. That study revealed the usability of the longitudinal motion as a predictor of vascular status and highlighted that RAlength displayed the highest correlations with arterial stiffness, being even better than the longitudinal amplitude indices.

In contrast to the RAlength, the Polydeg value displayed good repeatability but poor day-to-day reproducibility. It is possible that the Pearson's correlation coefficient value criterion used for the calculation of the Polydeg value ($r > 0.95$) was too strict, causing even the smallest changes in the longitudinal motion waveform and measuring artifacts to ruin the reproducibility. Therefore, Polydeg's correlations to other reference stiffness indices, presented in this thesis, must be considered carefully.

7.2.4 Waveform characterizing indices

This thesis revealed that the waveform of the carotid wall motion varies largely from one subject to the next, when measured during free breathing. The longitudinal waveforms observed in this thesis can be divided roughly into three categories: bidirectional, antegrade oriented and retrograde oriented waveforms. In general, the waveforms have been stated to remain unchanged over a 4-month period [130] and the bidirectional longitudinal motion has been reported to occur even during a breath hold [121, 129].

The majority of our test subjects displayed the primary longitudinal motion towards the retrograde direction. One common feature for all the longitudinal motion waveforms is that they all have a tendency to head towards the antegrade direction during early systole. The antegrade motion seem to occur at the same time as the local blood velocity peaks [128].

However, despite the temporal concurrency, the statistical significance between the blood flow velocity and the longitudinal carotid wall motion is lacking [128, 137]. The direction of the longitudinal motion changes towards the retrograde direction in the early diastole and the timing of the change of the direction has been reported to match with the peak apical and basal rotation of the heart [128]. Finally, the wall returns to its initial position during the late diastolic phase.

PCA is a widely used tool to summarize the information contained in a large dataset and here it was used to characterize the longitudinal waveform. The mathematics of the PCA does not entail any user dependent criteria and therefore it is a more elegant index to describe the complexity of the longitudinal motion than Polydeg. In addition, the repeatability of the index was good, but the day-to-day reproducibility of the PC values was not measured here.

The two most significant eigenvectors were able to account for over 92 % of the variation in the longitudinal motion data. This means that over 92 % of the information within the longitudinal motion curves can be packaged into two singular PC values and hence the usefulness of the higher PC values is rather insignificant if one is trying to reconstruct the longitudinal motion waveform from the eigenvectors.

According to the results, the amplitude and the main direction of the longitudinal motion of the intima-media and adventitia layer are related to the 1st PC defined from the motion waveform of the corresponding wall layer. In the case of the longitudinal motion of the intima-media complex, the 1st PC describes 86 % of the variance of the IO_{dev} and 53 % of the variance of the IO_{ampl}, which means that it is not such a valuable add-on for the amplitude and main direction indices. More interestingly, the 2nd PC is independent of the motion amplitude (explains only less than 2 % of the variance within the amplitudes) and is less affected than the 1st PC by the direction of the motion (i.e. it explains 37 % of the variance within the IO_{dev} values). The shapes of the eigenvectors reveal that the fine

details of the longitudinal motion, such as the amount of the back-and-forward motion, have a greater impact on the 2nd PC.

There were clear correlations between the 2nd PC, derived from the longitudinal motion curve of the adventitia layer, and multiple indices of local arterial stiffness e.g. DC, CC and E_Y. It seems that the longitudinal waveform of the outermost adventitia layer is more sensitive to change than the innermost intima-media complex when stiffening processes start in the vessel wall. The correlations between the 2nd PC of the longitudinal motion of the intima-media complex and the arterial stiffness indices only just failed to reach the statistical significance criterion ($p < 0.05$). In addition, there was no correlation to arterial stiffness with the PCs derived from the longitudinal motion between the intima-media complex and the adventitia layer.

All the participants in the study were healthy, thus the results highlight the potential of the PCA to detect the early signs of the arterial stiffening. The results might be different if diagnosed atherosclerotic or arteriosclerotic patients had been included to the study, as the longitudinal waveform has been shown to vary with the presence of blood vessel plaques [134, 135]. In addition, it has been reported that there is a significant difference in the longitudinal motion amplitude between young healthy and older diabetic populations [21]. A similar finding has also been made between healthy volunteers and patients with periodontal disease [132]. Based on the results of the above-mentioned studies, it is likely that at least the 1st longitudinal PC, which is highly associated with the longitudinal motion amplitude, would have a higher correlation to the arterial stiffness in arteriosclerotic study populations. The behavior of the 2nd PC in a diseased population is harder to predict, since it seems to be independent of the current longitudinal motion amplitude indices.

The pitfall in the PCA presented here, is the low number of subjects which were used to form the eigenvectors. If one wishes to obtain a more precise and accurate representation of the eigenvectors, a vastly enlarged number of subjects would be

needed, including diagnosed cardiovascular patients. In the future, if the input-output characteristics of the different driving forces and the resulting longitudinal motion prove to be rather consistent and logical, then the population-averaged eigenvectors might be a useful tool for analyzing the status of the patient's vascular system. By only measuring the longitudinal waveform of the carotid wall during a heart cycle and allowing the computer to calculate the optimal PCs to fit the universal eigenvectors, it should be possible to reveal the status of the patient's vascular system. The PCA is as fast and easy to perform as the amplitude measurement of the longitudinal motion, but nonetheless, it provides much more information about the longitudinal motion than the plain amplitude measurement.

Irrespective of the low number of subjects examined in this thesis, the use of PCA to study the longitudinal motion is promising. The 2nd PCs of different arterial layers are independent of the longitudinal peak-to-peak amplitudes and display significant correlation, especially on the adventitia layer, to the indices of arterial stiffness. In other words, the PCA of the longitudinal carotid wall motion is a measure of arterial stiffness and the results of this thesis can act as a foundation for larger clinical studies on this topic.

7.3 TRANSFER FUNCTION ANALYSIS

In this thesis, the more detailed changes within the waveform of the longitudinal motion have been connected to arterial stiffness. In order to characterize further the kinetics of the common carotid artery wall, a transfer function analysis was performed. The spectra of the longitudinal motion of the intima-media complex and the adventitia layer were defined. The main power in both spectra was on the band from 0 to 3 Hz, with a peak value within the 1.1 Hz frequency. The 1.1 Hz frequency is the frequency where the heart muscle operates. Similarly, the power spectrum of the blood pressure signal in carotid artery

was computed and the form of the power spectrum was found to be similar to the spectra derived from the longitudinal wall motion: main power was detected in the 0-3 Hz band with the peak at the 1.1 Hz frequency. The only visible difference is that the power spectrum of the blood pressure signal does not include an additional spike at the 0.2 Hz frequency, this spike is visible on the power spectra of the longitudinal wall motions.

The additional peak power on the 0.2 Hz frequency occurs in a typical frequency band of free breathing, from 0.2 Hz to 0.33 Hz [165]. This finding may be additional evidence that breathing modulates the longitudinal motion of the carotid wall. It has been reported previously that breathing can influence the longitudinal wall motion in the common carotid artery [112].

The transfer function between the intima-media complex and the adventitia layer displayed a high coherence, demonstrating that the wall layers are connected to one another and that the longitudinal motions of the wall layers exhibit a strong linear relationship. The amplitude of the longitudinal motion is on average 17 % higher in the intima-media complex than in the adventitia layer, when observed at the 1.0 Hz frequency where the abatement of the longitudinal motion reaches its maximum. At the same frequency, the delay between the longitudinal motions is 6.8 degrees (i.e. 19 ms), indicating that the longitudinal motion of the intima-media complex occurs prior to the longitudinal motion of the adventitia layer. Based on the transfer function analysis, it seems that the driving force for the longitudinal wall motion mainly affects the intima-media complex and possibly the intima-media simply pulls the adventitia layer along. However, it is also possible that the driving forces affect both layers directly even though they affect the intima-media complex first and with greater force.

Similar to the situation at the 1.0 Hz frequency, the 0.2 Hz component of the longitudinal motion occurs first in the intima-media complex and this is then followed by the adventitia layer and also with a small amplitude reduction. However, there was some variation within the study population, in the way that the longitudinal amplitudes compared to each other in that 0.2 Hz

frequency. In some individuals, the longitudinal amplitude was higher on the adventitia layer and the longitudinal motion of the adventitia occurred prior to the motion in the intima-media. This makes the interpretation harder, for example, to determine how breathing can modify the longitudinal motion of the carotid artery wall and thus more studies on the subject are needed. Another uncertainty emerging from the breathing results is the limited duration of the continuously recorded signals. Due to the technical limitation of the ultrasound imaging device being used, the maximum continuous signal length which could be obtained in the transfer function analysis was 10 seconds. According to the Nyquist theorem, this limits the lowest observable frequency to 0.2 Hz. Longer continuous signals would have been beneficial in order to achieve a more precise presentation of the frequencies being influenced by breathing. However, the key findings of the transfer function analysis are obtained from the heartbeat band, which is well covered in the analyzed spectrum.

The transfer function revealed a strong linear relationship between the blood pressure signal in the common carotid artery and the longitudinal motion of the intima-media complex. The coherence value was lower than in the transfer function between the longitudinal motions of the intima-media complex and the adventitia layer but on average still above 0.68 between frequencies 0 and 5 Hz. The amplitude part of the transfer function behaves as a low-pass filter with an additional notch on the heartbeat frequency (1.0 Hz).

The blood pressure has been suggested as the driving force for the longitudinal motion of the common carotid wall [129] and the high coherence of the transfer function supports it. However, the relationship between the blood pressure and the longitudinal motion is not as unambiguous as between the pulse pressure and the diameter change of the artery. This is because of the variety of waveforms displayed by longitudinal motion. It is unlikely that by only changing the pulse pressure inside the artery, that the main direction of the longitudinal wall motion

would change. Additional factors within the human body are needed to explain the waveforms.

The phase part of the transfer function between the blood pressure and the carotid wall longitudinal motion revealed that on average, the blood pressure signal occurs prior to the longitudinal motion on the heartbeat frequency. However, in some cases, the longitudinal motion seem to occur prior to the blood pressure signal but this of course should not be interpreted to mean that the longitudinal motion is the driving force for the pressure change inside the common carotid artery; the negative phase shift in the transfer function occurs, because of the retrograde oriented waveform of the longitudinal motion curve. The majority of the subjects had the main orientation of the longitudinal motion in the retrograde direction, i.e. against the main direction of the blood flow. This retrograde orientation of the longitudinal motion causes a 180-degree phase shift when compared to the blood pressure signal, which always has higher values during systole and lower values during diastole. The large phase shift is visible around the 1 Hz frequency on the quartile transfer functions, which have been sorted according to the IO_{dev} value. The population quartile, which displays the retrograde oriented longitudinal waveform (lower quartile), has negative phase values whereas the quartile with the antegrade oriented waveform has positive phase values. Another key difference in the quartile transfer functions is in the coherence functions between frequencies of 2 Hz and 3 Hz. The upper quartile had its peak coherence on the frequency band whereas the lower quartile displayed only a minor peak on the band and had its primary coherence at the 1 Hz frequency. This is an indirect sign that there is less oscillation occurring within the retrograde oriented longitudinal motion waveform.

A correlation was found to reference arterial stiffness values from the phase values of the heartbeat frequency of the transfer function between the blood pressure and the longitudinal motion. Both Aix@75 and E_Y displayed significant inverse correlations with the phase values in the 0.5 Hz wide heartbeat band ($p < 0.01$ and $p < 0.05$, respectively). Based on the

individual longitudinal motion curves, it is known that an approximately 180-degree phase shift is visible with subjects whose intima-media moves mainly in the retrograde direction during systole. However, the main direction of the longitudinal motion is not responsible for the correlation between the phase values in the heartbeat band and the arterial stiffness indices, since the correlation between IO_{dev} and arterial stiffness indices was statistically insignificant (Aix@75, $r = -0.01$, $p = 0.79$; E_Y, $r = -0.32$, $p = 0.18$).

The results of the transfer function analysis were obtained from rather young healthy adults and thus they do not represent average motion values in general population. If one examined larger sample populations, then because the longitudinal motion waveform is connected to the arterial stiffness, the amplitude attenuation and the delay between the longitudinal motions of different wall layers would be likely to change from the values reported here.

8 CONCLUSIONS

This thesis examined the unexplored features of the longitudinal motion of the common carotid artery, by applying a motion-tracking method with a series of newly devised waveform analysis tools. The developed tracking method proved to be useful and sufficiently accurate for measuring the longitudinal wall motion of the common carotid artery in clinical studies.

Arterial stiffness indices from the velocity and acceleration curves of the longitudinal motion were introduced and especially the new methods intending to summarize the whole motion waveform into a single useful value (RAlength and the 2nd principal component of the longitudinal motion) successfully detected stiffness changes within the artery wall. In side-by-side comparison, all of the above indices were superior to the amplitude measurements when evaluating the stiffness of the artery from the longitudinal motion of the carotid wall. In addition, the temporal characteristics of the longitudinal motion outperformed the spatial characteristics in the transfer function analysis, when assessing arterial stiffness.

The transfer function analysis revealed a strong linear relationship between the longitudinal motions of the intima-media complex and the adventitia layer. In this young healthy population, the longitudinal motion of the intima-media complex occurred prior to the longitudinal motion of the adventitia layer by 19 ms and, on average, it had a 17 % higher motion amplitude. In addition, a weaker linear relationship was found between the carotid blood pressure and the longitudinal motion of the intima-media complex. This emphasizes the role of blood pressure as the driving force for the longitudinal motion. However, other driving forces are needed to explain the variation within the carotid longitudinal motion waveforms.

Overall, the results highlight the need for more detailed investigations of longitudinal wall kinetics; these may demand the development of more advanced techniques. By focusing

solely on the amplitude of the motion, the full potential of the longitudinal wall motion is not being exploited as a tool for assessing arterial stiffening.

Bibliography

[1] D. N. Ku, "Blood flow in arteries," *Annu. Rev. Fluid Mech.,* vol. 29, pp. 399-434, 1997.

[2] R. Joshi, S. Jan, Y. Wu and S. MacMahon, "Global inequalities in access to cardiovascular health care: our greatest challenge," *J. Am. Coll. Cardiol.,* vol. 52, pp. 1817-1825, 2008.

[3] A. D. Lopez, C. D. Mathers, M. Ezzati, D. T. Jamison and C. J. Murray, "Global and regional burden of disease and risk factors, 2001: systematic analysis of population health data," *The Lancet,* vol. 367, pp. 1747-1757, 2006.

[4] C. J. Murray and A. D. Lopez, "Mortality by cause for eight regions of the world: Global Burden of Disease Study," *The Lancet,* vol. 349, pp. 1269-1276, 1997.

[5] E. Braunwald, K. J. Isselbacher, R. G. Petersdorf, J. D. Wilson, J. B. Martin and A. S. Fauci, *Harrison's Principles of Internal Medicine.* McGraw-Hill, Medical Publishing Division, 1987.

[6] C. Diehm, J. Allenberg, K. Nimura-Eckert and F. J. Veith, *Color Atlas of Vascular Diseases.* Springer Science & Business Media, 2013.

[7] W. Insull, "The pathology of atherosclerosis: plaque development and plaque responses to medical treatment," *Am. J. Med.,* vol. 122, pp. S3-S14, 2009.

[8] S. Gielen and U. Landmesser, "The Year in Cardiology 2013: cardiovascular disease prevention," *Eur. Heart J.,* vol. 35, pp. 307-312, Feb, 2014.

[9] M. L. Weisfeldt and S. J. Zieman, "Advances in the prevention and treatment of cardiovascular disease," *Health. Aff.,* vol. 26, pp. 25-37, 2007.

[10] G. S. Berenson, W. A. Wattigney, R. E. Tracy, W. P. Newman, S. R. Srinivasan, L. S. Webber, E. R. Dalferes and J. P. Strong, "Atherosclerosis of the aorta and coronary arteries and cardiovascular risk factors in persons aged 6 to 30 years and studied at necropsy (The Bogalusa Heart Study)," *Am. J. Cardiol.,* vol. 70, pp. 851-858, 1992.

[11] M. Juonala, M. J. Järvisalo, N. Mäki-Torkko, M. Kähönen, J. S. Viikari and O. T. Raitakari, "Risk factors identified in childhood and decreased carotid artery elasticity in adulthood: the Cardiovascular Risk in Young Finns Study," *Circulation,* vol. 112, pp. 1486-1493, Sep 6, 2005.

[12] J. Koskinen, M. Kähönen, J. S. Viikari, L. Taittonen, T. Laitinen, T. Rönnemaa, T. Lehtimäki, N. Hutri-Kähönen, M. Pietikäinen, E. Jokinen, H. Helenius, N. Mattsson, O. T. Raitakari and M. Juonala, "Conventional cardiovascular risk factors and metabolic syndrome in predicting carotid intima-media thickness progression in young adults: the cardiovascular risk in young Finns study," *Circulation,* vol. 120, pp. 229-236, Jul 21, 2009.

[13] O. T. Raitakari, M. Juonala, M. Kähönen, L. Taittonen, T. Laitinen, N. Mäki-Torkko, M. J. Järvisalo, M. Uhari, E. Jokinen and T. Rönnemaa, "Cardiovascular risk factors in childhood and carotid artery intima-media thickness in adulthood: the Cardiovascular Risk in Young Finns Study," *JAMA,* vol. 290, pp. 2277-2283, 2003.

[14] A. Veijalainen, T. Tompuri, T. Laitinen, N. Lintu, A. Viitasalo, D. E. Laaksonen, J. Jääskeläinen and T. A. Lakka, "Metabolic Risk Factors Are Associated With Stiffness Index, Reflection Index and Finger Skin Temperature in Children," *Circulation Journal,* vol. 77, pp. 1281-1288, 2013.

[15] L. A. Solberg and D. A. Eggen, "Localization and sequence of development of atherosclerotic lesions in the carotid and vertebral arteries," *Circulation,* vol. 43, pp. 711-724, May, 1971.

[16] H. C. Stary, A. B. Chandler, R. E. Dinsmore, V. Fuster, S. Glagov, W. Insull Jr, M. E. Rosenfeld, C. J. Schwartz, W. D. Wagner and R. W. Wissler, "A definition of advanced types of atherosclerotic lesions and a histological classification of atherosclerosis. A report from the Committee on Vascular Lesions of the Council on Arteriosclerosis, American Heart Association," *Circulation,* vol. 92, pp. 1355-1374, Sep 1, 1995.

[17] S. S. Franklin, "Blood pressure and cardiovascular disease: what remains to be achieved?" *J. Hypertens. Suppl.,* vol. 19, pp. S3-8, Sep, 2001.

[18] M. Naghavi, P. Libby, E. Falk, S. W. Casscells, S. Litovsky, J. Rumberger, J. J. Badimon, C. Stefanadis, P. Moreno, G. Pasterkamp, Z. Fayad, P. H. Stone, S. Waxman, P. Raggi, M. Madjid, A. Zarrabi, A. Burke, C. Yuan, P. J. Fitzgerald, D. S. Siscovick, C. L. de Korte, M. Aikawa, K. E. Juhani Airaksinen, G. Assmann, C. R. Becker, J. H. Chesebro, A. Farb, Z. S. Galis, C. Jackson, I. K. Jang, W. Koenig, R. A. Lodder, K. March, J. Demirovic, M. Navab, S. G. Priori, M. D. Rekhter, R. Bahr, S. M. Grundy, R. Mehran, A. Colombo, E. Boerwinkle, C. Ballantyne, W. Insull Jr, R. S. Schwartz, R. Vogel, P. W. Serruys, G. K. Hansson, D. P. Faxon, S. Kaul, H. Drexler, P. Greenland, J. E. Muller, R. Virmani, P. M. Ridker, D. P. Zipes, P. K. Shah and J. T. Willerson, "From vulnerable plaque to vulnerable patient: a call for new definitions and risk assessment strategies: Part I," *Circulation,* vol. 108, pp. 1664-1672, Oct 7, 2003.

[19] S. J. Zieman, V. Melenovsky and D. A. Kass, "Mechanisms, pathophysiology, and therapy of arterial stiffness," *Arterioscler. Thromb. Vasc. Biol.,* vol. 25, pp. 932-943, May, 2005.

[20] S. H. Taivainen, H. Yli- Ollila, M. Juonala, M. Kähönen, O. T. Raitakari, T. M. Laitinen and T. P. Laitinen,

"Interrelationships between indices of longitudinal movement of the common carotid artery wall and the conventional measures of subclinical arteriosclerosis," *Clin. Physiol. Funct. Imaging,* 2015.

[21] G. Zahnd, L. Boussel, A. Marion, M. Durand, P. Moulin, A. Sérusclat and D. Vray, "Measurement of two-dimensional movement parameters of the carotid artery wall for early detection of arteriosclerosis: a preliminary clinical study," *Ultrasound Med. Biol.,* vol. 37, pp. 1421-1429, 2011.

[22] S. Svedlund and L. Gan, "Longitudinal common carotid artery wall motion is associated with plaque burden in man and mouse," *Atherosclerosis,* vol. 217, pp. 120-124, 2011.

[23] M. Acar, A. Salbacak, M. E. Sakarya, I. Zararsiz, M. Ulusoy, M. ACAR, A. SALBACAK, M. SAKARYA, I. ZARARSIZ and M. ULUSOY, "The Morphometrical Analysis of the External Carotid Artery and its Branches with Multidetector Computerized Tomography Angiography Technique," *Int. J. Morphol.,* vol. 31, pp. 1407-1414, 2013.

[24] R. S. Snell, *Clinical Anatomy by Regions.* Lippincott Williams & Wilkins, 2011.

[25] P. Atluri, *The Surgical Review: An Integrated Basic and Clinical Science Study Guide.* Lippincott Williams & Wilkins, 2005.

[26] K. T. Patton and G. A. Thibodeau, *Anatomy & Physiology.* Elsevier Health Sciences, 2014.

[27] T. Nilsson, Å R. Ahlgren, T. Jansson, H. W. Persson, J. Nilsson, K. Lindström and M. Cinthio, "A method to measure shear strain with high spatial resolution in the arterial wall non-invasively in vivo by tracking zero-crossings of B-mode intensity gradients," in *IEEE IUS,* 2010, pp. 491-494.

[28] E. Gkaliagkousi and S. Douma, "The pathogenesis of arterial stiffness and its prognostic value in essential hypertension and cardiovascular diseases," *Hippokratia,* vol. 13, pp. 70-75, 2009.

[29] W. J. Krause, *The Art of Examining and Interpreting Histologic Preparations: A Laboratory Manual and Study Guide for Histology.* Universal-Publishers, 2004.

[30] Y. Sun, C. Lin, C. Lu, P. Yip and R. Chen, "Carotid atherosclerosis, intima media thickness and risk factors—an analysis of 1781 asymptomatic subjects in Taiwan," *Atherosclerosis,* vol. 164, pp. 89-94, 2002.

[31] A. M. Dart and B. A. Kingwell, "Pulse pressure—a review of mechanisms and clinical relevance," *J. Am. Coll. Cardiol.,* vol. 37, pp. 975-984, 3/15, 2001.

[32] C. Giannattasio, P. Salvi, F. Valbusa, A. Kearney-Schwartz, A. Capra, M. Amigoni, M. Failla, L. Boffi, F. Madotto, A. Benetos and G. Mancia, "Simultaneous measurement of beat-to-beat carotid diameter and pressure changes to assess arterial mechanical properties," *Hypertension,* vol. 52, pp. 896-902, Nov, 2008.

[33] G. Gamble, J. Zorn, G. Sanders, S. MacMahon and N. Sharpe, "Estimation of arterial stiffness, compliance, and distensibility from M-mode ultrasound measurements of the common carotid artery," *Stroke,* vol. 25, pp. 11-16, Jan, 1994.

[34] T. G. Pickering, J. E. Hall, L. J. Appel, B. E. Falkner, J. W. Graves, M. N. Hill, D. W. Jones, T. Kurtz, S. G. Sheps and E. J. Roccella, "Recommendations for blood pressure measurement in humans: an AHA scientific statement from the Council on High Blood Pressure Research Professional and Public Education Subcommittee," *J. Clin. Hypertens,* vol. 7, pp. 102-109, 2005.

[35] M. E. Safar and A. Kakou, "Carotid and brachial blood pressure–measurements in hypertensive subjects," *Revista Brasileira De Hipertensao,* vol. 15, pp. 122-124, 2008.

[36] K. D. Reesink, E. Hermeling, M. C. Hoeberigs, R. S. Reneman and A. P. Hoeks, "Carotid artery pulse wave time characteristics to quantify ventriculoarterial responses to

orthostatic challenge," *J. Appl. Physiol. (1985),* vol. 102, pp. 2128-2134, Jun, 2007.

[37] N. Westerhof, J. Lankhaar and B. E. Westerhof, "The arterial windkessel," *Med. Biol. Eng. Comput.,* vol. 47, pp. 131-141, 2009.

[38] J. Pfitzner, "Poiseuille and his law," *Anaesthesia,* vol. 31, pp. 273-275, 1976.

[39] J. E. Deanfield, J. P. Halcox and T. J. Rabelink, "Endothelial function and dysfunction: testing and clinical relevance," *Circulation,* vol. 115, pp. 1285-1295, Mar 13, 2007.

[40] J. A. Vita and J. F. Keaney Jr, "Endothelial function: a barometer for cardiovascular risk?" *Circulation,* vol. 106, pp. 640-642, Aug 6, 2002.

[41] T. Alam, A. Seifalian and D. Baker, "A review of methods currently used for assessment of in vivo endothelial function," *Eur. J. Vasc. Endovasc. Surg.,* vol. 29, pp. 269-276, 2005.

[42] H. Tomiyama and A. Yamashina, "Non-invasive vascular function tests: their pathophysiological background and clinical application," *Circulation Journal,* vol. 74, pp. 24-33, 2010.

[43] S. Laurent, J. Cockcroft, L. Van Bortel, P. Boutouyrie, C. Giannattasio, D. Hayoz, B. Pannier, C. Vlachopoulos, I. Wilkinson and H. Struijker-Boudier, "Expert consensus document on arterial stiffness: methodological issues and clinical applications," *Eur. Heart J.,* vol. 27, pp. 2588-2605, 2006.

[44] H. S. Bassiouny, C. K. Zarins, M. H. Kadowaki and S. Glagov, "Hemodynamic stress and experimental aortoiliac atherosclerosis," *J. Vasc. Surg.,* vol. 19, pp. 426-434, 1994.

[45] D. Beattie, C. Xu, R. Vito, S. Glagov and M. Whang, "Mechanical analysis of heterogeneous, atherosclerotic human aorta," *J. Biomech. Eng.,* vol. 120, pp. 602-607, 1998.

[46] Z. S. Galis and J. J. Khatri, "Matrix metalloproteinases in vascular remodeling and atherogenesis: the good, the bad, and the ugly," *Circ. Res.,* vol. 90, pp. 251-262, Feb 22, 2002.

[47] J. Amar, J. B. Ruidavets, B. Chamontin, L. Drouet and J. Ferrières, "Arterial stiffness and cardiovascular risk factors in a population-based study," *J. Hypertens.,* vol. 19, pp. 381-387, 2001.

[48] J. Blacher, A. P. Guerin, B. Pannier, S. J. Marchais, M. E. Safar and G. M. London, "Impact of aortic stiffness on survival in end-stage renal disease," *Circulation,* vol. 99, pp. 2434-2439, May 11, 1999.

[49] E. D. Lehmann, K. D. Hopkins, A. Rawesh, R. C. Joseph, K. Kongola, S. W. Coppack and R. G. Gosling, "Relation between number of cardiovascular risk factors/events and noninvasive Doppler ultrasound assessments of aortic compliance," *Hypertension,* vol. 32, pp. 565-569, Sep, 1998.

[50] A. H. Hoffman, Z. Teng, C. Mui, J. Zheng, P. K. Woodard and D. Tang, "Stiffness comparisons between adventitia, media and full thickness specimens from human atherosclerotic carotid arteries," in *ASME SBC,* 2009, pp. 525-526.

[51] J. C. Kohn, M. C. Lampi and C. A. Reinhart-King, "Age-related vascular stiffening: causes and consequences," *Front. Genet.,* vol. 6, pp. 112, 2015.

[52] M. O'Rourke, "Arterial stiffness, systolic blood pressure, and logical treatment of arterial hypertension," *Hypertension,* vol. 15, pp. 339-347, Apr, 1990.

[53] M. Cecelja and P. Chowienczyk, "Dissociation of aortic pulse wave velocity with risk factors for cardiovascular disease other than hypertension: a systematic review," *Hypertension,* vol. 54, pp. 1328-1336, Dec, 2009.

[54] J. Craft, C. Gordon, S. E. Huether, K. L. McCance and V. L. Brashers, *Understanding Pathophysiology-ANZ Adaptation*. Elsevier Health Sciences, 2015.

[55] C. L. Taylor, Z. Yuan, W. R. Selman, R. A. Ratcheson and A. A. Rimm, "Cerebral arterial aneurysm formation and rupture in 20,767 elderly patients: hypertension and other risk factors," *J. Neurosurg.,* vol. 83, pp. 812-819, 1995.

[56] A. J. Flammer, T. Anderson, D. S. Celermajer, M. A. Creager, J. Deanfield, P. Ganz, N. M. Hamburg, T. F. Luscher, M. Shechter, S. Taddei, J. A. Vita and A. Lerman, "The assessment of endothelial function: from research into clinical practice," *Circulation,* vol. 126, pp. 753-767, Aug 7, 2012.

[57] D. W. Morel, P. E. DiCorleto and G. M. Chisolm, "Endothelial and smooth muscle cells alter low density lipoprotein in vitro by free radical oxidation," *Arteriosclerosis,* vol. 4, pp. 357-364, Jul-Aug, 1984.

[58] R. B. Singh, S. A. Mengi, Y. J. Xu, A. S. Arneja and N. S. Dhalla, "Pathogenesis of atherosclerosis: A multifactorial process," *Exp. Clin. Cardiol.,* vol. 7, pp. 40-53, Spring, 2002.

[59] C. N. Gamble, "The pathogenesis of hyaline arteriolosclerosis," *Am. J. Pathol.,* vol. 122, pp. 410-420, Mar, 1986.

[60] G. Elzinga and N. Westerhof, "Pressure and flow generated by the left ventricle against different impedances," *Circ. Res.,* vol. 32, pp. 178-186, Feb, 1973.

[61] G. F. Mitchell, M. A. van Buchem, S. Sigurdsson, J. D. Gotal, M. K. Jonsdottir, O. Kjartansson, M. Garcia, T. Aspelund, T. B. Harris, V. Gudnason and L. J. Launer, "Arterial stiffness, pressure and flow pulsatility and brain structure and function: the Age, Gene/Environment Susceptibility--Reykjavik study," *Brain,* vol. 134, pp. 3398-3407, Nov, 2011.

[62] G. F. Mitchell, H. Parise, E. J. Benjamin, M. G. Larson, M. J. Keyes, J. A. Vita, R. S. Vasan and D. Levy, "Changes in arterial stiffness and wave reflection with advancing age in healthy men and women: the Framingham Heart Study," *Hypertension,* vol. 43, pp. 1239-1245, Jun, 2004.

[63] G. Fernandez-Fresnedo, E. Rodrigo, A. L. de Francisco, S. S. de Castro, O. Castaneda and M. Arias, "Role of pulse pressure on cardiovascular risk in chronic kidney disease patients," *J. Am. Soc. Nephrol.,* vol. 17, pp. S246-9, Dec, 2006.

[64] R. R. Townsend, I. B. Wilkinson, E. L. Schiffrin, A. P. Avolio, J. A. Chirinos, J. R. Cockcroft, K. S. Heffernan, E. G. Lakatta, C. M. McEniery, G. F. Mitchell, S. S. Najjar, W. W. Nichols, E. M. Urbina, T. Weber and American Heart Association Council on Hypertension, "Recommendations for Improving and Standardizing Vascular Research on Arterial Stiffness: A Scientific Statement From the American Heart Association," *Hypertension,* vol. 66, pp. 698-722, Sep, 2015.

[65] R. Loutzenhiser, A. Bidani and L. Chilton, "Renal myogenic response: kinetic attributes and physiological role," *Circ. Res.,* vol. 90, pp. 1316-1324, Jun 28, 2002.

[66] R. Loutzenhiser, K. Griffin, G. Williamson and A. Bidani, "Renal autoregulation: new perspectives regarding the protective and regulatory roles of the underlying mechanisms," *Am. J. Physiol. Regul. Integr. Comp. Physiol.,* vol. 290, pp. R1153-67, May, 2006.

[67] W. R. Milnor, *Hemodynamics.* Baltimore: Williams and Wilkins, 1982.

[68] S. Laurent, P. Boutouyrie, R. Asmar, I. Gautier, B. Laloux, L. Guize, P. Ducimetiere and A. Benetos, "Aortic stiffness is an independent predictor of all-cause and cardiovascular mortality in hypertensive patients," *Hypertension,* vol. 37, pp. 1236-1241, May, 2001.

[69] M. F. O'Rourke and R. P. Kelly, "Wave reflection in the systemic circulation and its implications in ventricular function." *J. Hypertens.,* vol. 11, pp. 327-337, 1993.

[70] G. M. London and A. P. Guerin, "Influence of arterial pulse and reflected waves on blood pressure and cardiac function," *Am. Heart J.,* vol. 138, pp. S220-S224, 1999.

[71] C. Russo, Z. Jin, Y. Takei, T. Hasegawa, S. Koshaka, V. Palmieri, M. S. Elkind, S. Homma, R. L. Sacco and M. R. Di Tullio, "Arterial wave reflection and subclinical left ventricular systolic dysfunction," *J. Hypertens.,* vol. 29, pp. 574-582, Mar, 2011.

[72] J. A. Franciosa, M. Wilen, S. Ziesche and J. N. Cohn, "Survival in men with severe chronic left ventricular failure due to either coronary heart disease or idiopathic dilated cardiomyopathy," *Am. J. Cardiol.,* vol. 51, pp. 831-836, 1983.

[73] A. Hofman, G. Verwoert, J. Wittemana, I. Wilkinson, J. Cockcroft, C. McEniery, L. S. Yasmin, P. Boutouyrie, E. Bozec and T. Hansen, "Determinants of pulse wave velocity in healthy people and in the presence of cardiovascular risk factors: 'establishing normal and reference values'," *Eur. Heart J.,* vol. 31, pp. 2338-2350, Oct, 2010.

[74] J. Nürnberger, A. Keflioglu-Scheiber, A. M. O. Saez, R. R. Wenzel, T. Philipp and R. F. Schäfers, "Augmentation index is associated with cardiovascular risk," *J. Hypertens.,* vol. 20, pp. 2407-2414, 2002.

[75] E. J. Benjamin, M. G. Larson, M. J. Keyes, G. F. Mitchell, R. S. Vasan, J. F. Keaney Jr, B. T. Lehman, S. Fan, E. Osypiuk and J. A. Vita, "Clinical correlates and heritability of flow-mediated dilation in the community: the Framingham Heart Study," *Circulation,* vol. 109, pp. 613-619, Feb 10, 2004.

[76] R. M. Henry, I. Ferreira, P. J. Kostense, J. M. Dekker, G. Nijpels, R. J. Heine, O. Kamp, L. M. Bouter and C. D. Stehouwer,

"Type 2 diabetes is associated with impaired endothelium-dependent, flow-mediated dilation, but impaired glucose metabolism is not: the Hoorn Study," *Atherosclerosis,* vol. 174, pp. 49-56, 2004.

[77] E. Ter Avest, A. F. Stalenhoef and J. de Graaf, "What is the role of non-invasive measurements of atherosclerosis in individual cardiovascular risk prediction?" *Clin. Sci. (Lond),* vol. 112, pp. 507-516, May, 2007.

[78] A. Bjallmark, B. Lind, M. Peolsson, K. Shahgaldi, L. A. Brodin and J. Nowak, "Ultrasonographic strain imaging is superior to conventional non-invasive measures of vascular stiffness in the detection of age-dependent differences in the mechanical properties of the common carotid artery," *Eur. J. Echocardiogr.,* vol. 11, pp. 630-636, Aug, 2010.

[79] A. Benetos, S. Laurent, A. P. Hoeks, P. H. Boutouyrie and M. E. Safar, "Arterial alterations with aging and high blood pressure. A noninvasive study of carotid and femoral arteries," *Arterioscler. Thromb.,* vol. 13, pp. 90-97, Jan, 1993.

[80] R. S. Reneman, J. M. Meinders and A. P. Hoeks, "Non-invasive ultrasound in arterial wall dynamics in humans: what have we learned and what remains to be solved," *Eur. Heart J.,* vol. 26, pp. 960-966, May, 2005.

[81] C. Yuan, J. Wang and M. Ying, "Predictive Value of Carotid Distensibility Coefficient for Cardiovascular Diseases and All-Cause Mortality: A Meta-Analysis," *PloS One,* vol. 11, pp. e0152799, 2016.

[82] M. F. O'Rourke, J. A. Staessen, C. Vlachopoulos and D. Duprez, "Clinical applications of arterial stiffness; definitions and reference values," *Am. J. Hypertens.,* vol. 15, pp. 426-444, 2002.

[83] J. Cutnell and K. Johnson, *Physics.* New Jersey: Wiley, 2007.

[84] C. H. Chen, E. Nevo, B. Fetics, P. H. Pak, F. C. Yin, W. L. Maughan and D. A. Kass, "Estimation of central aortic pressure waveform by mathematical transformation of radial tonometry pressure. Validation of generalized transfer function," *Circulation,* vol. 95, pp. 1827-1836, Apr 1, 1997.

[85] S. Skinner, E. Barin, E. Gallery, J. Beattie and P. Kamen, "SphygmoCor manual: a clinical guide; pulse wave analysis," *West Ryde, Australia: AtCor Medical Pty Ltd,* 2011.

[86] I. B. Wilkinson, K. Prasad, I. R. Hall, A. Thomas, H. MacCallum, D. J. Webb, M. P. Frenneaux and J. R. Cockcroft, "Increased central pulse pressure and augmentation index in subjects with hypercholesterolemia," *J. Am. Coll. Cardiol.,* vol. 39, pp. 1005-1011, 2002.

[87] T. Weber, J. Auer, M. F. O'Rourke, E. Kvas, E. Lassnig, R. Berent and B. Eber, "Arterial stiffness, wave reflections, and the risk of coronary artery disease," *Circulation,* vol. 109, pp. 184-189, Jan 20, 2004.

[88] B. A. Kingwell and C. D. Gatzka, "Arterial stiffness and prediction of cardiovascular risk," *J. Hypertens.,* vol. 20, pp. 2337-2340, 2002.

[89] I. B. Wilkinson, H. MacCallum, L. Flint, J. R. Cockcroft, D. E. Newby and D. J. Webb, "The influence of heart rate on augmentation index and central arterial pressure in humans," *J. Physiol. (Lond.),* vol. 525, pp. 263-270, 2000.

[90] S. M. Hughes, L. J. Dixon and G. E. McVeigh, "Arterial stiffness and pulse wave velocity: problems with terminology," *Circulation,* vol. 109, pp. 3, Jan 20, 2004.

[91] L. M. Van Bortel, S. Laurent, P. Boutouyrie, P. Chowienczyk, J. K. Cruickshank, T. De Backer, J. Filipovsky, S. Huybrechts, F. U. Mattace-Raso, A. D. Protogerou, G. Schillaci, P. Segers, S. Vermeersch, T. Weber, Artery Society, European Society of Hypertension Working Group on Vascular Structure

and Function and European Network for Noninvasive Investigation of Large Arteries, "Expert consensus document on the measurement of aortic stiffness in daily practice using carotid-femoral pulse wave velocity," *J. Hypertens.,* vol. 30, pp. 445-448, Mar, 2012.

[92] G. F. Mitchell, S. J. Hwang, R. S. Vasan, M. G. Larson, M. J. Pencina, N. M. Hamburg, J. A. Vita, D. Levy and E. J. Benjamin, "Arterial stiffness and cardiovascular events: the Framingham Heart Study," *Circulation,* vol. 121, pp. 505-511, Feb 2, 2010.

[93] J. Blacher, R. Asmar, S. Djane, G. M. London and M. E. Safar, "Aortic pulse wave velocity as a marker of cardiovascular risk in hypertensive patients," *Hypertension,* vol. 33, pp. 1111-1117, 1999.

[94] Y. Lee, K. Kim, C. Nam, S. Han, S. Hur, Y. Kim, K. Kim and J. Lee, "Clinical implication of carotid-radial pulse wave velocity for patients with coronary artery disease," *Korean Circ. J.,* vol. 36, pp. 565-572, 2006.

[95] B. Pannier, A. P. Guerin, S. J. Marchais, M. E. Safar and G. M. London, "Stiffness of capacitive and conduit arteries: prognostic significance for end-stage renal disease patients," *Hypertension,* vol. 45, pp. 592-596, Apr, 2005.

[96] A. Lerman and A. M. Zeiher, "Endothelial function: cardiac events," *Circulation,* vol. 111, pp. 363-368, Jan 25, 2005.

[97] O. T. Raitakari and D. S. Celermajer, "Research Methods in Human Cardiovascular Pharmacology edited by Dr S. Maxwell and Prof. D. Webb Flow- mediated dilatation," *Br. J. Clin. Pharmacol.,* vol. 50, pp. 397-404, 2000.

[98] M. C. Corretti, T. J. Anderson, E. J. Benjamin, D. Celermajer, F. Charbonneau, M. A. Creager, J. Deanfield, H. Drexler, M. Gerhard-Herman and D. Herrington, "Guidelines for the ultrasound assessment of endothelial-dependent flow-mediated vasodilation of the brachial artery: a report of the International

Brachial Artery Reactivity Task Force," *J. Am. Coll. Cardiol.,* vol. 39, pp. 257-265, 2002.

[99] A. Peretz, D. F. Leotta, J. H. Sullivan, C. A. Trenga, F. N. Sands, M. R. Aulet, M. Paun, E. A. Gill and J. D. Kaufman, "Flow mediated dilation of the brachial artery: an investigation of methods requiring further standardization," *BMC Cardiovasc. Disord.,* vol. 7, pp. 11, Mar 21, 2007.

[100] M. Juonala, M. Kähönen, T. Laitinen, N. Hutri-Kähönen, E. Jokinen, L. Taittonen, M. Pietikäinen, H. Helenius, J. S. Viikari and O. T. Raitakari, "Effect of age and sex on carotid intima-media thickness, elasticity and brachial endothelial function in healthy adults: the cardiovascular risk in Young Finns Study," *Eur. Heart J.,* vol. 29, pp. 1198-1206, May, 2008.

[101] C. Masoura, C. Pitsavos, K. Aznaouridis, I. Skoumas, C. Vlachopoulos and C. Stefanadis, "Arterial endothelial function and wall thickness in familial hypercholesterolemia and familial combined hyperlipidemia and the effect of statins. A systematic review and meta-analysis," *Atherosclerosis,* vol. 214, pp. 129-138, 2011.

[102] G. Brohall, A. Oden and B. Fagerberg, "Carotid artery intima- media thickness in patients with Type 2 diabetes mellitus and impaired glucose tolerance: a systematic review," *Diabetic Med.,* vol. 23, pp. 609-616, 2006.

[103] D. H. O'Leary, J. F. Polak, R. A. Kronmal, T. A. Manolio, G. L. Burke and S. K. Wolfson Jr, "Carotid-artery intima and media thickness as a risk factor for myocardial infarction and stroke in older adults," *N. Engl. J. Med.,* vol. 340, pp. 14-22, 1999.

[104] P. Touboul, J. Labreuche, E. Bruckert, H. Schargrodsky, P. Prati, A. Tosetto, R. Hernandez-Hernandez, K. Woo, H. Silva and E. Vicaut, "HDL-C, triglycerides and carotid IMT: a meta-analysis of 21,000 patients with automated edge detection IMT measurement," *Atherosclerosis,* vol. 232, pp. 65-71, 2014.

[105] S. Bartels, A. R. Franco and T. Rundek, "Carotid intima-media thickness (cIMT) and plaque from risk assessment and clinical use to genetic discoveries," *Perspectives in Medicine,* vol. 1, pp. 139-145, 2012.

[106] C. Cuspidi, E. Ambrosioni, G. Mancia, A. C. Pessina, B. Trimarco, A. Zanchetti and APROS Investigators, "Role of echocardiography and carotid ultrasonography in stratifying risk in patients with essential hypertension: the Assessment of Prognostic Risk Observational Survey," *J. Hypertens.,* vol. 20, pp. 1307-1314, 2002.

[107] A. Zanchetti, M. G. Bond, M. Hennig, A. Neiss, G. Mancia, C. Dal Palu, L. Hansson, B. Magnani, K. H. Rahn, J. L. Reid, J. Rodicio, M. Safar, L. Eckes, P. Rizzini and European Lacidipine Study on Atherosclerosis investigators, "Calcium antagonist lacidipine slows down progression of asymptomatic carotid atherosclerosis: principal results of the European Lacidipine Study on Atherosclerosis (ELSA), a randomized, double-blind, long-term trial," *Circulation,* vol. 106, pp. 2422-2427, Nov 5, 2002.

[108] A. Zanchetti, M. G. Bond, M. Hennig, R. Tang, R. Hollweck, G. Mancia, L. Eckes and D. Micheli, "Absolute and relative changes in carotid intima–media thickness and atherosclerotic plaques during long-term antihypertensive treatment: further results of the European Lacidipine Study on Atherosclerosis (ELSA)," *J. Hypertens.,* vol. 22, pp. 1201-1212, 2004.

[109] R. Lawton and L. Greene, "A method for the in situ study of aortic elasticity in the dog," *Authorized Medical Allowance List, US Naval and Air Development Center, Warminister, PA (Rep.no.NADC-MA-5603),* 1956.

[110] M. Persson, Å Rydén Ahlgren, T. Jansson, A. Eriksson, H. W. Persson and K. Lindström, "A new non- invasive ultrasonic method for simultaneous measurements of longitudinal and

radial arterial wall movements: first in vivo trial," *Clinical Physiology and Functional Imaging,* vol. 23, pp. 247-251, 2003.

[111] J. Albinsson, S. Brorsson, Å R. Ahlgren and M. Cinthio, "Improved Tracking Performance of Lagrangian Block-Matching Methodologies Using Block Expansion in the Time Domain: In Silico, Phantom and in Vivo Evaluations," *Ultrasound Med. Biol.,* vol. 40, pp. 2508-2520, 2014.

[112] M. Cinthio, Å R. Ahlgren, T. Jansson, A. Eriksson, H. W. Persson and K. Lindström, "Evaluation of an ultrasonic echo-tracking method for measurements of arterial wall movements in two dimensions," *Ultrasonics, Ferroelectrics, and Frequency Control, IEEE Transactions On,* vol. 52, pp. 1300-1311, 2005.

[113] A. Gastounioti, S. Golemati, J. Stoitsis and K. Nikita, "Comparison of Kalman-filter-based approaches for block matching in arterial wall motion analysis from B-mode ultrasound," *Measurement Science and Technology,* vol. 22, pp. 114008, 2011.

[114] A. Gastounioti, S. Golemati, J. Stoitsis and K. Nikita, "Carotid artery wall motion analysis from B-mode ultrasound using adaptive block matching: in silico evaluation and in vivo application," *Phys. Med. Biol.,* vol. 58, pp. 8647, 2013.

[115] S. Golemati, A. Sassano, M. J. Lever, A. A. Bharath, S. Dhanjil and A. N. Nicolaides, "Carotid artery wall motion estimated from B-mode ultrasound using region tracking and block matching," *Ultrasound Med. Biol.,* vol. 29, pp. 387-399, 2003.

[116] S. Golemati, J. S. Stoitsis, A. Gastounioti, A. C. Dimopoulos, V. Koropouli and K. S. Nikita, "Comparison of block matching and differential methods for motion analysis of the carotid artery wall from ultrasound images," *IEEE Trans. Inf. Technol. Biomed.,* vol. 16, pp. 852-858, 2012.

[117] T. Idzenga, S. Holewijn, H. H. Hansen and C. L. de Korte, "Estimating cyclic shear strain in the common carotid artery

using radiofrequency ultrasound," *Ultrasound Med. Biol.*, vol. 38, pp. 2229-2237, 2012.

[118] M. Larsson, B. Heyde, F. Kremer, L. Brodin and J. D'hooge, "Ultrasound speckle tracking for radial, longitudinal and circumferential strain estimation of the carotid artery–An in vitro validation via sonomicrometry using clinical and high-frequency ultrasound," *Ultrasonics,* vol. 56, pp. 399-408, 2015.

[119] T. Numata, H. Hasegawa and H. Kanai, "Basic study on detection of outer boundary of arterial wall using its longitudinal motion," *Jpn. J. Appl. Phys.*, vol. 46, pp. 4900, 2007.

[120] G. Zahnd, M. Orkisz, A. Sérusclat and D. Vray, "Minimal-path contours combined with speckle tracking to estimate 2D displacements of the carotid artery wall in B-mode imaging," in *IEEE Int. Ultrason. Symp.* 2011, pp. 732-735.

[121] G. Zahnd, M. Orkisz, A. Sérusclat, P. Moulin and D. Vray, "Evaluation of a Kalman-based block matching method to assess the bi-dimensional motion of the carotid artery wall in B-mode ultrasound sequences," *Med. Image Anal.,* vol. 17, pp. 573-585, 2013.

[122] G. Zahnd, M. Orkisz, S. Balocco, A. Sérusclat, P. Moulin and D. Vray, "Tracking arterial wall motion in a 2D t volume," in *IEEE J-BHI,* 2014, pp. 672-675.

[123] G. Zahnd, S. Salles, H. Liebgott, D. Vray, A. Sérusclat and P. Moulin, "Real-time ultrasound-tagging to track the 2D motion of the common carotid artery wall in vivo," *Med. Phys.*, vol. 42, pp. 820-830, 2015.

[124] J. S. Suri, *Advances in Diagnostic and Therapeutic Ultrasound Imaging*. Artech House, 2008.

[125] F. Yeung, S. F. Levinson, D. Fu and K. J. Parker, "Feature-adaptive motion tracking of ultrasound image sequences using a

deformable mesh," *IEEE Trans. Med. Imaging,* vol. 17, pp. 945-956, 1998.

[126] F. Yeung, S. F. Levinson and K. J. Parker, "Multilevel and motion model-based ultrasonic speckle tracking algorithms," *Ultrasound Med. Biol.,* vol. 24, pp. 427-441, 1998.

[127] S. Svedlund and L. Gan, "Longitudinal wall motion of the common carotid artery can be assessed by velocity vector imaging," *Clin. Physiol. Funct. Imaging,* vol. 31, pp. 32-38, 2011.

[128] J. S. Au, D. S. Ditor, M. J. MacDonald and E. J. Stohr, "Carotid artery longitudinal wall motion is associated with local blood velocity and left ventricular rotational, but not longitudinal, mechanics," *Physiol. Rep.,* vol. 4, pp. 10.14814/phy2.12872, Jul, 2016.

[129] M. Cinthio, A. R. Ahlgren, J. Bergkvist, T. Jansson, H. W. Persson and K. Lindstrom, "Longitudinal movements and resulting shear strain of the arterial wall," *Am. J. Physiol. Heart Circ. Physiol.,* vol. 291, pp. H394-402, Jul, 2006.

[130] Å R. Ahlgren, M. Cinthio, H. W. Persson and K. Lindström, "Different patterns of longitudinal displacement of the common carotid artery wall in healthy humans are stable over a four-month period," *Ultrasound Med. Biol.,* vol. 38, pp. 916-925, 2012.

[131] J. Tat, J. S. Au, P. J. Keir and M. J. MacDonald, "Reduced common carotid artery longitudinal wall motion and intramural shear strain in individuals with elevated cardiovascular disease risk using speckle tracking," *Clin Physiol Funct Imaging,* 2015.

[132] G. Zahnd, D. Vray, A. Sérusclat, D. Alibay, M. Bartold, A. Brown, M. Durand, L. M. Jamieson, K. Kapellas and L. J. Maple-Brown, "Longitudinal displacement of the carotid wall and cardiovascular risk factors: associations with aging, adiposity, blood pressure and periodontal disease independent of cross-

sectional distensibility and intima-media thickness," *Ultrasound Med. Biol.,* vol. 38, pp. 1705-1715, 2012.

[133] G. Zahnd, S. Balocco, A. Sérusclat, P. Moulin, M. Orkisz and D. Vray, "Progressive attenuation of the longitudinal kinetics in the common carotid artery: preliminary in vivo assessment," *Ultrasound Med. Biol.,* vol. 41, pp. 339-345, 2015.

[134] M. Bukac and S. Canic, "Longitudinal displacement in viscoelastic arteries: a novel fluid-structure interaction computational model, and experimental validation," *Math. Biosci. Eng.,* vol. 10, pp. 295-318, Apr, 2013.

[135] J. Tat, I. N. Psaromiligkos and S. S. Daskalopoulou, "Carotid Atherosclerotic Plaque Alters the Direction of Longitudinal Motion in the Artery Wall," *Ultrasound Med. Biol.,* 2016.

[136] A. R. Ahlgren, M. Cinthio, S. Steen, T. Nilsson, T. Sjoberg, H. W. Persson and K. Lindstrom, "Longitudinal displacement and intramural shear strain of the porcine carotid artery undergo profound changes in response to catecholamines," *Am. J. Physiol. Heart Circ. Physiol.,* vol. 302, pp. H1102-15, Mar 1, 2012.

[137] Å R. Ahlgren, S. Steen, S. Segstedt, T. Erlöv, K. Lindström, T. Sjöberg, H. W. Persson, S. Ricci, P. Tortoli and M. Cinthio, "Profound Increase in Longitudinal Displacements of the Porcine Carotid Artery Wall Can Take Place Independently of Wall Shear Stress: A Continuation Report," *Ultrasound Med. Biol.,* vol. 41, pp. 1342-1353, 2015.

[138] A. D. Gepner, L. A. Colangelo, N. Reilly, C. E. Korcarz, J. D. Kaufman and J. H. Stein, "Carotid Artery Longitudinal Displacement, Cardiovascular Disease and Risk Factors: The Multi-Ethnic Study of Atherosclerosis," *PloS One,* vol. 10, pp. e0142138, 2015.

[139] S. Svedlund, C. Eklund, P. Robertsson, M. Lomsky and L. M. Gan, "Carotid artery longitudinal displacement predicts 1-

year cardiovascular outcome in patients with suspected coronary artery disease," *Arterioscler. Thromb. Vasc. Biol.*, vol. 31, pp. 1668-1674, Jul, 2011.

[140] E. Soleimani, M. Mokhtari-Dizaji and H. Saberi, "A novel non-invasive ultrasonic method to assess total axial stress of the common carotid artery wall in healthy and atherosclerotic men," *J. Biomech.*, vol. 48, pp. 1860-1867, 2015.

[141] M. Bukač, S. Čanić, R. Glowinski, J. Tambača and A. Quaini, "Fluid–structure interaction in blood flow capturing non-zero longitudinal structure displacement," *J. Comput. Phys.*, vol. 235, pp. 515-541, 2013.

[142] R. K. Warriner, K. W. Johnston and R. S. Cobbold, "A viscoelastic model of arterial wall motion in pulsatile flow: implications for Doppler ultrasound clutter assessment," *Physiol. Meas.*, vol. 29, pp. 157, 2008.

[143] F. P. Capote and M. L. de Castro, *Analytical Applications of Ultrasound.* Elsevier, 2007.

[144] T. L. Szabo, *Diagnostic Ultrasound Imaging: Inside Out.* Academic Press, 2004.

[145] K. Hynynen, "The threshold for thermally significant cavitation in dog's thigh muscle in vivo," *Ultrasound Med. Biol.*, vol. 17, pp. 157-169, 1991.

[146] P. R. Hoskins, K. Martin and A. Thrush, *Diagnostic Ultrasound: Physics and Equipment.* Cambridge University Press, 2010.

[147] P. Suetens, *Fundamentals of Medical Imaging.* Cambridge university press, 2009.

[148] T. Misaridis and J. A. Jensen, "Use of modulated excitation signals in medical ultrasound. Part III: high frame rate imaging,"

IEEE Trans. Ultrason. Ferroelectr. Freq. Control, vol. 52, pp. 208-219, 2005.

[149] J. D'hooge, E. Konofagou, F. Jamal, A. Heimdal, L. Barrios, B. Bijnens, J. Thoen, F. Van de Werf, G. Sutherland and P. Suetens, "Two-dimensional ultrasonic strain rate measurement of the human heart in vivo," *IEEE Trans. Ultrason. Ferroelectr. Freq. Control,* vol. 49, pp. 281-286, 2002.

[150] M. Wicks and E. Mokole, *Principles of Waveform Diversity and Design.* The Institution of Engineering and Technology, 2011.

[151] K. Z. Abd-Elmoniem, A. Youssef and Y. M. Kadah, "Real-time speckle reduction and coherence enhancement in ultrasound imaging via nonlinear anisotropic diffusion," *IEEE Trans. Biomed. Eng.,* vol. 49, pp. 997-1014, 2002.

[152] R. N. Czerwinski, D. L. Jones and W. D. O'Brien, "Ultrasound speckle reduction by directional median filtering," in *IEEE ICIP,* 1995, pp. 358-361.

[153] R. G. Dantas and E. T. Costa, "Ultrasound speckle reduction using modified Gabor filters," *IEEE Trans. Ultrason. Ferroelectr. Freq. Control,* vol. 54, pp. 530-538, 2007.

[154] J. Yu, J. Tan and Y. Wang, "Ultrasound speckle reduction by a SUSAN-controlled anisotropic diffusion method," *Pattern Recognit,* vol. 43, pp. 3083-3092, 2010.

[155] P. D. Welch, "The use of fast Fourier transform for the estimation of power spectra: A method based on time averaging over short, modified periodograms," *IEEE Trans. Audio Electroacoust.,* vol. 15, pp. 70-73, 1967.

[156] W. Nichols, M. O'Rourke and C. Vlachopoulos, *McDonald's Blood Flow in Arteries: Theoretical, Experimental and Clinical Principles.* CRC Press, 2011.

[157] G. O. Barnett, A. J. Mallos and A. Shapiro, "Relationship of aortic pressure and diameter in the dog," *J. Appl. Physiol.,* vol. 16, pp. 545-548, May, 1961.

[158] D. J. Patel, F. M. De Freitas, J. C. Greenfield Jr and D. L. Fry, "Relationship of Radius to Pressure Along the Aorta in Living Dogs," *J. Appl. Physiol.,* vol. 18, pp. 1111-1117, Nov, 1963.

[159] M. Sugawara, K. Niki, H. Furuhata, S. Ohnishi and S. Suzuki, "Relationship between the pressure and diameter of the carotid artery in humans," *Heart Vessels,* vol. 15, pp. 49-51, 2000.

[160] L. J. Cronbach, "Coefficient alpha and the internal structure of tests," *Psychometrika,* vol. 16, pp. 297-334, 1951.

[161] D. Han, "Comparison of commonly used image interpolation methods," *ICCSEE, Hangzhou, China,* 2013.

[162] V. Patel and K. Mistree, "A review on different image interpolation techniques for image enhancement," *IJETAE,* vol. 3, pp. 129-133, 2013.

[163] S. Fekkes, A. E. Swillens, H. H. Hansen, A. E. Saris, M. M. Nillesen, F. Iannaccone, P. Segers and C. L. de Korte, "2D versus 3D cross-correlation-based radial and circumferential strain estimation using multiplane 2D ultrafast ultrasound in a 3D atherosclerotic carotid artery model," *IEEE Trans. Ultrason. Ferroelectr. Freq. Control,* vol. 63, pp. 1543-1553, Aug 25, 2016.

[164] H. Yli-Ollila, T. Laitinen, M. Weckström, M. P. Tarvainen and T. Laitinen, "Relation of arterial stiffness and axial motion of the carotid artery wall—A pilot study to test our motion tracking algorithm in practice," in *IEEE EMBC,* Chicago, 2014, pp. 246-249.

[165] J. W. Ball, J. E. Dains, J. A. Flynn, B. S. Solomon and R. W. Stewart, *Seidel's Guide to Physical Examination.* Elsevier Health Sciences, 2014.

HEIKKI YLI-OLLILA

Longitudinal motion of the carotid artery wall is a novel index of arterial wellbeing. Previous studies have focused on the amplitude of the motion. In this thesis, tools to measure and analyze the whole longitudinal motion waveform are presented and validated. The results indicate that the measurements with these novel tools are repeatable and that the small changes within the arterial waveform are a more sensitive way to detect early signs of arterial stiffness than can be achieved by measuring the amplitude of the motion.

UNIVERSITY OF
EASTERN FINLAND

uef.fi

PUBLICATIONS OF
THE UNIVERSITY OF EASTERN FINLAND
Dissertations in Forestry and Natural Sciences

ISBN 978-952-61-2521-3
ISSN 1798-5668